Investigation of the interfaces of solid electrolyte based supercapacitors and batteries

Dissertation

zur Erlangung des akademischen Grades
Doktor der Ingenieurwissenschaften
(Dr.-Ing.)
der Technischen Fakultät
der Christian-Albrechts-Universität zu Kiel

Tesfaye Shiferaw

Faculty of Engineering
Christian-Albrechts-University of Kiel
Chair for Sensors and Solid State Ionics

Kiel, Germany

2008

1. Gutachter:	Prof. Dr. W. Weppner
2. Gutachter	Prof. Dr. F. Faupel
Datum der mündlichen Prüfung	12 December 2008

Contents:

Chapter 1

1. Introduction

1.1 Capacitors and History of a Capacitor

1.1.1 History of a Capacitor

The invention of the capacitor varies somewhat depending on whom you ask. There are records that indicate a German scientist named Ewald Georg von Kleist invented the capacitor in November 1745. Several months later Pieter van Musschenbroek, a Dutch professor at the University of Leyden came up with a very similar device in the form of the Leyden jar, which is typically credited as the first capacitor [1]. Since Kleist didn't have detailed records and notes, nor the notoriety of his Dutch counterpart, he's often overlooked as a contributor to the capacitor's evolution. However, over the years, both have been given equal credit as it was established that their research was independent of each other and merely a scientific coincidence [1].

The Leyden jar was a very simple device. It consisted of a glass jar, half filled with water and lined inside and out with metal foil. The glass acted as the dielectric, although it was thought for a time that water was the key ingredient. There was usually a metal wire or chain driven through a cork in the top of the jar. The chain was then hooked to something that would deliver a charge, most likely a hand-cranked static generator. Once delivered, the jar would hold two equal but opposite charges in equilibrium until they were connected with a wire, producing a slight spark or shock [2].

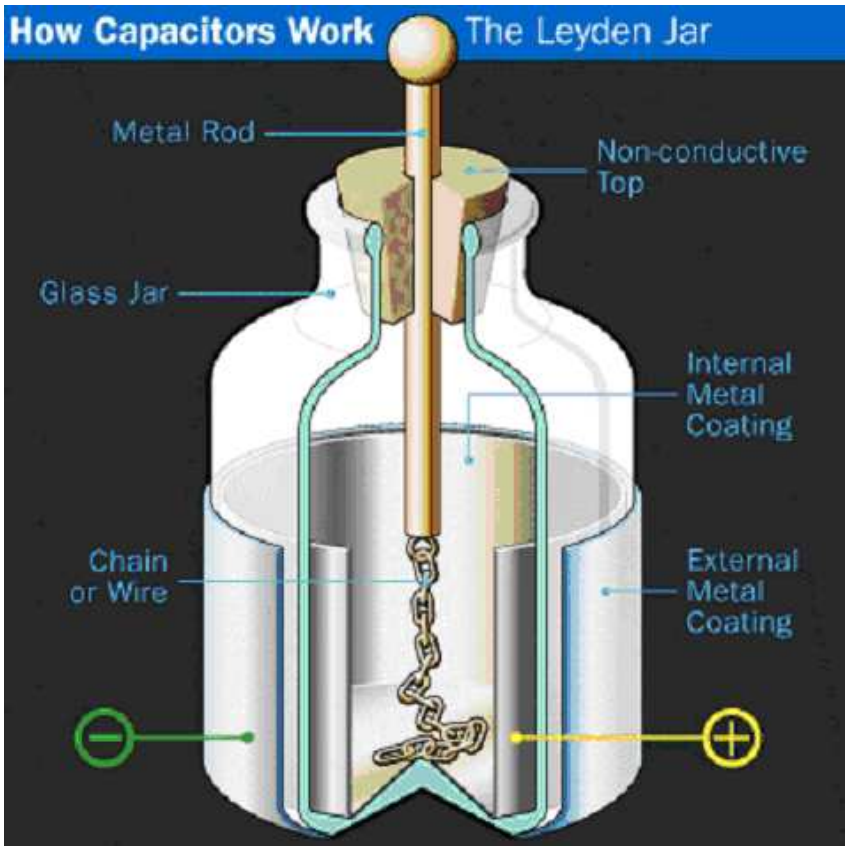

Fig. 1.1 The first Leyden jar model of a capacitor [Williams, 2]

Benjamin Franklin worked with the Leyden jar in his experiments with electricity and soon found that a flat piece of glass worked as well as the jar model, prompting him to develop the flat capacitor, or Franklin Square. Years later, English chemist Michael Faraday would pioneer the first practical applications for the capacitor in trying to store unused electrons from his experiments. This led to the first usable capacitor, made from large oil barrels. Faraday's progress with capacitors is what eventually enabled us to deliver electric power over great distances. As a result of Faraday's achievements in the field of electricity, the unit of measurement for capacitors, or capacitance, became known as the farad [1, 2].

This means that the principle that electrical energy can be stored in a charged capacitor was known since 1745; at a voltage difference, V, established between the plates accommodating charges +q and –q, the stored energy is $\frac{1}{2} CV^2$ or $\frac{1}{2} QV$, where Q is the electrical charge, V is the applied voltage and C is the capacitance Q/V.

The utilization of this principle to store electrical energy in large amounts for practical purposes, as in a capacitor or battery of capacitors seems to have been first proposed and claimed as an original development in the patent granted to Becker in 1957 [3]. The patent

described electrical energy storage by means of the charge held in the interfacial double layer at a porous carbon material perfused with an aqueous electrolyte. The principle involved was charging of capacitance, C_{dl}, of the double layer, which arises at all solid/electrolyte interfaces, such as metal, semi-conductor, and colloid surfaces (and also at the phase boundary between two immiscible electrolyte solutions [4].

Carbon is an element almost uniquely suited for fabrication of electrochemical capacitors of the double-layer type. It exists in several, well-known allotropic forms, i.e., diamond, the fullerences, and graphite; the latter and glassy carbon can be generated in the form of high-area fibers of felts. Amorphous carbons and carbon black are available as high specific-area powders. The fiber or felt materials are particularly convenient for formation of electrode structures having good mechanical integrity, while the high-area powders are more difficult to handle. However, glassy carbon, graphite, and carbon black materials are convenient for forming high-area electrode structures, often on a support matrix. From an electrochemical point of view, carbon is relatively, though not entirely, unreactive and thus has a potential voltage range of almost ideal polarizability, approaching 1.0 V in aqueous solution and possibly up to 3.5 V in nonaqueous media.

After Becker, the Sohio Corporation in Cleveland, Ohio, also utilized the double-layer capacitance of high-area carbon materials, but in a nonaqueous solvent containing a dissolved tetraalkylammonium salt electrolyte. Such systems provide higher operating voltage (3.4 - 4.0 V) owing to the larger decomposition voltage of nonaqueous electrolytes than those for aqueous ones. Thus they can accommodate higher charge densities and provide larger specific energy storage since the storable energy increases with the square of the voltage attainable on charge.

A different principle was utilized and developed in 1975 onward up to 1981 by Conway [5] in Ottawa, under contract with Continental group. This was based on the concept of D. Craig that was developed at Hooker Corp. Here, in one type of system, the large, so-called "pseudocapacitance" C_{ϕ}, which is associated with the potential dependence to the extentd of electrochemical adsorption of *H* or monolayer levels of electrodeposition of some base metals (Pb, Bi, Cu) at Pt or Au was used [6] as a basic for an energy-storing capacitor. In another type of system, the pseudocapacitance associated with solid oxide redox systems was used, especially that developed over some 1.4 V (practical range 1.2 V) in aqueous H_2SO_4 at RuO_2

films [7] This system approaches almost ideal capacitive behaviour, with a large degree of reversibility between charge and discharge, and multiple cyclability over some 10^5 cycles.

Pseudocapacitance arises whenever, for thermodynamic reasons, there is some continuous dependence of a charge, q, passed faradaically in oxidation or reduction, upon the electrode potential, V. Thus, a derivative *dq/dV* can arise that corresponds to a pseudocapacitance that is directly measurable, or utilizable, as a capacitance.

The large capacitances (on the order of several or more farads per gram) that can be developed with the RuO_2 film system and also with the carbon double-layer-type capacitors led to the terms “supercapacitors” or “ultracapacitor” being coined, respectively, for these two types of high specific capacitance devices. Recently it has been suggested that the more general term “electrochemical capacitors” be used to refer to these systems [6]. However, this name should not be confused with “electrolytic capacitor,” the latter term referring to the well-known, moderately high-capacitance device (on the order of tens of millifarads) that is based on a thin-film oxide dielectric formed electrolytically with a gel electrolyte on such metals as Ta, Zr, Ti, or Al.

The key practical factor that allows very high capacitances, on the order of farads or tens of farads rather than millifarads, to be achieved in a small volume, say $1cm^3$, is the utilization of high-area materials such as activated porous carbons for which real areas are up to 1000 to 2000 $m^2\ g^{-1}$. Similarly, with the RuO_2 pseudocapacitance system, the material, which is a hydrous oxide, has a quasi-3-dimensional, electronically conducting structure, giving accessibility to protons and electrons [7] that are involved in two or three successive, reversible oxidation or reduction steps in charge or discharge, respectively. The continuous dependence of the extents of oxidation or reduction on electrode potential (over 1.4 V), with corresponding passage of charge, leads to the high specific redox pseudocapacitance of this material [8], which is usually coupled with an appreciable double-layer capacitance component.

The use of high-area carbon or oxide redox systems has led to the commercial production of practical high-capacitance electrochemical capacitor devices such as that developed (the Gold Capacitor) by Matsushita Electric Industrial Co. (Osaka, Japan) and by Pinnacle Research; the latter has been developed mainly for military applications. The commercial products are designed to provide standby power for random access memory (RAM) devices or telephone equipment, as power sources for operating activators, and as elements for long time-constant circuits, etc.

An attractive technology employing RuO_2 in a thin film applied to a Nafion membrane, or a powder treated with Nafion, has been developed by Giner, Inc. (Waltham, Massachusetts) and gives high specific capacitance. The design avoids a liquid electrolyte and is analogous to membrane electrolyte fuel cell electrodes. Recent opportunities for the use and development of large scale capacitors arise from the possibility of using them in hybrid configuration with secondary batteries in electric vehicle power systems.

1.1.2 Some definitions and working principles of a Capacitor

In an electronic circuit, a capacitor is represented like shown in Fig. 1.2:

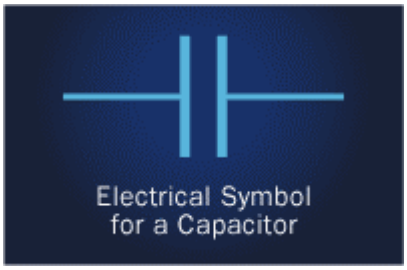

Fig. 1.2 Electrical symbol representation of a capacitor.

When a capacitor connected to a battery, here's what happens:

- The plate on the capacitor that attaches to the negative terminal of the battery accepts electrons that the battery is producing.
- The plate on the capacitor that attaches to the positive terminal of the battery looses electrons to the battery.

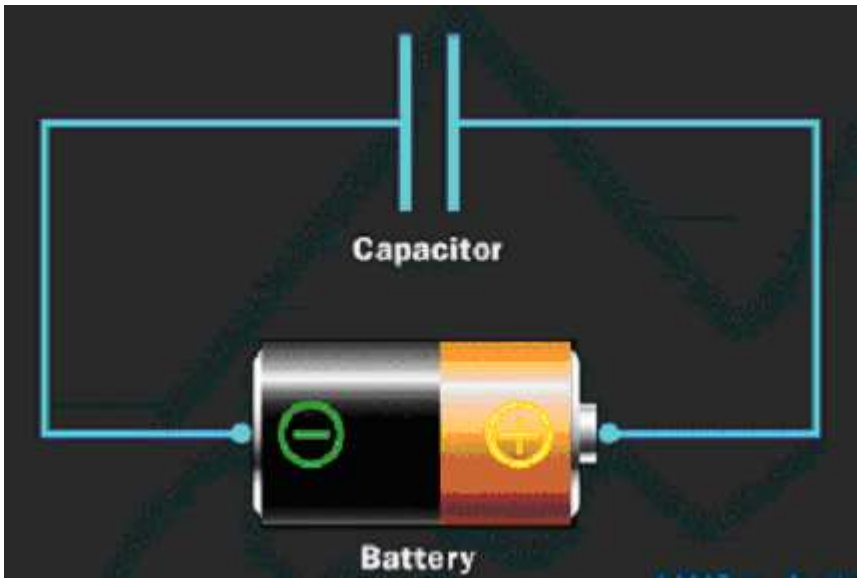

Fig. 1.3 A model showing when a capacitor is connected with a battery.

Once it's charged, the capacitor has the same voltage as the battery (1.5 volts on the battery means 1.5 volts on the capacitor). For a small capacitor, the capacity is small. But large capacitors can hold quite a bit of charge. One can find capacitors as big as soda cans that hold enough charge to light a flashlight bulb for a minute or more.

Even nature shows the capacitor at work in the form of lightning. One plate is the cloud, the other plate is the ground and the lightning is the charge releasing between these two "plates." Obviously, in a capacitor that large, you can hold a huge amount of charge!

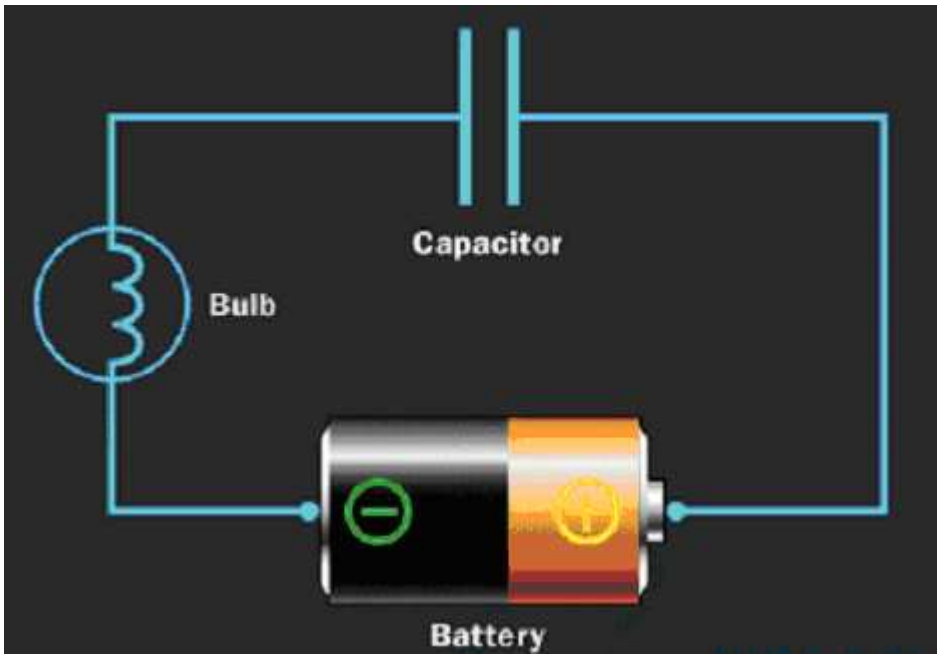

Fig. 1.4 Demonstration of the energy generating principle when a battery is connected to a capacitor.

Here are a battery, a light bulb and a capacitor. If the capacitor is pretty big, what one will notice is that, when the battery is connected, the light bulb will light up as current flows from the battery to the capacitor to charge it up. The bulb will get progressively dimmer and finally go out once the capacitor reaches its capacity. If then the battery is removed and replaced with a wire, current will flow from one plate of the capacitor to the other. The bulb will light initially and then dim as the capacitor discharges, until it is completely out.

One way to visualize the action of a capacitor is to imagine it as a water tower hooked to a pipe. A water tower "stores" water pressure -- when the water system pumps produce more water than a town needs, the excess is stored in the water tower. Then, at times of high demand, the excess water flows out of the tower to keep the pressure up. A capacitor stores electrons in the same way and can then release them later.

1.2 What are supercapacitors and batteries?

1.2.1 Supercapacitors or electrochemical capacitors (ECs)

1.2.1.1 Definitions and working principles:

A Supercapacitor or also called an electrochemical capacitor [1] is a device that stores electrical energy in the electrical double layer of a high-surface-area that forms at the interface between an electrolyte and an electronic conductor electrode. The term applies to charged carbon-carbon systems as well as carbon-battery electrode and conducting polymer electrode combinations sometimes called ultracapacitors, supercapacitors, or hybrid capacitors.

New potential applications for ECs include the portable electronic device market, the power quality market, due particularly to distributed generation, and low-emission hybrid cars, buses, and trucks.

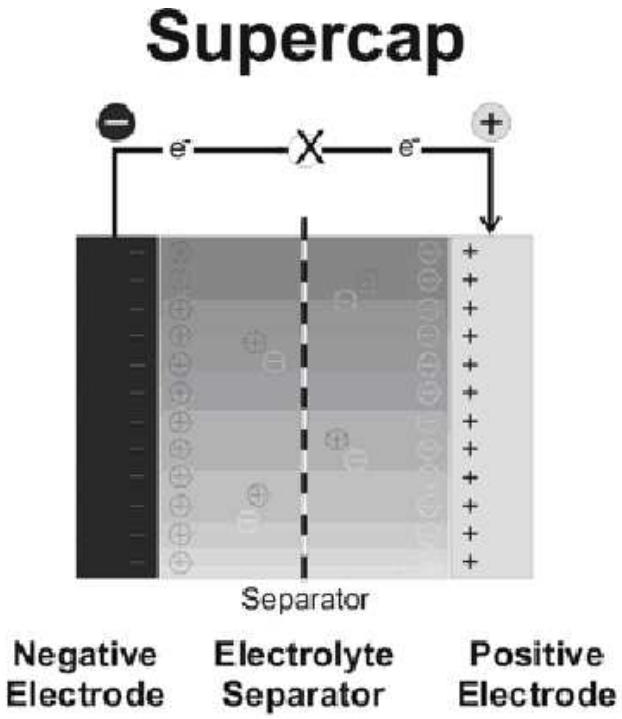

Fig. 1.5 Representation of an electrochemical capacitor (supercapacitor), illustrating the energy storage in the electric double layers at the electrode-electrolyte interfaces.

In electrochemical capacitors (or supercapacitors), energy may not be delivered via redox reactions and, thus the use of the terms anode and cathode may not be appropriate but are in common usage. By orientation of electrolyte ions at the electroode/electrolyte interface, so-called electrical double layers (EDLs) are formed and released, which results in a

parallel movement of electrons in the external wire, that is, in the energy-delivering process.

In a way, a capacitor is a little like a battery, although they work in completely different ways, capacitors and batteries both store electrical energy. Inside the battery, chemical reactions produce electrons on one terminal and absorb electrons on the other terminal. A capacitor is much simpler than a battery, as it can't produce new electrons -- it only stores them. Inside the capacitor, the terminals connect to two metal plates separated by a non-conducting substance, or dielectric. In theory, the dielectric can be any non-conductive substance. However, for practical applications, specific materials are used that best suit the capacitor's function. The dielectric dictates what kind of capacitor it is and for what it is best suited. Depending on the size and type of dielectric, some capacitors are better for high frequency uses, while some are better for high voltage applications. Capacitors can be manufactured to serve any purpose, from the smallest plastic capacitor in your calculator, to an ultra capacitor that can power a commuter bus.

1.2.1.2 Characteristics of the electrical double layer

When an electrode, that is, an electronic conductor, is immersed into an electrolyte solution, that is, an ionic conductor, there is a spontaneous organization of charges at the surface of the electrode and in the electrolyte facing the electrode. This EDL forms at the electrode-electrolyte interface with one layer at the surface inside the conductor and the other layer in the electrolyte as depicted in Fig. 1.6. The two charged layers are considered to behave as a physical capacitor, with the charges in the solution and in the conductor separated by a distance of the order of molecular dimensions. The characteristics of the EDL depend on the electrode surface structure, the composition of the electrolyte, and the potential field between the charges at the interface. Depending on the surface charge of the electrode materials, positive or negative ions from the electrolyte form the solution part of the EDL at the interface between the electrode and the electrolyte. A simplified structure is shown in Fig. 1.6A for the case of a negatively charged electrode surface. According to this simple Helmholtz model, the charges are concentrated on each side of the electrode surface. A more complex model of the EDL structure in Fig. 1.6B takes into account the different sizes of the ions and their reactivity with the surface. The outer Helmholtz plane (OHP) refers to the distance of closest approach of nonspecifically adsorbed ions (generally cations) in solution. Cations that populate the OHP are usually solvated and thus are generally larger than the less solvated anions. The interactions of the

ions of the OHP with the surface charge have the character of coulombic interactions. The inner Helmholtz plane (IHP) refers to the distance of closest approach of specifically adsorbed ions (generally anions) and/or adsorbed solvent molecules to the electrode surface. These adsorption processes are determined by chemical affinities of the ions to the electrode surface and the field strength in the EDL [1,8].

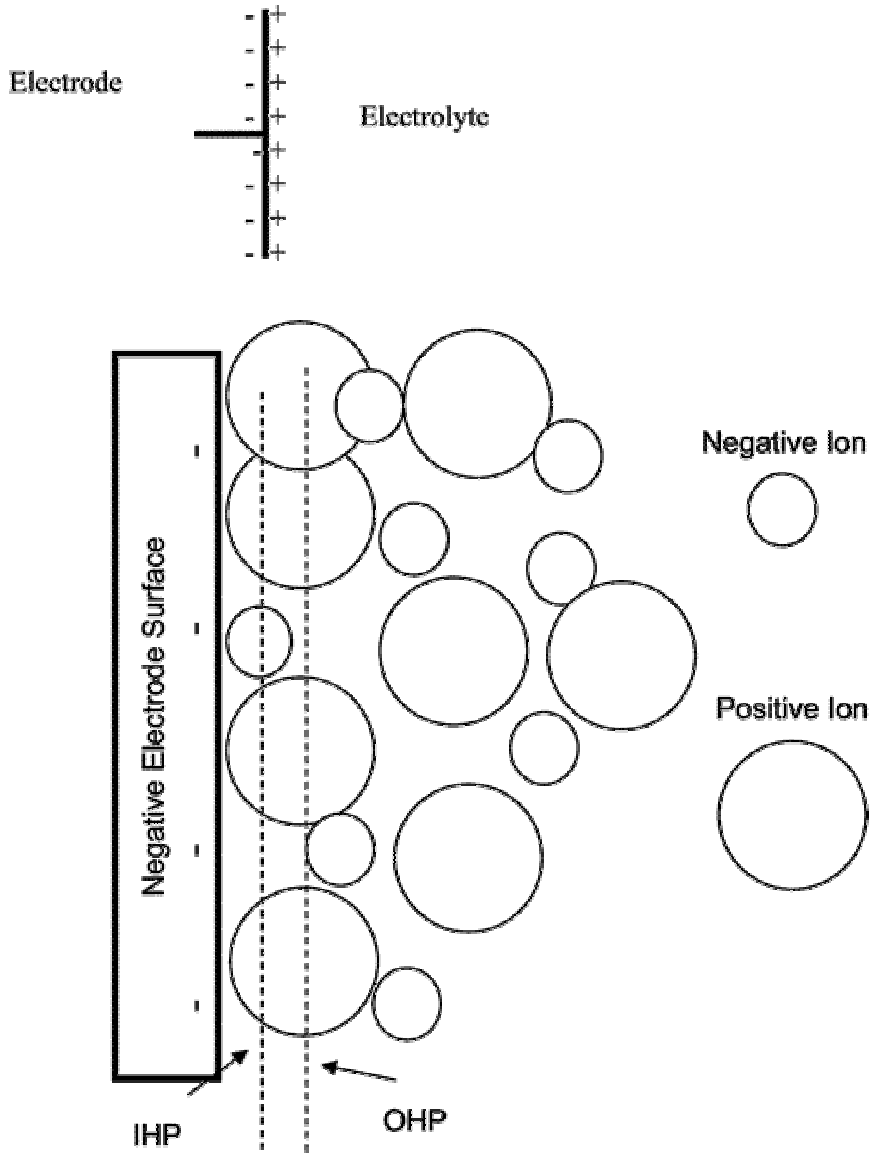

Fig. 1.6 (A, top) Simple Helmholtz model of the electrical double layer. It is essentially a picture of a conventional capacitor. (B, bottom) Depiction of the electrical double layer at the surface of the negative electrode showing the outer Helmholtz plane (OHP) and the inner Helmholtz plane (IHP). The inner Helmholtz plane (IHP) refers to the distance of closest approach of specifically adsorbed ions and solvent molecules to the electrode surface. The outer Helmholtz plane (OHP) refers to the distance of ions, which are oriented at the interface by coulomb forces [1].

The double layer at the electrode surface forms and relaxes almost instantaneously. It has a time constant, or time of formation, of ~10^{-8} s. Therefore, the structure of the double layer has the capability to respond rapidly to potential changes in the same time frame. The process involves only a charge rearrangement, not a chemical reaction. This rapid response to change is in contrast to the situation with the redox electrode reactions in batteries and fuel cells. The time constant for the redox reactions is much slower and in the range of 10^{-2}-10^{-4} s related to the impedance of the reaction. The redox reactions contribute to "polarization capacitance" associated with the electrode reactions. The other main difference between supercapacitors and batteries and fuel cells is the reversibility (short time constant) of the EDL process compared to the longer time constant of the redox reactions and the stress from detrimental side reactions, which reduce the cycle life and long-term stability of the device. Whereas cycle life and stability of the double layer electrochemical capacitor can easily exceed 1 million cycles, battery electrodes can reach this level only if charged and discharged at a low depth of discharge.

When carbons are placed in an electrolyte, they generally assume a voltage near the zero point of charge of the EDL. In aqueous solutions, this is near 0 V versus hydrogen. By applying an external voltage, many more additional ions and electrons can be moved to the double layer, increasing the capacitance (C = charge per applied voltage, C = Q/U). As a rule of thumb, carbons and metals typically have a double-layer capacitance in the range of 10 - 40 F/cm^2. The exact values depend mainly on the voltage and the extent of participation of the IHP in the electrical double layer. A high-surface-area carbon electrode can yield a capacitance of ~4 F/g.

1.2.1.3 Electrochemical capacitors operation

As noted above, electrochemical capacitors are closely related to batteries. The simple circuit shown illustrates their basic operation. Here, C_a and C_c are the double-layer capacitances of the anode and cathode, respectively. For capacitors in series,

$$\frac{1}{C} = \frac{1}{C_a} + \frac{1}{C_c} \tag{1.1}$$

If $C_a = C_c$, as would be expected for an ultracapacitor, then

$$C = 1/2C_a \tag{1.2}$$

High-surface-area carbon is the material of choice, as it combines a large surface area wetted by the electrolyte, high electronic conductivity, and chemical and electrochemical stabilities with low cost. The capacitance of these devices can be orders of magnitude larger than those of conventional dry and electrolytic capacitors [9]. The voltage for electrochemical capacitors with aqueous electrolytes is ~1 V, limited by the voltage stability of the electrolyte. By switching to an organic-based electrolyte, voltages of up to 2.7 V can be found in practice. However, the organic electrolytes have lower double-layer capacitance and poorer conductivity. Because the energy storage is given by:

$$E = {}^1/_2QV^2, \tag{1.3}$$

the higher voltage permitted by an organic electrolyte significantly increases the energy storage capability of the EC. Because the resistivity is ~100 times larger than for aqueous electrolytes, the time constant for response to a large pulse is slower for the nonaqueous electrolyte-based ECs.

The charge-discharge of a symmetric EC composed of two carbon electrodes with approximately the same mass immersed in an aqueous or nonaqueous electrolyte is shown in Fig. 1.7. With zero applied charge Q, both electrodes of a cell are at the same voltage. The potential of the electrodes increases in opposite directions during charge, as each has approximately the same capacitance. Maximum cell operating voltage is reached when one of the electrodes reaches the stability limit of the electrolyte.

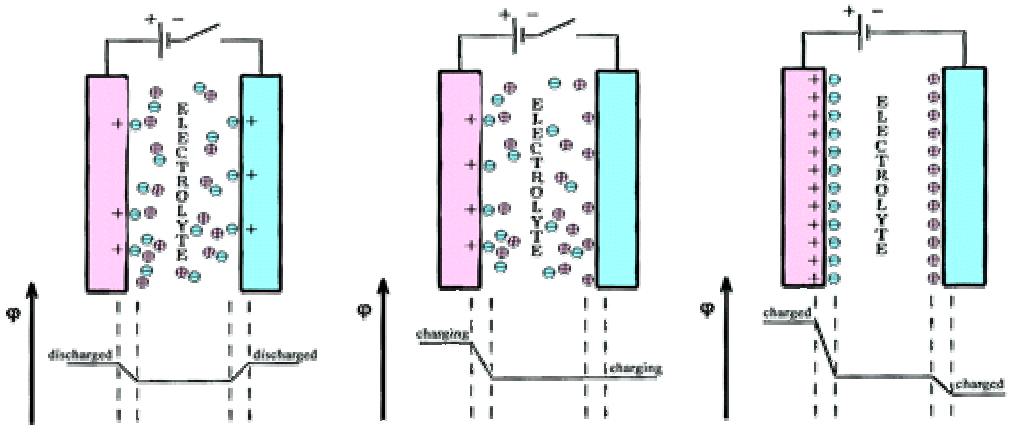

Fig. 1.7 Depiction of the charging process of a symmetric capacitor composed of two carbon electrodes with approximately the same mass immersed in an aqueous electrolyte showing the level of potential changes when there is no charging and where there is a charging process applied.

The asymmetric type of EC incorporates a battery electrode as one of the electrodes. The battery electrode has a capacitance associated with the redox battery reaction of ~10 times the capacitance of the electrical double layer. For instance, if the nickel battery cathode is substituted for the cathode in a symmetric capacitor, for example, NiOOH for carbon, then substituting $C_c = 10C_a$ in eq 1.1, the capacitance of the EC is essentially doubled.

$$\frac{1}{C} = \frac{1}{C_a} + \frac{1}{10C_a} \tag{1.4}$$

which means then, $C \approx C_a$

This asymmetric type of EC is often termed a "hybrid" capacitor. The typical discharge curve for this hybrid EC is shown in Fig. 1.8. Because the battery electrode has a capacity of 3-10 times that of the double-layer electrode, it remains at an invariant voltage during charge and discharge. As a result, the discharge voltage of the hybrid capacitor decreases more slowly than that of the carbon-carbon EDL capacitor.

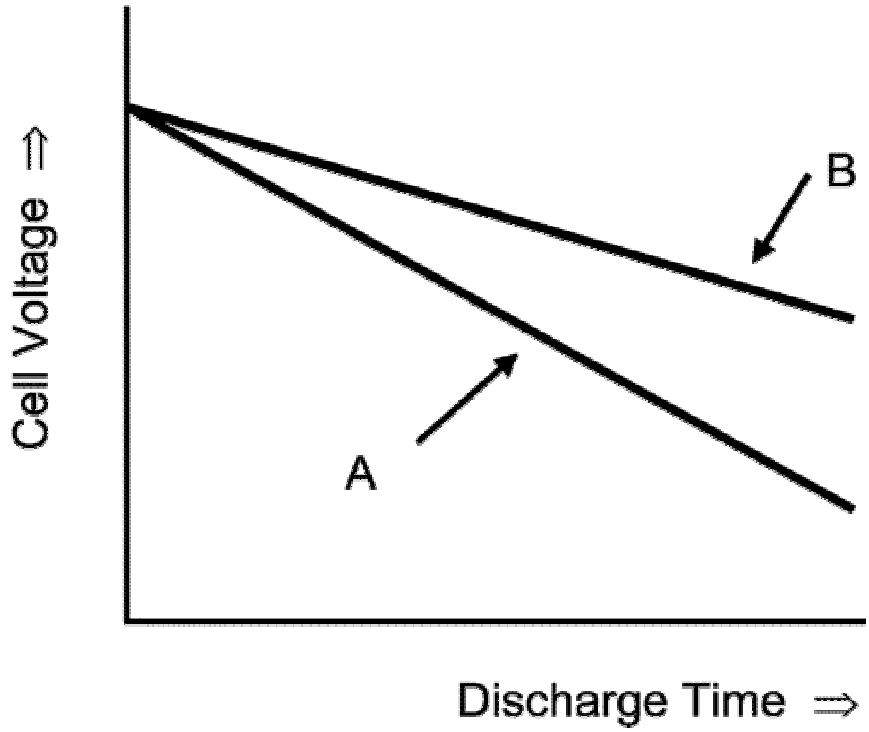

Fig. 1.8 Operation principle of an EC in the discharged state, during charging, and in the charged state: (A) for a symmetric construction and (B) for an asymmetric construction [8].

In some cases, the kinetics of the redox charge-discharge reactions can proceed almost as quickly and reversibly as EDL charging. Thin film redox electrodes, based on the lithium intercalation/insertion principle such as $Li_4Ti_5O_{12}$, exhibit high reversibility and fast kinetics. The RuO_2 materials deposited on carbon show "pseudo-capacitive" charge-discharge behavior as do polymeric materials such as polyaniline, polypyrrole, and polydiaminoanthraquinone (DAAQ). These have facile kinetics and have shown high capacitance and long life. The insertion of anions and cations into their structure can yield capacitances of up to 200 $\mu F/cm^2$ and, moreover, they can be easily fabricated as thin films.

1.2.2 Batteries (Some important definitions for batteries)

A battery is one or more electrically connected electrochemical cells having terminals/contacts to supply electrical energy.

A primary battery is a cell, or group of cells, for the generation of electrical energy intended to be used until exhausted and then discarded. Primary batteries are assembled in the charged state; discharge is the primary process during operation.

A secondary battery is a cell or group of cells for the generation of electrical energy in which the cell, after being discharged, may be restored to its original charged condition by an electric current flowing in the direction opposite to the flow of current when the cell was discharged. Other terms for this type of battery are rechargeable battery or accumulator. As secondary batteries are usually assembled in the discharged state, they have to be charged first before they can undergo discharge in a secondary process.

The anode is the negative electrode of a cell associated with oxidative chemical reactions that release electrons into the external circuit.

The cathode is the positive electrode of a cell associated with reductive chemical reactions that gain electrons from the external circuit.

Active mass is the material that generates electrical current by means of a chemical reaction within the battery.

An electrolyte is a material that provides pure ionic conductivity between the positive and negative electrodes of a cell.

A separator is a physical barrier between the positive and negative electrodes incorporated into most cell designs to prevent electrical shorting. The separator can be a gelled electrolyte or a microporous plastic film or other porous inert material filled with electrolyte. Separators must be permeable to the ions and inert in the battery environment.

Open-circuit voltage is the voltage across the terminals of a cell or battery when no external current flows. It is usually close to the thermodynamic voltage of the system.

Closed-circuit voltage is the voltage of a cell or battery when the battery is producing current into the external circuit.

Discharge is an operation in which a battery delivers electrical energy to an external load.

Charge is an operation in which the battery is restored to its original charged condition by reversal of the current flow.

Internal resistance or impedance is the resistance or impedance that a battery or cell offers to current flow.

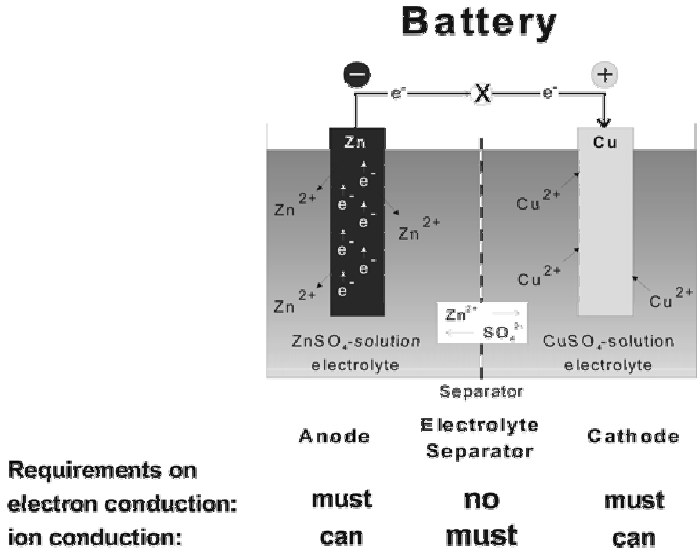

Fig. 1.9 Representation of a battery (Daniel cell) showing the key features of battery operation and the requirements on electron and ion conduction [10].

In batteries, electrical energy is generated by conversion of chemical energy via redox reactions at the anode and cathode. As reactions at the anode usually take place at lower electrode potentials than at the cathode, the terms negative and positive electrode (indicated as minus and plus poles) are used. The more negative electrode is designated the anode, whereas the cathode is the more positive one. Unlike fuel cells, batteries are closed systems, with the anode and cathode being the charge-transfer medium and taking an active role in the redox reaction as "active masses". In other words, energy storage and conversion occur in the same compartment. Fuel cells are open systems where the anode and cathode are just charge-transfer media and the active masses undergoing the redox reaction are delivered from outside the cell, either from the environment, for example, oxygen from air, or from a tank, for example, fuels such as hydrogen and hydrocarbons. Energy storage (in the tank) and energy conversion (in the fuel cell) are thus locally separated [10]

In comparison to supercapacitors and fuel cells, batteries have found by far the most application markets and have an established market position. Whereas supercapacitors have found markets as memory protection in several electronic devices, fuel cells are basically still in the development stage and are searching to find a "killer application" that allows their penetration into the market. Fuel cells established their usefulness in space applications with the advent of the Gemini and Apollo space programs. The most promising future markets for fuel cells and supercapacitors are in the same application sector as batteries. In other words, supercapacitor and fuel cell development aim to compete with, or even to replace, batteries in several application areas. Thus, fuel cells, which originally were intended to replace combustion engines and combustion power sources due to possible higher energy conversion efficiencies and lower environmental impacts, are now under development to replace batteries to power cellular telephones and notebook computers and for stationary energy storage. The motivation for fuel cells to enter the battery market is simple. Fuel cells cannot compete today with combustion engines and gas/steam turbines because of much higher costs, inferior power and energy performance, and insufficient durability and lifetime. With operation times of typically <3000 h and, at least to an order of magnitude, similar costs, batteries are less strong competitors for fuel cells.

1.2.3 Similarities and differences between supercapacitors and batteries for storing electrical energy.

1.2.3.1 Energy storage systems

A modern technological society demands the use and storage of energy on a major scale, employing large and small systems for that purpose. Energy stored as potential energy is involved in hydroelectric systems through the hydrostatic "head" of water behind dams; it is also stored in a potential sense in fuels (e.g., coal, oil and cryogenic hydrogen) and becomes available, albeit with rather poor efficiency, through combustion utilizing steam-piston, steam turbine, and internal combustion engines of various kinds as energy transduction devices. Energy may also be stored as rotational kinetic energy in flywheels.

Electrical energy can be stored in two fundamentally different ways:

1) indirectly in batteries as potential available chemical energy requiring Faradaic oxidation and reduction of the electrochemically active reagents to release charges that can perform electrical work when they flow between two electrodes having different electrode potentials (i.e., across the voltage difference between the poles of battery cells; and
2) directly in an electrostatic way, as negative and positive electric charges on the plates of a capacitor, a process known as non-Faradaic electrical storage.

The efficiency of these two modes of storing electrical energy is usually substantially larger than that of fuel combustion systems, which are limited by thermodynamic Carnot cycle considerations while electrochemical systems usually involve more reversible processes, with direct conversion of potentially available chemical energy to free energy, ΔG.

1.2.3.2 Modes of electrical energy storage by capacitors and batteries

An important difference arises between the reversibility of Faradaic and non-Faradaic systems mentioned above. In energy storage by capacitors, only an excess and deficiency of electron charges on the capacitor plates have to be established on charge and the reverse on discharge; no chemical changes are involved. However, with storage of electrochemical energy in battery cells through Faradaic reactions, chemical interconversions of the anode

and cathode materials must take place, usually with phase changes. Although the overall energy change can be conducted in a relatively reversible thermodynamic way, the charge and discharge processes in a battery often involve irreversibility in interconversion of the chemical energy reagents; thus the cycle life of battery cells is usually restricted to one thousand to several thousand discharge and recharge cycles, depending on the type of battery. By contrast, a hardware capacitor has an almost unlimited cyclability since no chemical and phase changes are involved in its charging and discharging processes.

Ordinary capacitors have, however, a very small amount of charge storage unless they are large, i.e., they have low energy density for electrical energy storage. However, charged electrode/electrolyte solution interfaces contain double layers that have capacitances of about 16 to 50 $\mu F\ cm^{-2}$; hence, with the sufficiently large accessible electrode areas that are realizable with high-area carbon powders, very large double layer capacitances on the order of 10 to 100 F per gram can be achieved. It is the practical realization of the possibility in recent years that has led to the relatively new field of electrochemical capacitors. These are now actively progressing as energy storage devices to complement batteries [11].

Because the charging and discharging of such double-layer capacitors involves no chemical phase and composition changes which, in batteries, lead to materials irreversibility, such capacitors have a high degree of recyclability, on the order of 10^5 to 10^6 times. Only electrons need to be moved to and from the electrode surfaces through the external circuit, and cations and anions of the electrolyte transported within the electrolyte to the charged interfaces. It is for these reasons that capacitor charging and discharging processes are highly reversible.

In the cyclic voltammetry of such systems, the charging and discharging voltammograms are almost mirror images of one another, while for battery processes they are rarely of this kind. This is a major and characteristic difference between battery and capacitor electrical energy storage systems.

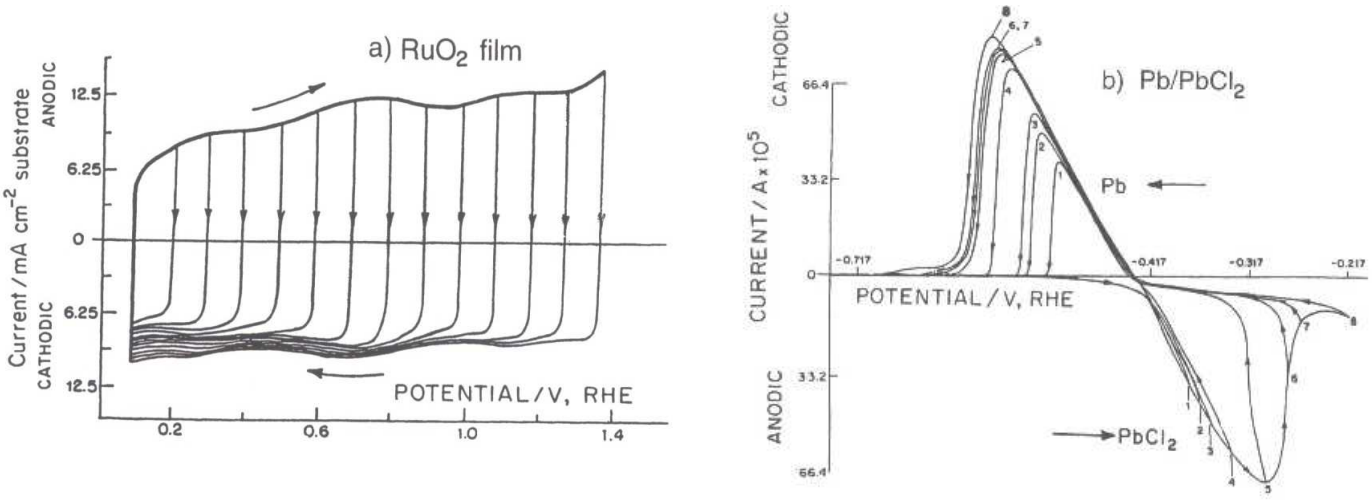

Fig. 1.10 (a) Cyclic Voltamogram for RuO_2 in 1 M aqueous H_2SO_4 at RT showing mirror-image symmetry and responses to successive switching along the scanned potential range. (b). Cyclic Voltamogram for Pb-$PbCl_2$ battery electrode showing typical irreversibility arising with 3-dimentional materials undergoing chemical phase changes [11].

It must be emphasized at the outset that there has never been an aim or projection of a possible substitution of batteries by supercapacitors; rather, opportunities arise for complementary operation of electrochemical capacitors that are electrically coupled in discharge and recharge with batteries, while other kinds of applications especially favor capacitor-type behavior, e.g., for backup power systems. Also, there are stand-alone opportunities for using multiply rechargeable electrochemical capacitors in a variety of independent functions and technology of batteries are to be found [12].

In the early stages of the development of electrochemical capacitor technology and related fundamental work, there was some confusion in the electrochemical engineering field and at symposia about the differences between properties and operation of a battery and a supercapacitor, and what advantages one might have over the other. Some groups calling the capacitor devices “ultracapacitors” and others “supercapacitors” may have assisted this confusion. The present preferred name, proposed by Burke, is now more scientific and generic, namely “electrochemical capacitors.”

It is therefore important to explain some of the similarities and differences between batteries and electrochemical capacitors in relation to the electrochemical processes that are involved in their discharge and recharge cycling, and in their potential uses as

electrical energy storage devices. In particular, the fundamentally different mechanisms of charge storage that are normally involved will be emphasized, along with the consequent, usually different, relations between the extents of charge accommodated at the electrodes and the electric potential differences (cell voltage) between pairs of electrodes having conjugate, plus/minus, polarities [13, 14].

One of the main and kinetically significant differences between capacitors and batteries is that the electrodes of the later usually undergo substantial phase changes during discharge and recharge, which lead to kinetic and thermodynamic irreversibility. On the other hand, capacitors of the double-layer type require only electrostatic charge accommodation with virtually no phase change, though some small but significant reversible electrostriction of the electrolyte can rise upon charging.

1.2.3.3 Faradaic and non-faradaic processes

There is a general and fundamental difference between the mechanisms of operation of electrochemical capacitors and battery cells: for the double-layer type of capacitor, the charge storage process is non-Faradaic, i.e., ideally no electron transfer takes place across the electrode interface and the storage of electric charge and energy is electrostatic.
In battery-type processes, the essential process is Faradaic, i.e., electron transfer does take place across the doubly layers, with a consequent change of oxidation state, and hence the chemistry of the electroactive materials.
Intermediate situations arise where Faradaic charge transfer occurs, but owing to special thermodynamic conditions that apply, the potential, V, of the electrode is some continuous function of the quantity of charge, q, passed so that a derivative, dq/dV, arises. This is equivalent to and measurable as a capacitance and is designated as a pseudocapacitance.

Non-Faradaic:- the charge accumulation is achieved electrostatically by positive and negative charges residing on two interfaces separated by a vacuum or molecular dielectric (the double layer or, e.g., a film of mica, a space of air or an oxide film, as in electrolyte capacitors)

Faradaic:- the charge storage is achieved by an electron transfer that produces chemical or oxidation state changes in the electroactive materials according to Faraday's laws related to electrode potential. Pseudocapacitance can arise in some cases. The energy storage is indirect and is analogous to that in battery.

Some of the advantages and disadvantages as well as differences and similarities of batteries and electrochemical capacitors are summarized with the tables below [1].

Table 1.1 Perceived Advantages and disadvantages of electrochemical capacitor for storing electrical energy [1].

Advantages	➢ Long cycle life, > 100,000 cycles; some systems up to 10^6 ➢ Good power density [under certain condition, limited by IR or equivalent series resistance (esr) complexity of equivalent circuit] ➢ Simple principle and mode of construction (can employ battery construction technology) ➢ Cheap materials (for aqueous embodiments) ➢ Combines state-of-charge indication, $Q = f(V)$ ➢ Can be combined with rechargeable battery for hybrid applications (electric vehicles)
Disadvantages	➢ Limited energy density ➢ Poor volume energy density ➢ Low working voltages (compared with electrolytics; satisfactory compared with batteries) ➢ Aq. voltage range 0 ~ 1.4 V; nonaq. to 4.5 V. In practice, 3.5 V. ➢ Nonaq. embodiments require pure, H_2O-free materials; more expensive ➢ Requires stacking for high potential operations (electric vehicles) ➢ Hence, good matching of cell units is necessary

Table 1.2 Comparative electrical characteristic of battery and electrochemical capacitor behavior [1].

Battery	Electrochemical capacitor
1. Ideally has single-valued free energies of components	1. Has continuous variation of free energy with degree of conversion of materials or extent of charge held
2. emf is ideally constant with degree of charge and discharge, except for nonthermodynamic incidental effects, or phase changes during discharge	2. Potential is thermodynamically related to state of charge through log [X/1 – X] factor, in a continuous manner for a pseudocapacitor, or directly to Q for a double-layer capacitor
3. Behavior is not capacitive, except in very general sense	3. Behavior is capacitive
4. Irreversibility is usual behavior (materials irreversibility and kinetic irreversibility)	4. High degree of reversibility is common (10^4 – 10^6 cycles with RuO_2 or C double-layer capacitors)
5. Response to linear modulation of potential gives irreversible I vs. V profile with nonconstant currents	5. Response to linear modulation of potential gives more or less constant charging current profile but with some dependence on material
6. Discharge at constant current arises at a more or less constant potential except for intercalation Li batteries	6. Discharge at constant current gives mainly linear decline of potential with time, which is characteristic of a capacitor

Table 1.3 An overall comparison of electrochemical capacitor and battery characteristics [1].

Capacitor	Battery
1. Has intrinsically sloping charge and discharge curve	1. Ideally has constant (thermodynamic) discharge or recharge potential, except for Li intercalation systems
2. Because of (1), has good intrinsic state-of-charge indication	2. Does not have good intrinsic state-of-charge indication except for Li intercalation system
3. Has relatively poor energy density	3. Has moderate or good energy density, depending on equivalent weights and electrode potentials of active materials
4. Has good power density	4. Has relatively poor power density, depending on kinetics
5. Has excellent cyclability or cycle life due to simple addition or withdrawal of charges (in double-layer type)	5. Has less cycle life by a factor of 1/100 ~ 1/1000 due to irreversibility of redox and phase-change processes in three dimensions
6. Has internal IR due to high-area matrix + electrolyte	6. Has internal IR due to electrolyte and active materials
7. Has little or no activation polarization but C may be temperature-dependent	7. Has significant T-dependent activation polarization (Faradaic resistance)
8. Has long lifetime except for corrosion of current collectors, etc	8. Has poorer lifetime due to degradation or reconstruction of active materials
9. Electrolyte conductivity can diminish on charging due to ion adsorption	9. Electrolyte conductivity can decrease or increase on charging, depending on chemistry of cell reactions, e.g., with Pb-acid
10. Can be constructed in bipolar configuration	10. Can be constructed in bipolar configuration

1.2.4 Supercapacitors as a bridge between batteries and ordinary capacitors

Energy-storing supercapacitors have electrical parameters and occupy a functional position between ordinary capacitors and batteries; where the components are used primarily as power sources or reserves. Although they are used to store energy, supercapacitors' characteristics differ fundamentally from those of batteries. They are useful because their parameters exactly complement some of batteries' shortcomings and also the shortcomings of many other power sources. The "super" prefix refers to a supercapacitor's capacitance-value range; it's around three orders of magnitude higher than that of a conventional electrolytic capacitor in a similar package size. A supercapacitor is, however, still a simple capacitor a two-terminal component (usually unpolarized) available in a variety of physical formats from surface-mountable coin cells for the smallest devices, to screw-terminal prismatic or cylindrical cans for the largest [1, 2].

The idea of an energy cache comes into play for many common applications, especially those complementing batteries. Batteries achieve a high level of total energy stored (energy density). The rate at which they can yield this energy is limited, so they have a rather low "power density." You can most usefully express these units, depending on application constraints, as true density - the energy or power per unit volume - or energy/power per unit of weight. Supercapacitors mirror those parameters; they have a fairly low total energy stored (energy density), but they can quickly yield that energy, exhibiting a high power density.

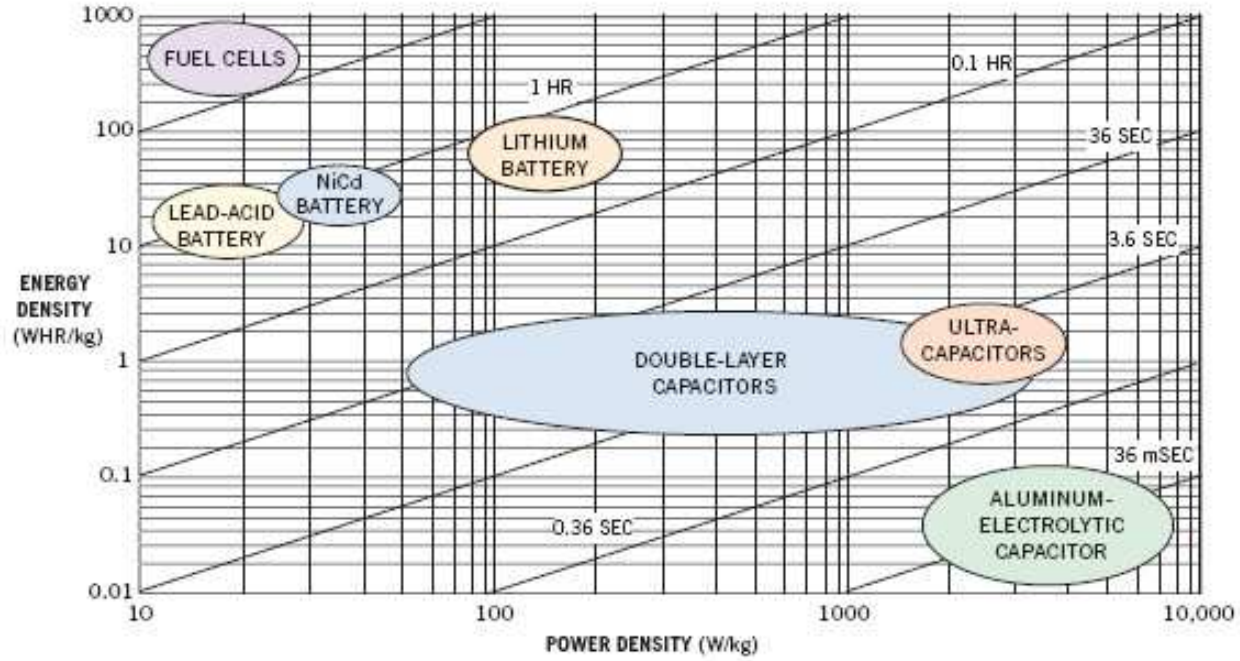

Fig. 1.11 Energy density against power density (Ragone plot): conventional batteries occupy the top-left position of high energy and low power density, and conventional aluminum-electrolytic capacitors occupy the bottom-right position of high power and low energy density, whereas Supercapacitors bridge the space between the conventional batteries and capacitors. Diagonal lines are lines of equal discharge time into a specified load [15].

In the simplest cases, therefore, one can connect battery and supercapacitor in parallel. The supercapacitor floats at the same terminal voltage as the battery. When the load demands a sudden high current peak, it sees a very low supply resistance in the capacitor and a much higher one in the battery, so the charge in the capacitor supplies the current peak. The battery then restores that charge during the period when the load demands a low current.

Virtually all applications employ supercapacitors in the same way: compensating for the shortcomings of a primary power source. In one of the most familiar applications, the memory-maintenance battery on a processor board, the supercapacitor floats on the supply line and provides power to hold up SRAM or other volatile memory in the absence of main system power. In this case, the shortcoming of the power supply is its absence during the critical period. A supercapacitor's advantage over a rechargeable battery cell in this application is that you can treat it as any other component, without the finite life restriction of a battery.

A GSM (Global System for Mobile communications) cellular-phone system typifies a situation in which you supply pulse currents in conjunction with a power source a battery, for example. Due to the bursty nature of the GSM signal, its power demand comprises short pulses of several amps with a much lower current between them. Rather than rate the battery to supply the whole current, you can use a supercapacitor to handle the peaks. Because of their physical dimensions, supercapacitors are not an option for today's handsets. But for the many applications (telemetry, for example) that use GSM transceivers in power- but not space-constrained situations, the combination can raise efficiency.

Moving up the power scale, the automotive environment provides a range of possible applications. In a conventional car, you can use a supercapacitor to assist with engine starting, reducing the "cranking load performance" rating of the main battery. You can also use the devices to provide local, point-of-load support for systems around the car. The dc motor that operates a window lift, for example, might peak at tens of amps (especially if it's stalled). The vehicle's main power system might be perfectly capable of providing that current peak, but if you augment it with a supercapacitor close to the motor, you can reduce the rating-and the weight of power-supply wiring to the subsystem.

Step up again in power level, and you enter a regime in which the key word is "hybrid." One architecture for the "hybrid car" is that of an internal combustion engine driving a generator with an electric drive motor or motors to propel the vehicle. If you design such a system with a supercapacitor energy cache, the supercapacitor can supply the transient loads of starting and acceleration, and regenerative braking can recharge it. Aside from the efficiency of recovering the energy of braking, you would be able to run the internal combustion engine at nearly constant speed and power output. In this mode, I-C engines are at their most efficient; also, under the dynamic loads of acceleration, they emit their highest pollution levels.

Likewise, in traction systems in trains and metro systems, supercapacitors may find further application. The opportunity for a cache on an individual vehicle is obvious, but a "systemwide" possibility also exists.

The term "hybrid" also applies to power-generation systems. Some proposals for future environmentally friendly systems rely heavily on supercapacitor caches to overcome either the primary energy source's inability to supply peak demand (such as fuel cells) or the inherent uneven supply characteristics (such as wind power).

Somewhere in that power spectrum, then, you may find an application for a supercapacitor. You can also partition the spectrum into "standby supply" or "load leveling" (pulse- or peak-load absorbing) uses.

The general process of designing with a supercapacitor begins with working out the energy needed from the device every discharge cycle, together with the knowledge of the acceptable endpoint voltage for correct circuit operation. One then look at the exponential dV/dt curve for the capacitor and the load supplied as well as published graphs of chosen device's available capacitance versus pulse width to arrive at a component value. With typical applications, one won't see the discharge curve at all. The initial drop due to the supercapacitor's ESR, as the capacitor begins to supply the pulse load, is much more significant; the actual capacitance value is somewhat irrelevant.

The basics of a supercapacitor are no different from those of any other capacitor: Capacitance varies directly with the area of the parallel plates and inversely with the distance between the plates of the capacitor. Supercapacitors achieve their very high values by maximizing the effective area of the "plates" in their structures and by reducing the effective separation between the plates to molecular dimensions. Most commercial devices employ carbon as an electrode material, exploiting that element's well-known ability to present a very high surface area in finely divided, granulated, or powder forms.

Electrical contacts comprise two carbon (cloth or powder) electrodes. You place a separator material between them that carries an electrolyte that readily provides high concentrations of mobile ions. When you place a potential across the resulting "sandwich," ions migrate toward charges of opposite polarity on the carbon electrodes, as shown in Fig. 1.12. The phase boundary between the electrode and the electrolyte is the dielectric layer of the capacitor and is only a few nanometres thick. Across this phase boundary are two layers of excess charge and opposite polarity, called the electrochemical double layer. The double layer constitutes a capacitor. This structure is mirrored on the other side of the separator layer but with reversed polarities. Internally, therefore, the structure is actually two capacitors that are series-connected via the conducting electrolyte.

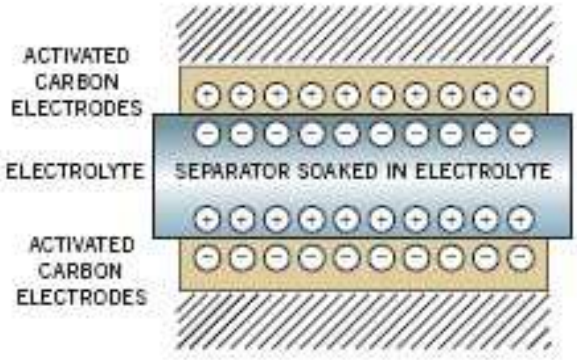

Fig. 1.12 Showing that when a potential is placed on the terminals of a double-layer electrochemical capacitor, charge accumulates on the surface of the carbon electrodes and is balanced by ions drawn from the separating electrolyte.

As an electrochemical device, the supercapacitor has a significant ESR at dc; this parameter is key, and manufacturers are constantly striving to reduce it. Manufacturers often quote supercapacitor ESR at, say, 1 kHz, where it is at a minimum but may have little useful capacitance. You need to carefully interpret the data sheet to derive both capacitance and ESR at the exact point you propose to operate the component.

In designing in a supercapacitor, it is important to note that its main parameters vary with environmental and circuit conditions in a way that those of an electronic capacitor do not.

Most supercapacitors' construction enforces an operating voltage limit of around 2.3V, which some manufacturers are working to extend. If one wants the design to operate at higher voltage, you must stack the devices in series and, as with any other capacitor, the effective capacitance decreases accordingly. Maintaining the same capacitance at higher voltage therefore requires an array of (individually) larger value devices or a series/parallel array; some manufacturers provide pre-packaged arrays of supercapacitors in a single housing to achieve higher ratings. Some units, however, are rated for operation at, say, 3 or 4V. This exercise often involves simple derating, which trades life for the higher voltage. It is useful for applications such as toys, whose reduced lifetime is unlikely to be a constraint.

A completely separate strand of supercapacitor research is actively investigating the use of conductive polymers as a charge-storage media. By storing ions in the bulk of polymer materials, rather than on a surface, researchers believe that you can achieve even higher

capacitance values. In a manner somewhat analogous to doping in semiconductor materials, polymers can provide sites to accept ions within the organic molecules that comprise the polymers; conduction mechanisms roughly analogous to semiconductor electron/hole propagation provide the conductivity. Researchers are exploring numerous mechanisms and materials, including some hybrids of polymer and existing supercapacitor techniques, such as the use of carbon nanotubes together with the polymer polypyrrole. Among the challenges this technology faces is the ability to achieve commercially useful lifetimes. However, the largest supercapacitor charge-storage capacities yet reported have been in polymer systems [16, 17].

[1] B. E. Conway, Electrochemical Supercapacitors: Scientific Fundamentals and Technological Applications, Kluwer Academic, New York (1999)

[2] Williams; William J. Beaty http://amasci.com/ele-edu.html.

[3] H. E. Becker, U.S Patent 2,800,616 (to General Electronic Co.) (1957)

[4] Z. Samec, J. Elecroanal. Chem., **103**, 1(1979)

[5] B. E. Conway, J. Electrochem. Soc., **138**, 1539 (1991)

[6] B.E. Conway and H. A. Kozlowska, Acct. Chem. Res., **14**, 49 (1981)

[7] R. Galizzioli, F, Tantardini and S. Trasatti, J. Appl. Electrochem., **4**, 57 (1974)

[8] B. E. Conway, in Proc. Symp. on Electrochemical Capacitors, F. M. Delnick and M. Tomkiewicz, eds., vol. 95-29, 15, Electrochem. Soc., Pennington, N.J. (1996)

[9] D. Linden, ed., Handbook of Batteries, 2nd ed., McGraw-Hill, New York (1995).

[10] H. A. Kiehne, Battery Technology Handbook, Marcel Dekker, New York (1989)

[11] B. E. Conway and P. L. Bourgault, Can. J. Chem., **37**, 298 (1959).

[12] B. V. Tilak and B. E. Conway, Electrochem. Acta, **21**, 745 (1976).

[13] D. A. Harrington and B. E. Conway, J. Electroanal. Chem**., 221**, 1 (1987)

[14] W. G. Pell, T. –C. Liu and B. E. Conway, Electrochim. Acta, **42**, 3541 (1997)

[15] G. Prophet http://www.edn.com/article/CA268379.html?text=supercaps

[16] J. Y. Kim, I. J. Chung, J. Electrochem. Soc. **149** (10) A1376-A1380 (2002)

[17] A. Burke, J. Power Sources, **91**, 37 (2000)

Chapter 2:

2. General theoretical backgrounds to experimental methods used and related terms on this work

2.1. X-Ray powder diffraction

X-rays are electromagnetic radiation with photon energies in the range of 100 eV-100 keV. For diffraction applications, only short wavelength x-rays in the range of a few angstroms to 0.1 angstrom (1 keV - 120 keV) are used. Because the wavelength of x-rays is comparable to the size of atoms, they are ideally suited for probing the structural arrangement in a wide range of materials. The energetic x-rays can penetrate deep into the materials and provide information about the bulk structure.

In laboratory x-ray instruments, x-rays are normally generated in x-ray tubes by a focused electron beam bombarding a solid target. Common targets used include Cu and Mo, which emit 8 keV and 14 keV x-rays with corresponding wavelengths of 1.54 Å and 0.8 Å, respectively. Diffracted waves from different atoms can interfere with each other. If the atoms are arranged periodically as in crystals, the diffracted waves will consist of sharp interference peaks, which contain the information of the atomic arrangement. The peaks in an x-ray diffraction pattern are directly related to the atomic distances through the Bragg's law, which is shown in Fig. 2.1, where d is the distance between the lattice plane, λ is the wavelength of the x-ray and n is an integer representing the order of the diffraction peak.

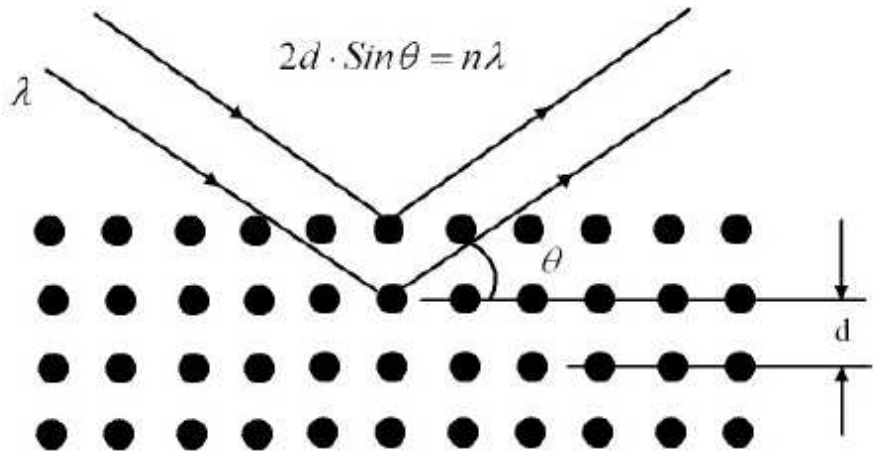

Fig. 2.1 Bragg's Law

Powder XRD (X-ray Diffraction) is perhaps the most widely used x-ray diffraction technique for characterizing materials. The term 'powder' really means that the crystalline domains are randomly oriented in the sample. The positions and the intensities of the peaks are used for identifying the structure, lattice constant and grain size of the material. Detailed discussions about XRD can be found in a lot of books and journal articles on this subject [1].
The database of diffraction patterns used is from the Joint Committee for Powder Diffraction Studies (JCPDS).

2.2. Impedance spectroscopy

Importance of interfaces: At an interface, physical, properties-crystallographic, mechanical, compositional and particularly, electrical-change precipitously and heterogeneous charge distributions (polarization) reduce the overall electrical conductivity of a system. Proliferation of interfaces is a distinguished feature of solid state electrolytic cells, where not only is the junction between electrode and electrolyte considerably more complex than in aqueous cells, but the solid electrolyte is commonly polycrystalline. Each interface will polarize in its unique way when the system is subjected to an applied potential difference. The rate at which the a polarized region will change when the applied voltage is reversed is characteristic of the type of interface: slow for chemical reaction s at the triple phase contacts between atmosphere, electrode and electrolyte, appreciably faster across grain boundaries in the polycrystalline electrolyte. The emphasis in electrochemistry has consequently shifted from a time-concentration dependency to frequency-related phenomena, a trend toward small signal as studies. Electrical double layers and their inherent capacitive reactances are characterized by their relaxation times, or more realistically by the distribution of their relaxation times. The electrical response of s heterogeneous cell can vary substantially depending on the species of charge present, the microstructure of the electrolyte, and the texture and nature of the electrodes [2, 5].

Electrochemical impedance spectroscopy (EIS) or impedance spectroscopy (IS) is one of the most powerful tools to analyze the characteristics of an electrochemical system. Compared to the DC techniques, which are mostly complicated and difficult to overcome the problems due to the nonlinear polarizations at the interfaces, impedance spectroscopy is easier to perform,

with the capability to separate the contributions from different processes. Impedance spectroscopy is a relatively new and powerful method of characterizing many of the electrical properties of materials and their interfaces with electrically conducting electrodes, which may be used to investigate the dynamics of bound or mobile charge in the bulk or interfacial regions of any kind of sold or liquid material which can be ionic, semiconducting or mixed electronic-ionc, and even insulators (dielectrics).

Basic applications of EIS:

- to indicate whether the overall resistance of a material is dominated by bulk or grain boundary components
- to assess the quality and electrical homogeneity of an electroceramic, since there is generally a link between sintering/microstructure and AC response
- to measure the values of the component resistances and capacitances.

Electrochemical Impedance is normally measured using a small excitation signal. This is done so that the cell's response is pseudo-linear, and the current response to a sinusoidal potential will be a sinusoid at the same frequency but shifted in phase. By applying a small AC voltage at varying frequencies, the phase shift and amplitude of the resulting current are recorded, from which the contributions from the bulk materials, grain boundaries in case of polycrystal, electrode processes and ionic junctions to the electrical properties could be distinguished from each other. The frequencies most employed in this technique can range from several mHz to more than 10 MHz, which are determined by the components of interest in the system. This is because in solid state systems all phenomenon have a characteristic capacitance and relaxation time [2]. Such capacitances are shown in Table 2.1.

Table. 2.1 Capacitance values with their possible interpretations.

Capacitance (F)	Characteristic responsible
10^{-12}	Bulk
10^{-11}	Second phase in minor quantities
10^{-12}~10^{-8}	Grain boundary
10^{-10}~10^{-9}	Bulk ferroelectric
10^{-9}~10^{-7}	Surface layer
10^{-7}~10^{-5}	Sample-electrode interface
10^{-4}	Electrochemical reactions

Basics of impedance:
There are three different types of electrical stimuli which are used in IS.

First, in transient measurements a step function of voltage [$v(t) = v_o$ for $t > 0$, $v(t) = 0$ for $t < 0$] may be applied at $t = 0$ to the system and the resulting time-varying current i(t) measured. The ratio $v_o/i(t)$, often called the indicial impedance or the time-varying resistance, measures the impedance resulting from the step function voltage perturbation at the electrochemical interface. This quantity is not the usual impedance referred to in IS, rather such time-varying results are generally Fourier or Laplace-transformed into the frequency domain, yielding a frequency dependent impedance.

A second in technique in IS is to apply a signal v(t) composed of random noise to the interface and measure the resulting current. This approach offers the advantage of fast data collection because only one signal is applied to the interface for a short time. The technique has the disadvantages of requiring true random (white) noise and then the need to carry out a Fourier analysis.

The third approach, the most common and standard one is to measure impedance by applying a single-frequency voltage or current to the interface and measuring the phase shift and amplitude, or real and imaginary parts, of the resulting current at that frequency using either analog circuit or fast Fourier transform (FFT) analysis of the response

If a small voltage is applied in a sinusoidal manner with time as follows:

$$V(t) = V_o \cos(\omega t) \tag{2.1}$$

where V_o is the amplitude of the signal, ω is the angular frequency (radians/s), which is related to the frequency f (hertz) by $\omega = 2\pi f$:

then the current response is also sinusoidal, but with a phase difference between voltage and current θ, which is zero for purely resistive behavior :

$$I(t) = I_o \cos(\omega t + \theta) \tag{2.2}$$

where I_o is the current amplitude.

The impedance is defined as the ratio between the voltage and current in the complex plane:

$$\dot{Z} = \frac{\dot{V}}{\dot{I}} \tag{2.3}$$

where $\dot{}$ represents the complex number.

Generally, it's convenient to describe these quantities in terms of real and imaginary coordinate. Then the ac voltage V can be expressed as a complex number:

$$V = V' + V''J \tag{2.4}$$

where $j = \sqrt{-1}$, V' and V'' are the real and imaginary part, respectively.

Using the Euler's relationship: $\exp(j\theta) = \cos\theta + j\sin\theta$, the above equation, 2.4, can be written as:

$$V = V_o \cos\omega + jV_o \sin\omega = V_o \exp(j\omega) \tag{2.5}$$

the same way the current equation can also be rewritten as:

$$I = I_o \exp(j\omega - \theta) \tag{2.6}$$

According to equation, 2.3; the real part of Z is in the direction of the real axis x-axis, and the imaginary part along the y-axis. An impedance Z(ω) = Z' + jZ'' is such a vector quantity and may be plotted in the plane with either rectangular or polar coordinates.
The two rectangular coordinate values are clearly

$$\mathrm{Re}(Z) = Z' = |Z|\cos(\theta) \text{ and } \mathrm{Im}(Z) = Z'' = |Z|\sin(\theta) \tag{2.7}$$

with the phase angle,

$$\theta = \tan^{-1}\frac{Z''}{Z'}$$

and the modulus

$$Z = \sqrt{(Z')^2 + (Z'')^2} = \left|\frac{V_o}{I_o}\right|$$

$$Z = Z' + Z''j = |Z|\exp(j\theta) \tag{2.8}$$

with $Z = \sqrt{(Z')^2 + (Z'')^2} = \left|\frac{V_o}{I_o}\right|$, $\theta = \tan^{-1}\frac{Z''}{Z'}$, we can plot it in a complex plane as shown below.
This type of plot is also known as Nyquist plot or Cole-Cole plot. Another type is called Bode plot, which is a plot of $\log Z$ vs. $\log\omega$.

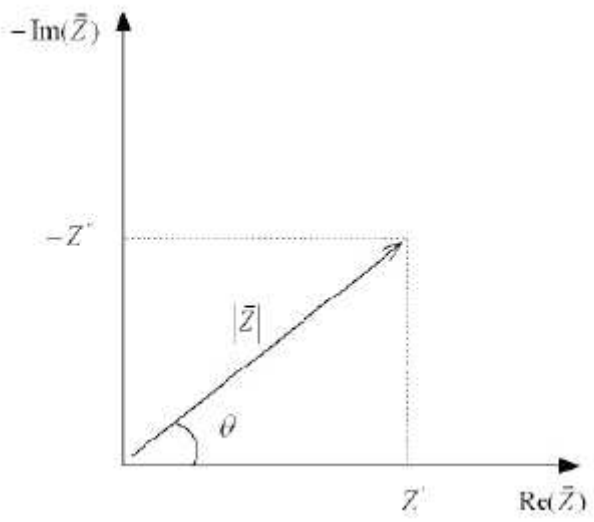

Fig. 2.2. The Impedance Z plotted as a planar vector using rectangular and polar coordinates.

Circuit elements:

Given the basic theory, we can now look at impedance expressions for some simple electrical circuits as shown in Table 2.2 below. The impedance of a resistor Z_R is simply the resistance R, which is represented by a single point on the real axis in the Nyquist plot, while a capacitance $Z_C = 1/j\ C\ \omega$ is shown as a straight line on the imaginary axis. If there is a resistance in series with a capacitance the impedance $Z_{R\text{-}C}$ is given by:

$$Z_{R-C} = Z_R + Z_C = R + {}^{1}\!\!\diagup\!\!{}_{j\omega C} \tag{2.9}$$

if they are combined in parallel, then the impedance Z_{RC} is given by:

$$1/Z_{R-C} = 1/Z_R + 1/Z_C = 1/R + j\omega C \tag{2.10}$$

which gives:

$$Z_{RC} = \frac{R}{1+(R\omega C)^2} - \frac{R^2\omega C}{1+(R\omega C)^2}\,j \tag{2.11}$$

Z_{RC} has the shape of a semicircle on the complex impedance plane. At very low frequencies, all the current flows through the resistor, while at very high frequencies, the current is short circuited by the capacitor. On the top of the semicircle, the real and imaginary parts are equal, which define the relaxation time τ of the 'RC' element:

$$\tau = RC = \frac{1}{\omega} \tag{2.12}$$

Table 2.2. Basic circuit elements and their Nyquist plots.

Circuit elements	Impedance equation	Nyquist plot
	R	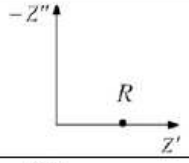
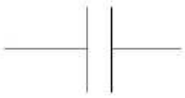	$Z_C = 1/j\omega C$	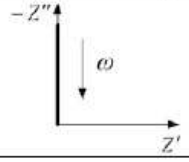
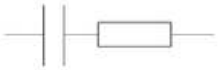	$Z_{R-C} = R + 1/j\omega C$	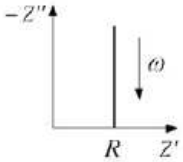
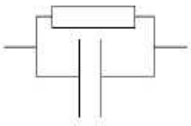	$Z_{RC} = \frac{R}{1+R^2\omega^2C^2} - \frac{R^2\omega C}{1+R^2\omega^2C^2}j$	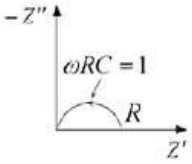

The electrochemical cell can be described by an equivalent circuit, which is a combination of capacitors and resistors. A simple example is given in Fig. 2.3, where two ionic blocking electrodes are used on top of a solid electrolyte. The Ohmic resistance of the electrolyte can be represented as a pure resistor, R_i in Fig. 2.4. The capacitive properties of the two-electrolyte/electrode interfaces are combined into one capacitor, C_{int}, with the subscript 'int' being the abbreviation of interface. C_{int} is sometimes also call the double layer capacitor C_{dl}.

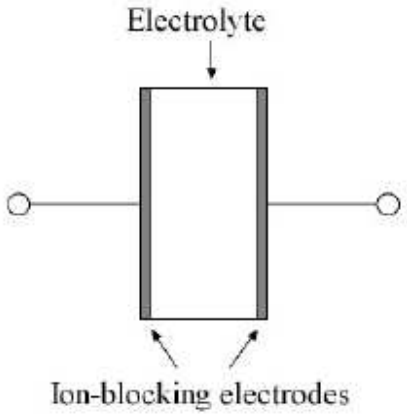

Figure 2.3. Solid electrolyte with two ion-blocking electrodes.

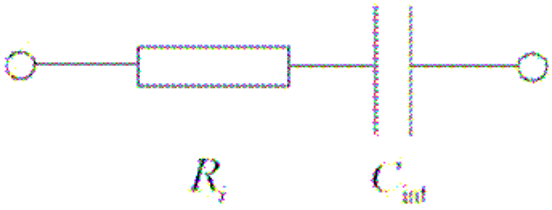

Figure 2.4. Equivalent circuit for the cell shown in Fig. 2.3 at low frequency.

At higher frequencies an additional geometrical capacitance, C_{geom}, due to the presence of a dielectric material between the two parallel metallic electrodes is involved as shown in Fig. 2.5. This is often called the "Debye circuit". The corresponding Nyquist plot is shown in Fig..2.6.

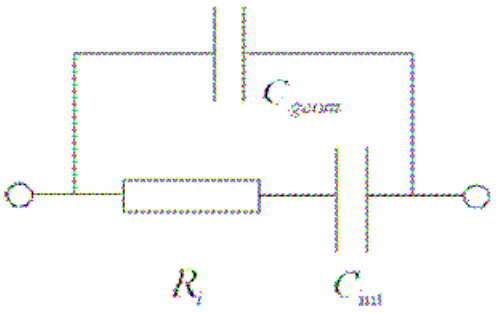

Figure 2.5. Debye circuit.

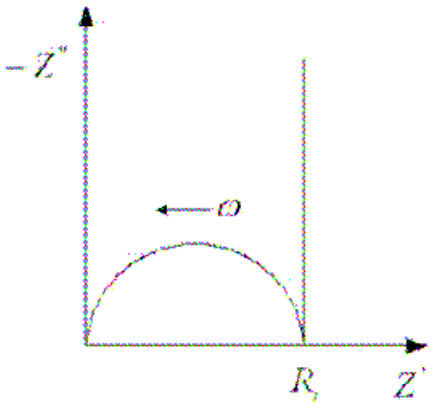

Figure 2.6. Nyquist plot of Debye circuit.

In Fig. 2.6, the impedance may not go all the way down to the real axis at intermediate frequencies if the values of C_{geom} and C_{int} are not sufficiently different from each other. The low frequency tail is not vertical in most cases, but is inclined at an angle from the vertical, as illustrated in Fig. 2.7.

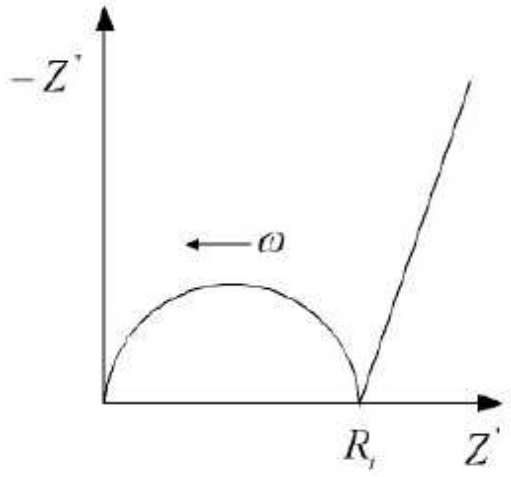

Figure 2.7. Nyquist plot showing tilted tail at low frequencies.

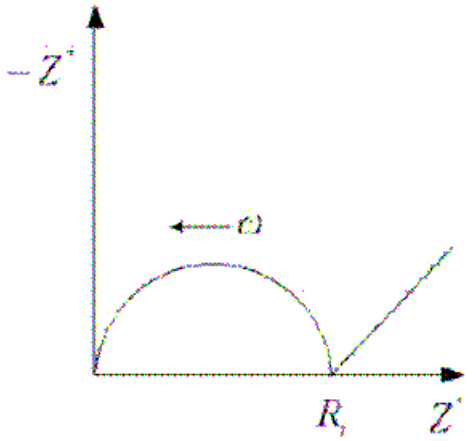

Figure 2.8. Nyquist plot showing Warburg impedance.

Such kind of deviation from the ideal Debye circuit behaviour is related to the processes occurring at the electrolyte/electrode interfaces [3]. These processes can be represented in the equivalent circuit by the following element:

$$Z = A\omega^{-\alpha} - jB\omega^{-\alpha} \tag{2.13}$$

If the electrodes are not completely blocking for the transport of ion, then the electroactive species can diffuse to or from the electrodes as a neutral reaction product according to Fick's second law. In this case, the low frequency tail will fall onto a straight line with a slope of 45 degrees, as shown in Fig. 2.8. Eq. (2.13) can then be written as:

$$Z_W = A\omega^{-1/2} - jB\omega^{-1/2} \tag{2.14}$$

where Z_W is the so called Warburg impedance, A and B include the information of the diffusion coefficient, the charge-transfer resistance, R_{ct}, and the interfacial capacitance, C_{int}.

If ionic transport through the solid is hindered by the presence of internal interfaces, e.g. grain boundaries, the additional ionic impedance, R_{gb}, must act in series with the bulk ionic

resistance. The blocking effect from the grain boundaries can be represented by a parallel local capacitance, C_{gb}.

The equivalent circuit, considering the Warburg impedance and the grain boundary effect is shown in Fig. 2.9. The corresponding Nyquist plot consists of three semicircles with a straight line at the low frequency end following 45 degrees slope, as shown in Fig. 2.10. In the real electrochemical systems, the Nyquist plots may differ from Fig. 2.10, in view of the different material properties and working conditions. Detailed discussion about impedance spectroscopy and their applications can be found elsewhere [4,5].

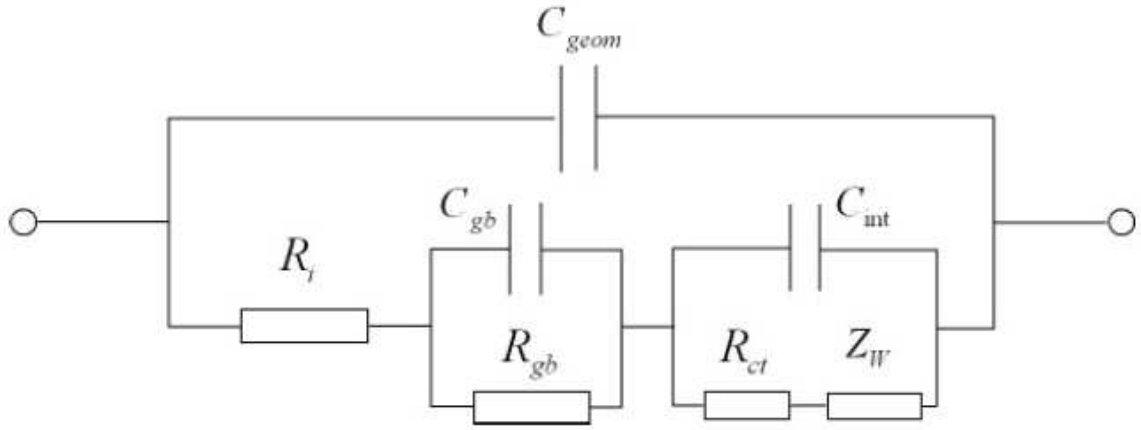

Fig. 2.9. Equivalent circuit with the Warburg impedance and grain boundary impedance.

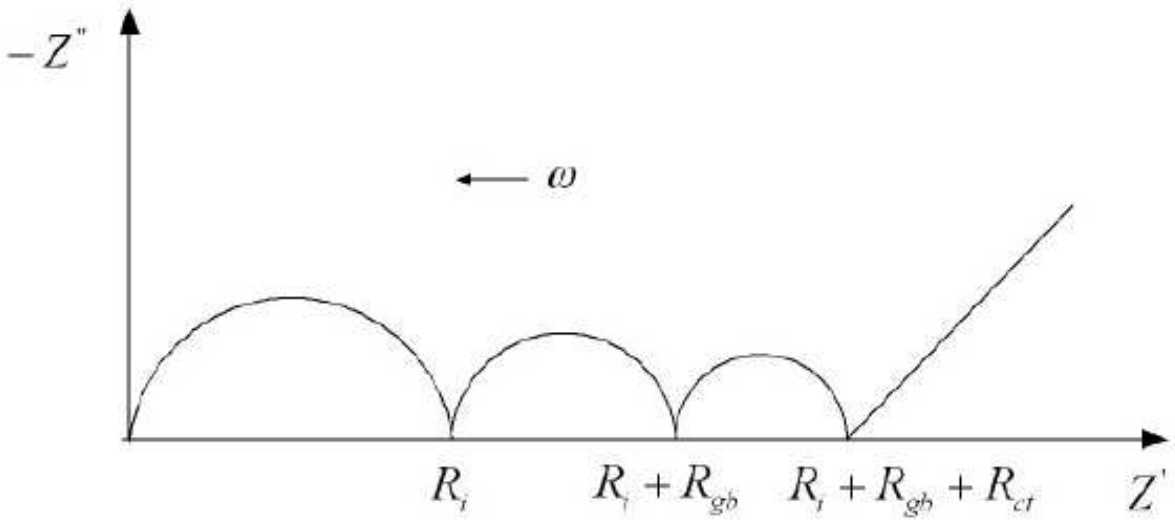

Fig. 2.10. Nyquist plot of the equivalent circuit shown in Fig. 2.9.

2.3 Dielectric materials and dielectric constant:

Dielectric materials are electrical insulators, which are used principally in capacitors and electrical insulators. They should posses the following properties in order to be of use in practical applications. They should possess high dielectric strength, i.e. they should be able to withstand high voltages without undergoing degradation and becoming electrically conducting. They should have low dielectric loss, i.e. in an alternating electric field, the loss of electrical energy, which appears as heat, should be minimized.

Application of a potential difference across a dielectric does lead to a polarization of charge within the material although long range motion of ions or electrons cannot occur. The polarization disappears when the voltage is removed. Ferroelectric materials are a special type of dielectric in that they retain a large, residual polarization of charge after the electric field has been removed.

Dielectric properties may be defined by the behaviour of the material in a parallel plate capacitor. This is a pair of conducting plates, parallel to one another and separated by a distance, *d*, that is small compared with the linear dimensions of the plates as shown in the Fig. below (Fig 2.11). With a vacuum between the plates, the capacitance C_o is defined as:

$$C_o = \frac{\varepsilon_o A}{d} \tag{2.15}$$

where ε_o *is the permitivity of the space*, 8.854×10^{-12} Fm^{-1}, and A is the area of the plates and d the separation between the two metallic plates. Since ε_o is constant, the capacitance depends only on the dimensions of the capacitor. On applying a potential difference, V, between the plates a quantity of charge, Q_o, is stored on them, given by:

$$Q_o = C_o V \tag{2.16}$$

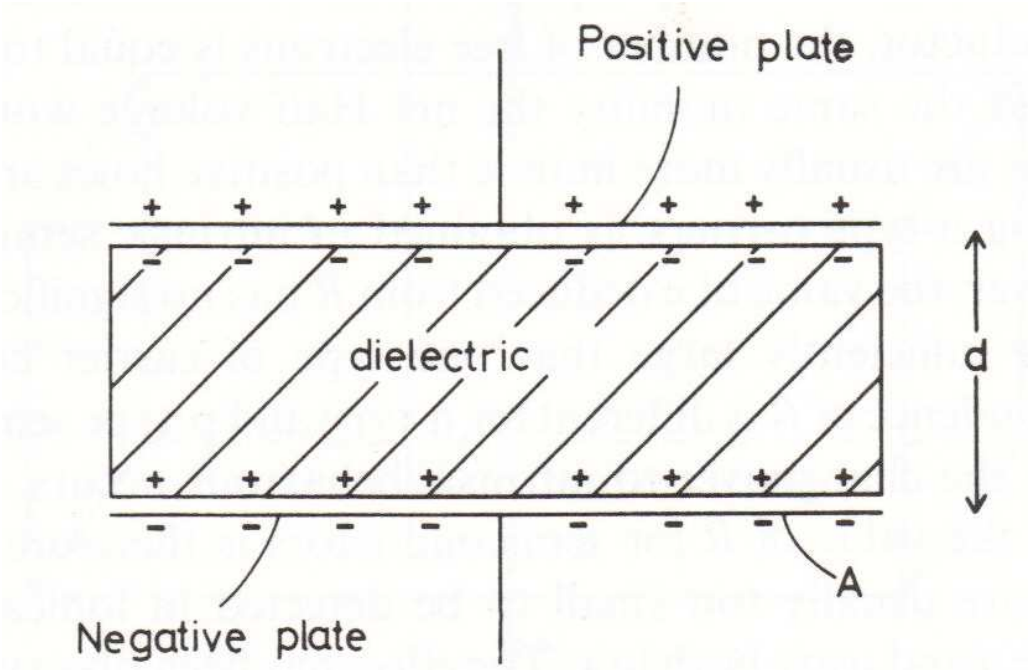

Fig. 2.11 Dielectric material between the plates of a parallel plate capacitor [27].

If a dielectric substance is now placed between the plates and the same potential difference is applied, the amount of charge stored increases to Q_1 and the capacitance therefore increases to C_1. The dielectric constant or relative permitivity, ε', of the dielectric is related to this increase in capacitance by:

$$\varepsilon' = \frac{C_1}{C_o} \tag{2.17}$$

The magnitude of ε'depends on the degree of polarization or charge displacement than can occur in the material. For air, $\varepsilon' = 1$. For most ionic solids, $\varepsilon' = 5$ to 10 and for ferroelectric materials such as $BaTiO_3$, $\varepsilon' = 1000$ to 10,000.

The polarizability, α, of the dielectric is defined by:

$$p = \alpha E \tag{2.18}$$

where p is the dipole moment induced by the local electric field, E. The polarizability has four possible components and is given by the summation:

$$\alpha = \alpha_e + \alpha_i + \alpha_d + \alpha_s \qquad (2.19)$$

where these four components are as follows:

1. The *electric polarizability*, α_e, is caused by a slight displacement of the charged electron cloud in an atom relative to the positively charged nucleus. Electronic polarizability occurs in all solids and some, such as diamond, it is the only contributor to the dielectric constant since ionic, dipolar and space charge polarizabilities are absent.
2. The *ionic polarizability*, α_i, arises from a slight relative displacement or separation of an ions and cations in a solid. It is the principal source of polarization in ionic crystals.
3. *Dipolar polarizability*, α_d , arises in materials such as HCl or H_2O that contain permanent electronic dipoles. These dipoles may change their orientation and they tend to align themselves with an applied electric field. The effect is usually very temeperature dependent since the dipoles may be frozen in at low temperatures.
4. *Space charge polarizability,* α_s, occurs in materials that are not perfect dielectrics but in which some long range charge migration may occur. In NaCl, for instance, cations migrate preferentially towards the negative electrode by means of crystal defects such as cation vacancies; consequently, an electrical double layer builds up at the electrode – NaCl interface. When such effects are appreciable, the material is better regarded as a conductor or solid electrolyte than as a dielectric. Apparent dielectric constants 10^6 to 10^7 may be measured (corresponding to double-layer capacitances of ~10^{-6} F) but these values have no significance in a conventional dielectric sense.

The magnitude of α usually decreases in the order, $\alpha_s > \alpha_d > \alpha_i > \alpha_e$, although, clearly, not all materials show all types of polarization. Experimentally, the four contributions to α and ε' may be separated by making measurements over a wide range of a.c. frequencies using a combination of capacitance bridge, microwave and optical measurements as shown in (Fig. 2.12). At low frequencies, e.g., audiofrequencies (~10^3 Hz), all four (if present) may contribute to α. At radio frequencies, (10^6 Hz), space charge effects may not have time to build up in most ionically conducting materials and are effectively "relaxed out". At microwave frequencies (~10^9 Hz) dipoles do not usually reorient themselves and are effectively relaxed out. The timescale of ionic polarizations is such that they do not occur at frequencies higher than infrared (~10^{12} Hz). This then leaves the electronic polarization which is observable into the UV but relaxed out at X-ray frequencies.

In good dielectric materials which do not contain contributions from α_s and α_d, the limiting low frequency permitivity, ε'_o, is composed mainly of α_i and α_e polarizations. The permitivity ε'_o may be obtained from a.c. capacitance bridge measurements in which the value of the capacitance is determined with and without the dielectric substance placed between the plates of the capacitor or cell. The value of ε'_o which contains α_e contributions only may be obtained from refractive index measurements (visible light frequencies) using the simple relation:

$n^2 = \varepsilon'_\infty$

values of ε'_o and ε'_∞ for NaCl, which are fairly typical of ionic crystals, are 5.62 and 2.32, respectively.

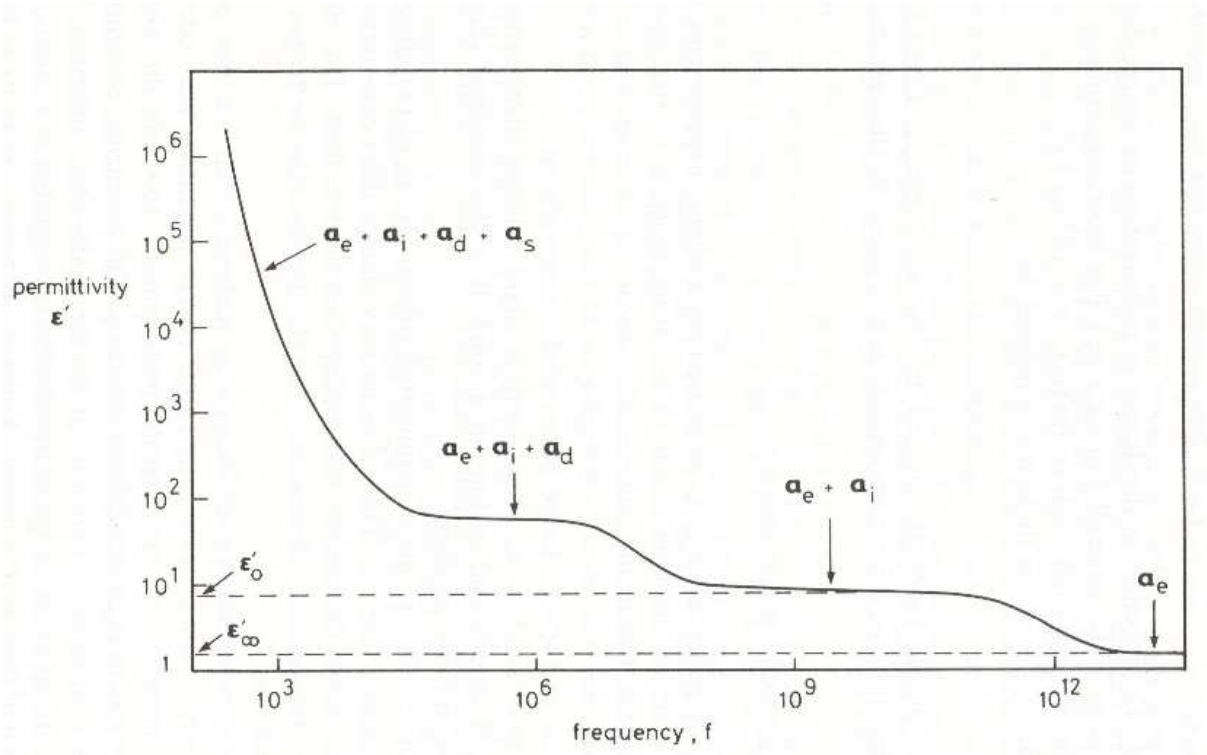

Fig. 2.12 Polarization effects in a dielectric [27].

A low-k dielectric is a dielectric that has a low permittivity, or low ability to polarize and hold charge. Low-k dielectrics are very good insulators for isolating signal-carrying conductors from each other. Thus, low-k dielectrics are a necessity in very dense multi-layered IC's, wherein coupling between very close metal lines need to be suppressed to prevent degradation in device performance.

A high-k dielectric, on the other hand, has a high permittivity. Because high-k dielectrics are good at holding charge, they are the preferred dielectric for capacitors. High-k dielectrics are also used in memory cells that store digital data in the form of charge.

2.4 . Kinetic and thermodynamic properties

Many different electrochemical techniques have been used to measure kinetic and thermodynamic properties in solids. In spite of the variety of experimental arrangements, several fundamental features are common to such studies. The galvanic cell phenomenon is one of the most relevant to the attainment of thermodynamic and kinetic information about the constituent solids in such cells.

The electrical current that passes through a galvanic cell is directly related to the dynamic processes involved in the transport of mobile ionic and electronic species in one or more parts of the experimental cell arrangement. However, the voltage difference across the cell is primarily determined by thermodynamic considerations. Despite this clear separation between kinetic and thermodynamic information, well-defined observations of material properties often involve the determination or the control of both types of electrical quantities.

The energy storage and power characteristics of electrochemical energy conversion systems follow directly from the kinetic and thermodynamic formulations for chemical reactions as adapted to electrochemical reactions.

2.4.1 Kinetic properties

If an electrical current is either forced or permitted to pass through any part of the experimental arrangements to be discussed, the partial current density i_n of any species n is, in general, proportional to the overall transport force acting upon that species. This force can be expressed as the gradient of the electrochemical potential η_n of the species in question. If transport involves no volume change, we can neglect all but chemical and electrostatic forces; correlation with the fluxes of other particles may be neglected [6]. The proportionality constant between the current and the electrochemical potential gradient is given by the partial specific electrical conductivity σ_n, of species n,

$$i_n = -\frac{\sigma_n \partial \eta_n}{z_n q \partial x} \quad , \tag{2.20}$$

where z_n is the charge number (effective valence) and q the elementary charge. To provide further insight into the parameters that determine the transport of species within a solid, the electrochemical potential may be divided into an electrostatic potential component ϕ and a chemical potential component μ_n according to the relation,

$$\eta_n = \mu_n + z_n q \phi \, , \tag{2.21}$$

The chemical potential may be replaced by the activity a_n by the use of the defining equation

$$\mu_n = \mu_n^0 + kT \ln a_n \tag{2.22}$$

where μ^0_n, k, and T stand for the chemical potential in the standard state ($a_n = 1$), Boltzmann's constant, and the absolute temperature, respectively.

The conductivity may be written in terms of the product of the concentration of the mobile species c_n and the diffusivity D_n:

$$\sigma_n = \frac{c_n D_n z_n^2 q^2}{kT} \tag{2.23}$$

This diffusivity, which is identical to quantities that are sometimes called the "component diffusion coefficient" [6], "elementary diffusion coefficient" [7], "self diffusion constant" [8], or "self diffusion coefficient" [9], is defined as the quantity that obeys the Nernst-Einstein relation [10, 11] between the electrical mobility u_n (drift velocity per unit electric field) or the general mobility b_n (drift velocity per unit general force) [8], and the diffusion coefficient, regardless of whether the material can be considered to be an ideal or a non-ideal solution:

$$D_n = u_n \frac{kT}{|z_n| q} = b_n kT \tag{2.24}$$

The diffusivity D_n is a measure of the random motion of the particles of species n in the absence of concentration gradients. It is related to the diffusion coefficient [also sometimes called the "self diffusion coefficient"], which is determined by the use of radioactive isotopic

tracers, D_n^T by $D_n^T = f_n D_n$ where f_n the correlation factor, or more generally, the Haven ratio [12].

From equation 2.23 it can be seen that D_n is also the quantity that contains the kinetic contribution to the conductivity of species *n*.

With the help of equations 2.21, 2.22 and 2.23, equation 2.20 can now be cast into the form,

$$i_n = -\sigma_n \frac{\partial \phi}{\partial x} - z_n q D_n \frac{\partial \ln a_n}{\partial \ln c_n} \frac{\partial c_n}{\partial x} \tag{2.25}$$

The first term on the right-hand side is identical to Ohm's law for the migration of species *n* under the influence of an internal electrostatic field. The second term is related to Fick's first law for diffusion under a concentration gradient. Equation 2.25 is general for isothermal conditions and is valid at any point in a galvanic cell, assuming that there is no mass motion or volume change and that no other forces are involved in the transport of species *n*, such as correlation effects due to the simultaneous transport of other components.

The movement of the various species in a simple galvanic cell is schematically shown in Fig. 2.13. It should also be pointed out that under these conditions this formulation is independent of the identity of both the defect species within the solid and the mechanism whereby their motion results in the effective transport of species *n*. Equation 2.25 holds both in an electrolyte phase, in which the transport of charge is primarily due to the motion of ionic species, and in mixed ionic and electronically conducting phases, it may be simplified by considering special cases when dealing with the properties of the different constituents of an electrochemical system and when being applied to specific species.

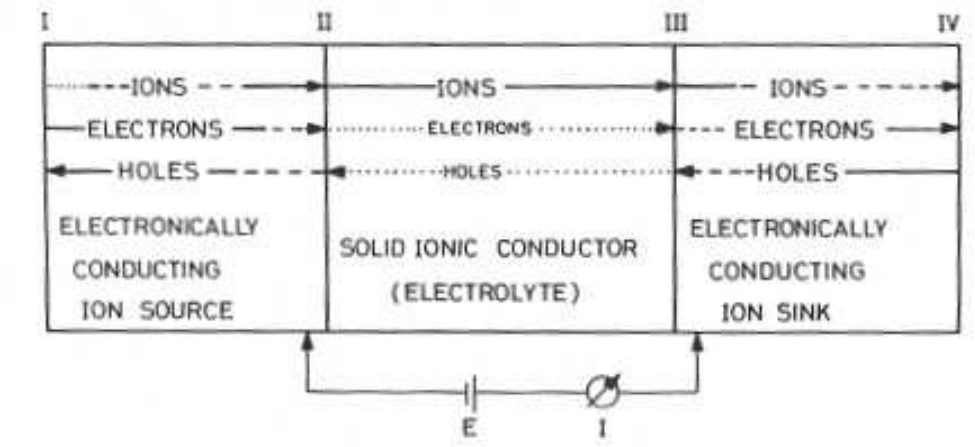

Fig. 2.13 General arrangement of galvanic cells. The arrows indicate the motion of the charge carriers and their relative magnitudes.

In most cases of interest we can assume that a phase realistically used as an electrolyte in a galvanic cell is characterized by a very large concentration of mobile ions or ionic defects. As a result, the chemical potential of the mobile ionic species, which is proportional to the logarithm of the activity, may be regarded as essentially independent of position within the material. Thus any ionic transference in such phases must be predominantly due to the influence of an internal electrostatic field:

$$i_{ion(electrolyte)} = -\sigma_{ion} \frac{\partial \phi}{\partial x} \tag{2.26}$$

For the electronic defects, itinerant (or "excess") electrons and holes, which can be considered relatively dilute in an electrolyte, the situation is different, and either an internal electrostatic field, a concentration gradient, or both may be important. This will depend upon the differences of the chemical potentials of the electronic species at the two sides of the electrolyte. When the concentration of the electronic species is high, the influence of an internal electric field is more important than when the concentrations of such species are low.

If the ionic current is blocked by the use of ionically polarizing electrodes so that only electrons and holes may pass through the electrolyte, the internal electrostatic field must become negligible under steady-state conditions, in accordance with equation 2.26. In that case, the transport of electronic species may occur only as the result of a concentration gradient.

A different situation holds in the case of phases that we categorize as electrodes and that we can assume to transport charge predominantly by the motion of electronic species. In that case the chemical potentials of the itinerant electrons or holes may be regarded as practically independent of location within the solid, due to their high concentrations. Thus their transport is primarily due to the effect of an internal electric field in such materials. Because of the large concentrations of these electronic species, as well as their high mobilities, this field will, of course, be very small. Therefore if ionic transport occurs across an electrode/electrolyte interface in connection with current flow by the motion of ionic species in the electrolyte, the ionic flux within the electrode material must be predominantly determined by the presence of a local ionic concentration gradient in that phase.

That is,

$$i_{ion(electrode)} = -z_{ion} q D_{ion} \frac{\partial \ln a_{ion}}{\partial \ln c_{ion}} \frac{\partial c_{ion}}{\partial x} \tag{2.27}$$

It should be noted that the factor $(\partial ln\ a_{ion}/\partial ln\ c_{ion})$, which is often called the "thermodynamic factor" and which can sometimes be very large, acts to enhance the ionic flux density above that which would be expected from the concentration gradient alone [13,14]. In a predominantly electronic conductor in which the concentration of excess electrons or holes is very large, so that the chemical potentials of the electronic species are essentially uniform throughout the body, the gradients of the chemical potentials of neutral atoms and their respective ions are identical. Thus the transport of ions may be considered to be the same as the net transport of neutral species.

If an electrode material is not overwhelmingly an electron or hole conductor so that the sum of the transference numbers of the electronic species differs appreciably from unity, the internal electrostatic field may not be completely neglected with regard to the movements of ions. In such a case the transport of ionic species occurs under the combined influence of electrostatic and chemical potential gradients. This situation can be expressed by an equation similar to equation 2.27 by replacing $(\partial\ ln\ a_n/\partial\ ln\ c_n)$, by a more general "enhancement factor," W, which is also named “Wagner factor” [15]:

$$i_{ion(mixed\ \ conductor)} = -z_{ion} q D_{ion} W \frac{\partial c_{ion}}{\partial x} \tag{2.28}$$

In addition to being expressible in terms of thermodynamic quantities, this enhancement factor can be interpreted kinetically as the generation of an internal electric field by a displacement of the concentration profiles of two differently charged mobile species within the solid. If one of them, e.g. electrons, has a significantly greater mobility than the other, e.g. ions, in a concentration gradient the more mobile species will tend to move ahead of the other. The requirement for overall charge flux neutrality causes the more mobile species to be slowed down and provides an additional driving force for the less mobile one [15]. The total charge transport current within a solid (e.g. an electrode material) may be composed of several partial currents whose magnitudes vary with position. Such a situation would, of course, not be measured by instruments in an external circuit, since they observe only the total

current passing through the overall cell. However, an electrolyte serves as an ion-pass filter if the electron and hole conductivities within it are very small. As a result, only ionic species can cross phase boundaries between electrodes and such an electrolyte. Since under steady-state conditions the ionic current must be continuous across an electrolyte-electrode interface, the total externally measurable current must be equal to the partial ionic current, as expressed in equation 2.28, within the electrode material just inside the interface. However, it is possible that the most mobile ions within the electrolyte are not those that are predominantly transferred in the electrode. In such a case, the overall cell current is given by equation 2.28 when it is written in terms of the species that are most mobile in the electrode phase.

2.4.2 Thermodynamic properties

The basic thermodynamic equations for a reversible electrochemical transformation are given as

$$\Delta G = \Delta H - T\Delta S \tag{2.29}$$

and

$$\Delta G^o = \Delta H^o - T\Delta S^o \tag{2.30}$$

where ΔG is the Gibbs free energy, or the energy of a reaction available (= free) for useful work, ΔH is the enthalpy, or the energy released by the reaction, ΔS is the entropy, and T is the absolute temperature, with $T\Delta S$ being the heat associated with the organization/disorganization of materials. The terms ΔG, ΔH, and ΔS are state functions and depend only on the identity of the materials and the initial and final states of the reaction. The degree symbol is used to indicate that the value of the function is for the material in the standard state at 25 °C and unit activity.

Because ΔG represents the net useful energy available from a given reaction, in electrical terms, the net available electrical energy from a reaction in a cell is given by

$$\Delta G = -nFE \tag{2.31}$$

and

$$\Delta G^o = -nFE^o \tag{2.32}$$

where n is the number of electrons transferred per mole of reactants, F is the Faraday

constant, being equal to the charge of 1 equiv of electrons, and E is the voltage of the cell with the specific chemical reaction; in other words, E is the electromotive force (emf) of the cell reaction. The voltage of the cell is unique for each reaction couple. The amount of electricity produced, nF, is determined by the total amount of materials available for reaction and can be thought of as a capacity factor; the cell voltage can be considered to be an intensity factor. The usual thermodynamic calculations on the effect of temperature, pressure, etc., apply directly to electrochemical reactions. Spontaneous processes have a negative free energy and a positive emf with the reaction written in a reversible fashion, which goes in the forward direction. The van't Hoff isotherm identifies the free energy relationship for bulk chemical reactions as

$$\Delta G = \Delta G^o + RT \ln(A_P / A_R) \tag{2.33}$$

where R is the gas constant, T the absolute temperature, A_P the activity product of the products and A_R the activity product of the reactants. Combining eqs 2.32 and 2.33 with the van't Hoff isotherm, we have the Nernst equation for electrochemical reactions:

$$E = E^o + (RT / nF) \ln(A_P / A_R) \tag{2.34}$$

Faraday's laws, as summarized in equation 2.35, give the direct relationship between the amount of reaction and the current flow. There are no known exceptions to Faraday's laws.

$$g = \frac{It(MW)}{nF} \tag{2.35}$$

g is the grams of material transformed, I is the current flow (amps), t is the time of current flow (seconds, hours), MW is the molecular or atomic weight of the material being transformed, and n is the number of electrons in the reaction.

A process is thermodynamically reversible when an infinitesimal reversal in a driving force causes the process to reverse its direction. Since all actual processes occur at finite rates, they cannot proceed with strict thermodynamic reversibility and thus additional nonreversible effects have to be regarded. In this case, under practical operation conditions, voltage losses at internal resistances in the cell (these kinetic effects are discussed below) lead to the

irreversible heat production (so-called Joule heat) in addition to the thermodynamic reversible heat effect.

Assuming thermodynamic reversibility, of the cell reaction and with the help of equations 2.29 and 2.31, we can obtain the reversible heat effect:

$$\Delta G = -nFE = \Delta H - T\Delta S \tag{2.36}$$

$$= \Delta H - nFT(dE/dT) \tag{2.37}$$

By measuring the cell voltage as a function of temperature, the various thermodynamic quantities for the materials in an electrode reaction can be determined experimentally. If dE/dT is positive, the cells will heat on charge and cool on discharge. Lead acid is an example of a negative dE/dT, where the cells cool on charge and heat on discharge. Ni-Cd is an example of a positive dE/dT, where the cells heat on charge and cool on discharge. Heating and cooling of the cell can proceed with heat exchange with the environment. In general, the entropic heat is negligibly small compared to the irreversible heat released, q, when a cell is in operation. Equation 10 describes total heat release, including the reversible thermodynamic heat release along with the irreversible joule heat from operation of the cell in an irreversible manner, during charge or discharge at finite current/rate. Irreversible behavior manifests itself as a departure from the equilibrium or thermodynamic voltage. In this situation, the heat, q, given off by the system is expressed by an equation in which E_T is the practical cell terminal voltage and E_{OCV} is the voltage of the cell on open circuit.

$$q = T\Delta S + I(E_{OCV} - E_T) \tag{2.38}$$

$$q = heat \quad given \quad off \quad by \quad system$$

The total heat released during cell discharge is the sum of the thermodynamic entropy contribution plus the irreversible contribution. This heat is released inside the battery at the reaction site on the surface of the electrode structures. Heat release is not a problem for low-rate applications; however, high-rate batteries must make provisions for heat dissipation. Failure to accommodate/dissipate heat properly can lead to thermal runaway and other catastrophic situations.

2.4.3 Chemical diffusion and methods of determination.

An important kinetic phenomenon in solids is the relaxation of composition gradients to achieve a more homogeneous composition. The kinetic parameter related to this process is the chemical diffusion coefficient $\tilde{D}$. This quantity is also an important parameter for many phenomena of practical interest, e.g. for corrosion processes or the kinetic behavior of electrodes in battery applications. In addition, an analysis of the physical processes underlying chemical diffusion may allow the determination of other kinetic parameters in a sample from a single set of experiments.

As shown in Fig. 2.14, an auxiliary electrolyte may be used both to measure the flux of ions into and out of a sample and to determine the concentration of the electroactive species at the electrolyte-sample interface. In contrast to other well-established transient electrochemical techniques such as chronoamperometric and chronopotentiometric methods, the rate-determining factor in this case is the diffusion of species within the mixed-conducting solid that is used as the electrode.

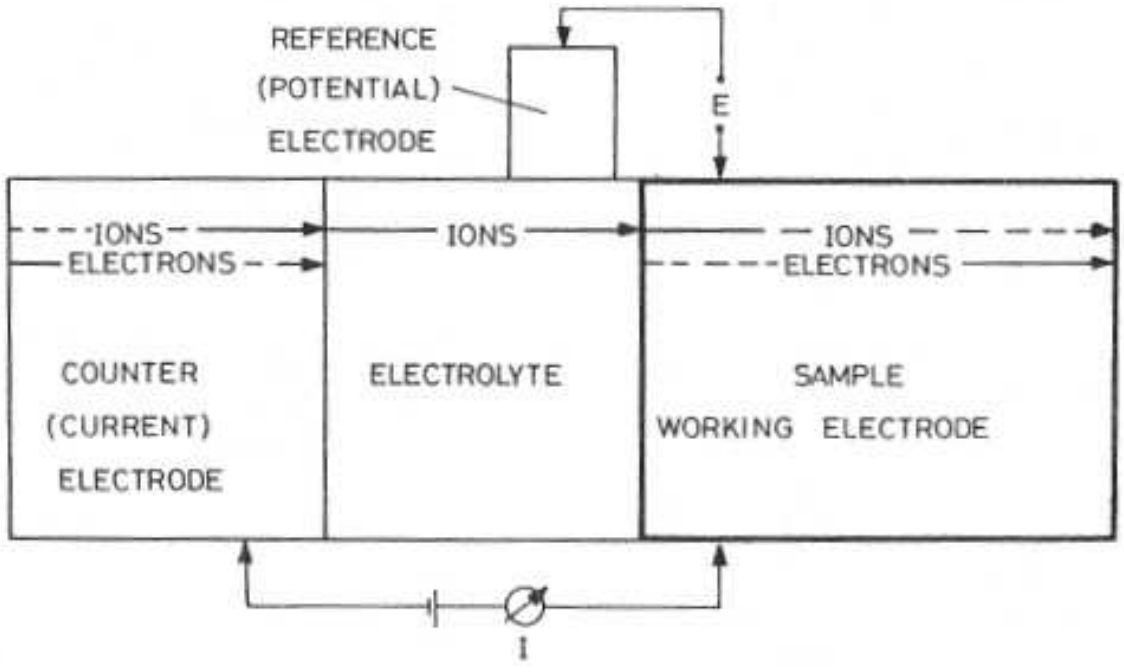

Fig. 2.14 Arrangement for determining chemical diffusion coefficients and other transport quantities by transient techniques. A separate reference electrode is used to determine the activity of the relevant species at the interface between the sample and the electrolyte.

The transport of ions across the electrolyte is assumed not to be the rate-determining process. The validity of this assumption can easily be determined by performing experiments in the absence of the sample, using only the electronic lead at that side of the cell. Under this circumstance all equilibration processes should be much faster than when transport within the sample is also present.

The change in the double layer charge at the interface between the sample and the electrolyte must also be small compared to the charge transported into or out of the bulk of the sample. This is generally the case, as can be calculated by using typical values for the double layer capacitance. Further experimental verification may be obtained by studying samples with different lengths (or radii, if cylindrical geometry is chosen). The double layer charging is not dependent on these parameters, whereas they are important in diffusion processes under certain conditions.

In order to avoid the coupling or involvement of kinetically slow processes (polarizations) at the current-supplying counterelectrode with the diffusion phenomena to be investigated, it is preferable to use a separate reference electrode for potential measurements. This reference electrode should be attached to the electrolyte near the working electrode (sample). (In some cases its position is unimportant, however, and it is not always necessary to use a reference electrode; the applied voltage across the cell may sometimes be used for this purpose.)

Early electrochemical measurements involved the diffusion of foreign atoms in small concentrations into a host lattice, a solid metal or alloy, or into liquid metals [16, 17]. To date, most work has involved the diffusion of oxygen, silver, or copper. In these cases the situation is simplified; because the concentration of the diffusing species is very low, no enhancement effects are involved. Under such circumstances one can therefore assume the laws of ideal dilute solid solutions. In some cases it was necessary to have further information concerning the concentration of the diffusing species. This could be acquired from prior experiments, or could be determined separately. In other cases, the activity-versus-concentration question could be avoided, and concentration and mobility effects separated by selecting suitable time periods, e.g. long-time behavior [18]. The ability to determine the diffusion coefficient separately has been erroneously attributed only to special geometries [19]. Methods for the determination of the diffusion coefficients of solute species in metals can be treated as special simplified cases of chemical diffusion within compounds, and they are therefore included in

the following general description of experimental methods. In simple metallic solid solutions it is usually assumed that the thermodynamic enhancement factor is equal to one. Furthermore, the coulometric titration procedure is often not practical.

Diffusion coefficients may also be determined from single galvanic cells by combining both current-supplying and potential-measuring electrochemical devices. In such cases transient signals are generally used. The first theoretical considerations of transient processes were reported by Yokota [20], and some early experiments on copper halides were carried out by Miyatani [21].

The electroneutrality requirement leads to the fact that, in principle, any transient transport measurement method involving either mobile -ionic or electronic species may be employed to determine the chemical diffusion coefficient, if the proper solution to Fick's second law is used. The mathematical solutions of the diffusion equation, by which the experimental results are analyzed, are known and tractable for a number of different cases. Amongth ose are arrangements involving potentiostatic, galvanostatic, current pulse, and ac conditions. The two monographs by Crank [22] and Carslaw & Jaeger [23], which deal with diffusion the mathematically equivalent problem of heat transfer, offer a wide variety of solutions for many initial, boundary, and geometrical conditions.

2.4.3.1 Chemical diffusion analysis using potential step mode

In the commonly used potential step mode, the activity of the electroactive species, and therefore the concentration of the mobile species, is suddenly changed from a spatially uniform distribution to one in which a new time-independent value is imposed at the phase boundary in contact with the electrolyte. A time-dependent current flows when transport occurs across the interface as species diffuse into (or out of) the bulk of the sample in response to the internal concentration gradient until a new homogeneous composition is reached. Fig. 2.15 shows the time variation of the concentration profiles of the diffusing species in the sample for linear and cylindrical geometries. It is assumed that no transport of species occurs across the phase boundary opposite from the electrolyte in the linear geometry, or across the axis in the cylindrical geometry. The observed currents are plotted on the right-hand side against linearizing time scales for short and long intervals after the start of the experiment [24, 25].

As long as the electroactive species obey the laws of infinitely dilute solutions, or as long as the activity coefficients are independent of the concentration for other reasons, the voltage change directly gives the change in the concentration at the sample-electrolyte phase boundary in accordance with Nernst's law.

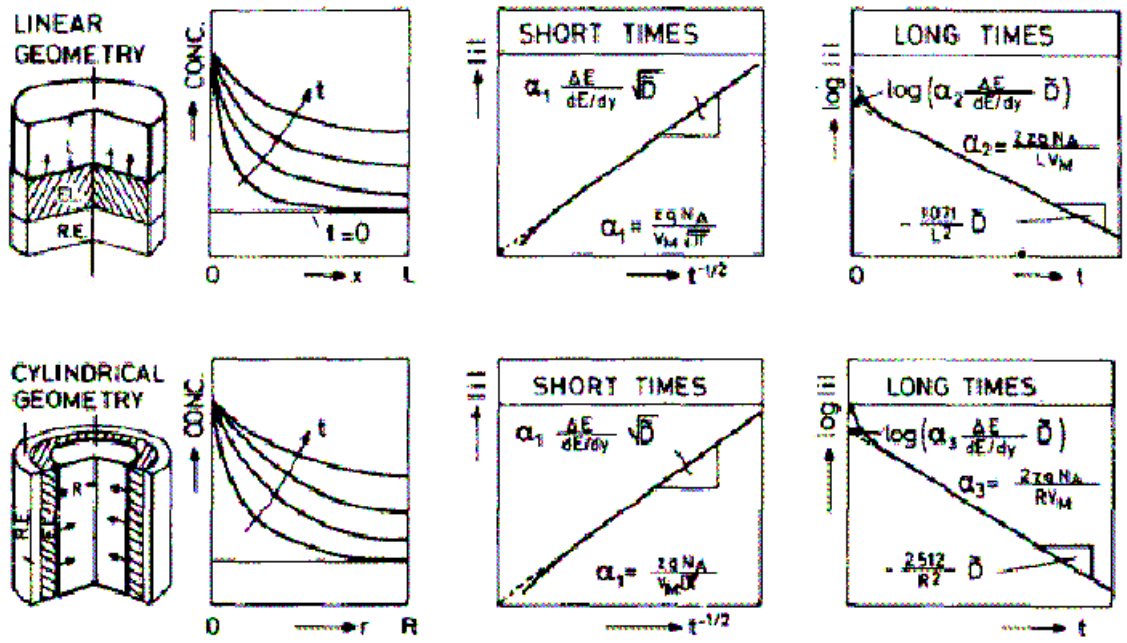

Fig. 2.15 Procedures for measuring chemical diffusion coefficients using the potential step mode with the application of voltage steps for linear and cylindrical geometric arrangements. The concentrations of the mobile ions as a function of location are shown in the second row for several times. Linearized plots of the current response are given in the 3rd and 4th row for short ($t << L^2/\tilde{D}$ or $R^2/\tilde{D}$) and long times ($t >> L^2/10\,\tilde{D}$ or $R^2/10\,\tilde{D}$).

i: current density; t: time; y: stoichiometric number; q: elementary charge; z: charge number of mobile species; Δc: total change of the overall concentration during the pulse; N_A: Avogadro's number; V_M: molar volume of the sample [24].

In many systems, these conditions may not fulfilled, especially in compounds. This difficulty is overcome by measurements of the relationship between the voltage and the composition. This may be done by changing the composition electrochemically by charge transfer across the galvanic cell. This procedure is called *coulometric titration* [26]. The relation between the changes in the cell voltage E and the concentration of the mobile species is obtained from the

slope of the curve, which varies as a function of the stoichiometry. It is assumed that the lattice of the other species remains unchanged to a first approximations, so that

$$\frac{dE}{d\ln c_m} = y\frac{dE}{dy}, \tag{2.39}$$

where c_m is the concentration of the mobile species in the crystal, and y is the stoichiometric number of species m in the sample.

Instead of determining the coulometric titration curve in separate experiments, it is possible simply to measure the total amount of charge passed through the galvanic cell during the full transient period until the new equilibrium is reached in an experimental run. This can be achieved with a sensitive but wide-range coulometer (the magnitude of the current changes by a number of orders of magnitude) or by integrating the current-versus-time curve. The relation between the charge ΔQ and the concentration change Δc_m is:

$$\Delta c_m = \Delta Q/zqV \tag{2.40}$$

where V is the sample volume and z the charge number of the mobile species.

Equations 2.39 with Nernst's equation can be used to give the kinetically important thermodynamic factor ($\partial \ln a/\partial \ln c$) by which diffusion is enhanced if a composition gradient is present in the case of predominantly electronically conducting mixed conductors,

$$\left|\frac{\partial \ln a_m}{\partial \ln c_m}\right| = -\frac{zqy}{kT}\frac{dE}{dy} \tag{2.41}$$

where a_m, stands for the activity of the mobile species, which is assumed to be the electroactive component. For the case that the mobile ionic species is not the electroactive species, the Gibbs-Duheme equation may be used to relate the activity of the electroactive species to that of the mobile one.

2.4.3.2 Chemical diffusion determination using galvanostatic mode

In the galvanostatic mode constant current is applied to the same type of cell used for the Potentiostatic mode. In this way, according to Fick's first law, a time-independent concentration gradient of the mobile species is established in the sample just inside the interface with the electrolyte, if the diffusion coefficient is independent of concentration [3]. The change in the cell voltage with time that results from this condition is measured.

An experimentally important advantage of this method is the fact that the *IR*-drop of the cell arrangement is time-independent and is merely added to the cell voltage as a constant. Thus any fixed impedances in the system do not change the shape of the voltage-time curve. Also for this reason, the location of the reference electrode is quite unimportant. This is in contrast to the potential step mode, in which an infinitely large current should pass through the cell initially in order to fulfill the boundary conditions precisely. This means that even when a reference electrode is placed very close to the sample, a considerable time-dependent *IR*-drop is superimposed upon the potentiostatically applied potential, thus reducing the effective voltage. Thus the concentration of the mobile species is not time-independently fixed at the interface. Deviations from the theoretical current-time curve in the potential step mode are usually observed for short times. The time dependence of the current at longer times may also be affected because of these initial deviations. On the other hand, the galvanostatic mode does not allow determination of the chemical diffusion coefficient from the long-time behavior, since the slope of the concentration profile, and therefore the diffusion coefficient, does not influence the measured concentration change at the interface. Another advantage in the use of the galvanostatic mode is that the charge, and therefore the overall concentration change of the sample, is easily determined from the current-time product.

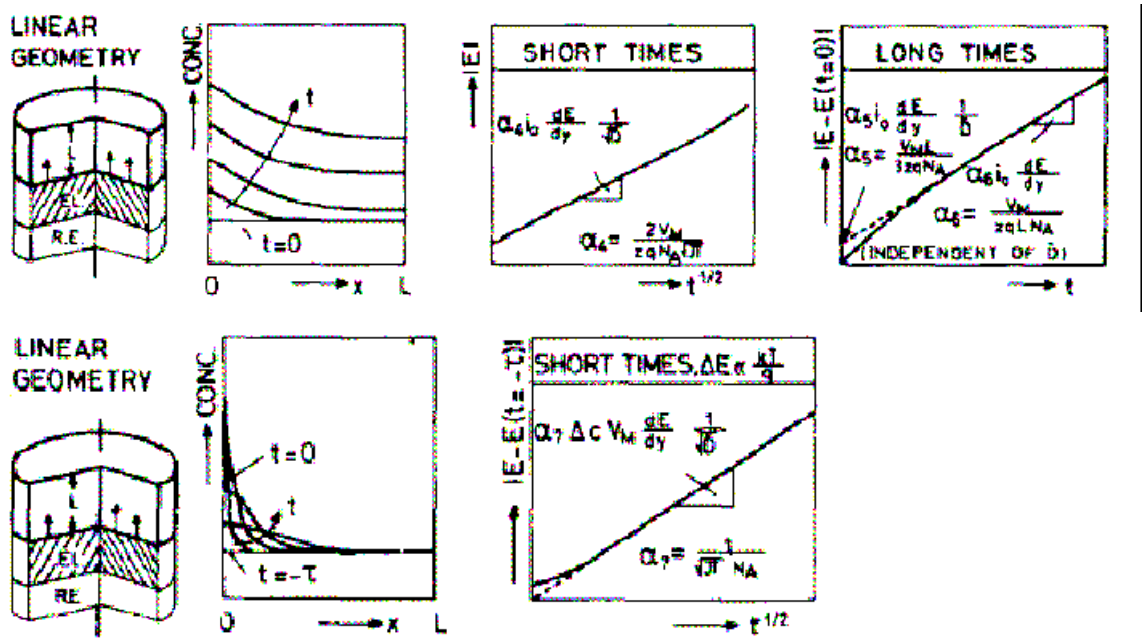

Fig. 2.16 Procedures for measuring chemical diffusion coefficients using the galvanostatic mode with the application of constant current for linear and cylindrical geometric arrangements. The concentrations of the mobile ions as a function of location are shown in the second row for several times. Linearized plots of the voltage response are given in the 3rd and 4th row for short ($t << L^2/\tilde{D}$ or $R^2/\tilde{D}$) and long times ($t >> L^2/10\,\tilde{D}$ or $R^2/10\,\tilde{D}$).

E: cell voltage; i_o: galvanostatically controlled current density; t: time; y: stoichiometric number; q: elementary charge; z: charge number of mobile species; Δc: total change of the overall concentration during the pulse; N_A: Avogadro's number; V_M: molar volume of the sample [24].

[1] E. Fuchs; H. Oppolzer; H. Rehme, *Particle Beam Microanalysis: Fundamentals, Methods and Applications*, VCH, Weinheim, 1990.

[2] John T.S. Irvine, Derek C. Sinclair, Anthony R. West, *Advanced Materials* **2**, 1990, No.3, 132.

[3] I.D. Raistrick, C. Ho, R.A. Huggins, *J. Electrochem. Soc.* **123**, (1976), 1469.

[4] Robert A. Huggins, *Ionics* 8, 2002, 300.

[5] J. R. Macdonald, *Impedance Spectroscopy*, Wiley, New York (1987)

[6] C. Wagner, Prog. Solid State Chem. **10** (1) 1975.

[7] C. Wagner, *Z. Phys. Chem., Bodenstein Festband,* pp. 177-86, (1931)

[8] C. Wagner, *Z. Phys. Chem.* Bll: 139-51, (1930)

[9] J. B.Wagner, In *Mass Transport in Oxides, Natl. Bur. Stand. Spec. Publ. 296,* ed. J. B. WachtmanA, . D. Franklin, pp. 65-77, (1968).

[10] W. Nernst, *Z. Phys. Chem.* **2**: 613-37, (1888)

[11] A.Einstein, *Ann. Phys. (4: Drude)* **17** : 549-60, (1905)

[12] A. D. LeClaire, In *Physical Chemistry,* ed. W. Jost, **10**:261-330, 1970, New York/London: Academic.

[13] Darken, L. S. 1948. *Trans. AIME* **175**: 184-201

[14] C. Wagner, In *Atom Movements,* pp. 153-73. Cleveland: Am. ~oc. Met.1951

[15] W. Weppner, R. A. Huggins, J.*Electrochem. Soc.* **124**:1569-78 (1977)

[16] H. Rickert, In *Electromotive Force Measurements in Hiyh Temperature Systems,* ed. C. B. Alcock, pp. 59-90. London:'Inst. Min, Metall (1968)

[17] D.O. Raleigh, *J. Electrochem. Soc.* **114** : 493-94 (1967)

[18] W. Weppner, R. A. Huggins, In *Electrode Materials and Processes for Energy Conversion and Storaoe.* Princeton, N.J. : Electrochem. Soc. pp. 833-46 (1977)

[19] H.Rickert, A. A. E1Miligy, In *Reactivity of Solids,* ed. J. W. Mitchell, R. C. DeVries, R. W. Roberts, P. Cannon, pp. 17-28. New York: Wiley (1969)

[20] I.Yokota, *J. Phys. Soc. Jpn.* **8**:595-602 (1953)

[21] S. Miyatani, Y. Suzuki, *J. Phys. Soc. Jpn.* **8** : 680-81 (1953)

[22] J. Crank, *The Mathematics of Diffusion.* London : Oxford Univ. Press. 347 pp. (1970)

[23] H. S. Carslaw, J. C. Jaeger, *Conduction of Heat in Solids.* London: Oxford Univ. Press. 510 pp. (1959)

[24] W. Weppner, *J. Solid State Chem.* **20**:305-14 (1977)

[25] H. Rickert, W. Weppner, Z. *Naturforsch.* **29a** : 1849-59 (1974)

[26] C. Wagner, *J. Chem. Phys. **21**:* 1819-27 (1953)

[27] A.R. West, Solid State Chemistry and it's Applications, Chapter 13, Wiley (1984)

Chapter 3

3. Experimental part: experimental methods used in this work:

3.1 X-Ray diffractometer (XRD)

The structure of all the electrolyte materials synthesized in for this work were investigated by X-ray powder diffraction using a SEIFERT XRD 3000TT and 3000PTS, with monochromized Cu Kα radiation, where Cu K_α radiation was used at room temperature with the operation conditions U = 40kV and I = 30mA. For preliminary investigation the materials used in this work were either in a powder or a circular pellet form. The initial position was adjusted with respect to the strongest reflection peak of silicon from time to time. Very thin film samples were characterized by GIXRD mode, for the electrode material deposited by sputtering method. Scans of both film and powdered samples were performed in a step-wise procedure using 0.02° 2θ steps with a 2 s hold at each position. Due to their small particle sizes, coherently scattering regions below a certain extension were not distinguishable from the amorphous background. Therefore, the evaluation of the X-ray patterns was mainly done to check the apparent crystallographic phases and estimate the particle size according to the *Scherrer* equation [1]

$$d = \frac{K\lambda}{\beta \cos\theta}$$

where d is the crystallite diameter, K is the Scherrer constant, λ is the wavelength of the Kα radiation from the Cu target, β is the integral breadth of the peak at 2θ, i.e., β is the FWHM (full width at half-maximum) for a Gaussian shaped peak and θ is the Bragg angle for the peak at 2θ.

3.2 Impedance and Kiel-Cell (Electrical conductivity measurements)

Impedance measurements were carried out with a device called A 4192A LF Hewlett Packard Impedance Analyzer which was used for the frequency region 13MHz to 5Hz. The amplitude of the perturbation was in the range 40-100 mV. For electrochemical cells with an open circuit voltage under the experimental conditions when the complex impedance has been measured, compensation of the voltage was performed during the impedance measurements. The impedance devices were placed as close as possible to the experimental setup to

minimize inductive or capacitive effects at high frequencies. Impedance measurements were repeated to avoid any stray capacitive effects.

The cell was put in a Kiel-cell, which is shown in Fig. 3.1 below for the impedance measurement.

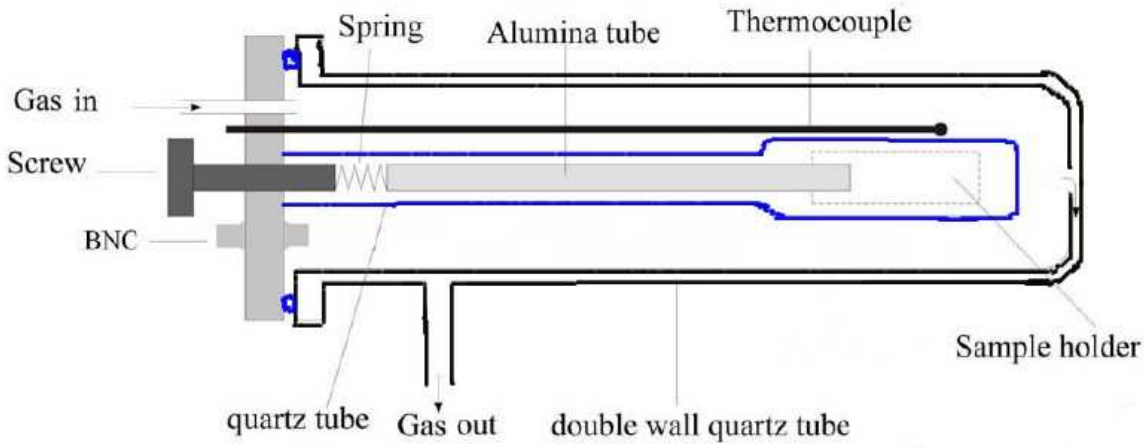

Fig. 3.1 Schematic representation of the apparatus for electrochemical measurements under defined temperature using a Kiel cell.

It can be used for measurements at temperatures up to 1000 °C, and may accomplish nominal experimental conditions for long term measurements, thus providing suitable experimental conditions for investigations on electrochemical processes. The apparatus was placed and fastened in a tubular furnace with the steel support to be maintained just outside the furnace. The temperature of the furnace was controlled with commercial NiCr / Ni thermocouples allowing the temperature to be maintained constant during the experiment. Furthermore, inside the quartz tube an additional thermocouple (Pt / Pt - 13% Rh or NiCr / Ni) placed near to the sample, for controlling the temperature of the sample under investigation. Platinum wires inside alumina tubes with small diameter were used to transfer the electrical signal from the electrochemical cell to the steel support base of the apparatus where it was further processed via BNC connectors to the electrical instruments. In the gas outlet a glycerin bubbler has been installed, and each time the apparatus has been assembled for measurements, its gas tightness has been individually checked before inserting the sample, where in most of the measurements of this work were done at normal environment, as there was no need of inert atmosphere for much of the experiments performed.

3.3 RF Sputtering

In this work sputtered layers were made using Alcatel 450 sputtering machine.This plant consists of a vacuum chamber that can be evacuated with a turbomolecular pums to a pressure of 10^{-7} mbar. In the chamber, there are three planar magnetron sputter sources. Through the magnetrons, the plasma will be fixed to the sputtering source. The outer diameter of the magnetrons is ~7.6 cm (3-inch) and the internal diameter ~1.2 cm (1/2 inch). The geometry of the magnetrons runs to a strong ring formation on the targets. The targets possess a diameter of 10 cm and a thickness of ~ 5 mm which are connected with copper disks and cooling water systems. The Sputtering machine possesses a sputter-down- geometry, which means that the targets are arranged above by the substrate. The advantage lies in a simple and fast bringing in of the substrates through a lock without interrupting the vacuum. The disadvantage is that there is possibility of depositing small particles on the substrate and that will raise formation of layers called Pinholes. This can be diminished however by very perusal and regular cleaning of the vacuum chamber. Each target is covered with a mechanical shutter to regulate around the pre-sputter. This is to be reached especially in reactive sputtering requiring a dynamic balance around. All three magnetrons are respectively with a high-frequency change tension with f = 13.56 MHz designed and can be coupled with a maximal potential of up to 600 W. The substrate plate is connected to a separate high frequency generator. So that is coupled with maximally 300 W on the substrate. 99.999% Ar gas is used as a sputtering gas, whereas for the reactive sputtering cases, O_2 and N_2 gases are let into the sputtering chamber with appropriate proportion for the material to be deposited on the substrate. All gas flows are controlled by gas flow measuring devices. The sputtering targets for this work are pressed and plated on a copper disc from different companies. To summarize in table form,

Substrate – Target distance	4 – 10 cm
Sputtering pressure	5.10^{-3} – 3.10^{-2} mbar
Power max. to	600 W
Gas flow max. to	100 sccm
Substrate temperature max.	600°C
Gas flow max. to	100 sccm

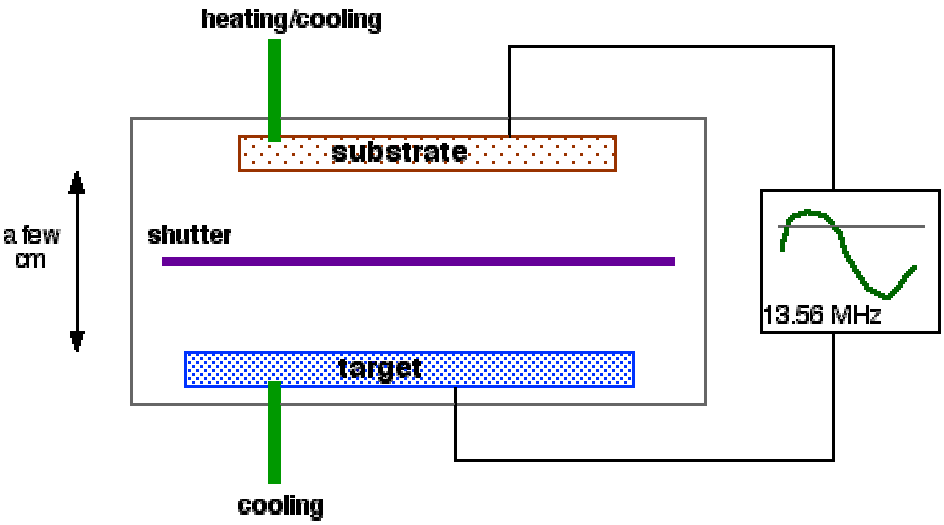

Fig.3.2 A schematic representation of RF Sputter deposition method

3.4 Electrochemical charging/discharging (Interrupted and non-interrupted current)

The Galvanostatic method and GITT were well explained in the theoretical chapter and here will be explained the experimental setups used in this work. A constant current was applied to the full cell under investigation from the potentiostat of Ionic System instruments. This instrument was controlled with a software program called Lab View^{TM}5.0 with which measurements were automatically converted to digital values in the computer. So, the cell was connected to the potentiostat and computer to obtain the information needed from the cell where a controlled current is applied and the output voltage versus time was recorded into the computer. Using this software, it was also possible to get automatic data for the GITT analysis with which one can determine the diffusion coefficient in the cell. Normally the program records the voltage against data points at the applied constant current and was later changed to voltage versus time plots from which the quantities like charge and capacitance of the charging and discharging processes can be calculated based on the applied and obtained values.

Fig.3.3 A photographic representation of the Galvanostatic/potentiostatic full measurement setups with the computer and potentiostat. The sample was kept in the Kiel-Cell where it was also used for measurements at different temperatures of the cell.

3.5 Electrochemical relaxation followed by oscilloscope

Electrochemical measurements were measured with high input impedance potentiostat PG 2.0 (Ionic Systems, Stuttgart, Germany). This device is simple and excellent in performance in both Potentiostatic and Galvanostatic mode provided with analog to digital interface converter [2, 3] The cell current in response to a step is monitored across a variable measuring resistor, using a Tektronix TDS 1002 storage oscilloscope with a Type 63 differential amplifier and Type 3B3 time base. In this manner, noise-free voltage steps with a 20-psec rise time were obtained and peak currents as high as 20 mA could be examined. In this method, a constant voltage of different values at different temperatures were applied and the response current as a function of temperature was digitally recorded for the determination of charge stored at the electrode electrolyte interface and of course the possible capacitance of the system assembled.

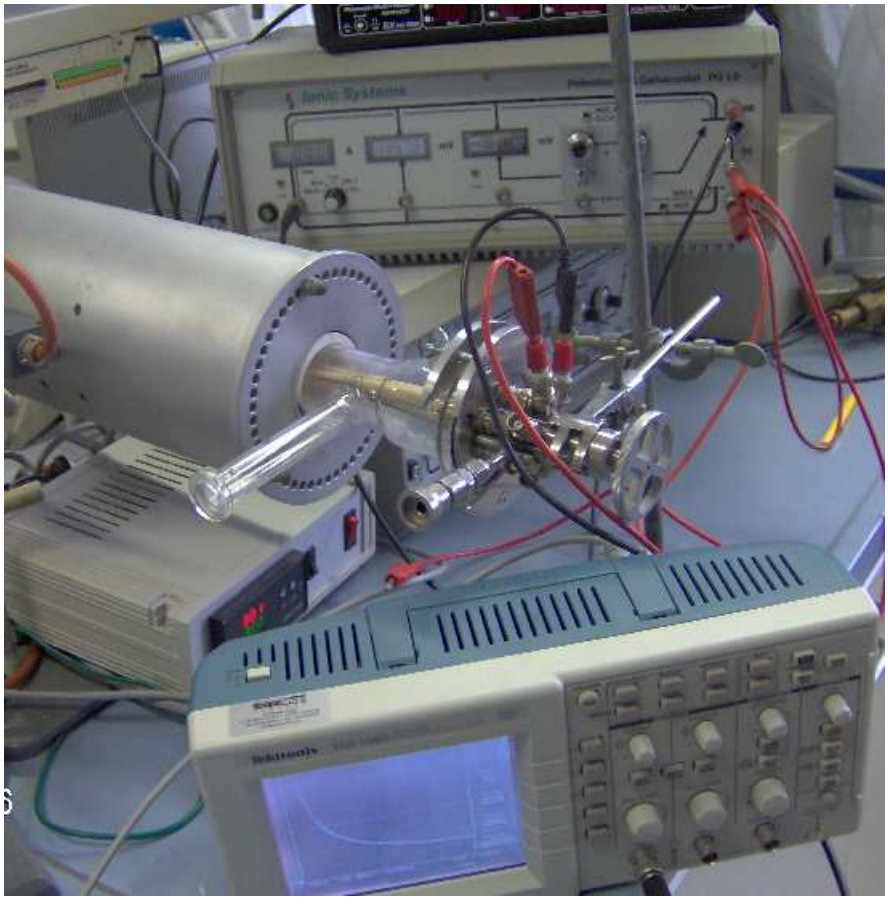

Fig.3.4 A photographic representation of the oscilloscopic full measurement setups with the heating furnace potentiostat and oscilloscopic instrument

3.6 DTA Thermal analysis

Differential thermal analysis (DTA) is a dynamic technique where the temperature difference between the material under investigation and a reference material is measured as a function of temperature. The sample typically in fine powder form is inserted into a furnace where both substance and reference material are heated up to a certain temperature. Because this is a differential technique sensitive changes can be easily registered. Thermogravimetric analysis (TGA, TG) is a technique in which the mass of a substance is measured as a function of temperature or time while substance and reference material are subjected to a temperature program. For both differential thermal analysis and thermogravimetric analysis the temperature raise is typically linear. The reference substance should show no phase transitions within the measured temperature range, have a similar heat conductivity and heat capacity as the measured one and should not react with the substance under study. A computer controlled thermal analyzer (STA 409 C NETZSCH) was used in this work, where simultaneously DTA and TGA/TG could be performed. The temperature raised with 5 °C/min if not otherwise noted. As reference material Al_2O_3 has been used. The temperature difference of substance and reference material was registered with PtPh10%-Pt (S– type) thermocouples whereas the surrounding atmosphere could be controlled by having a special gas, or left open to air.

3.7 Scanning electron microscope SEM

Images of the electrode-electrolyte cross-section to control the nature of the electrode material film deposited on the electrolyte were obtained, using a field emission gun scanning electron microscope (Philips XL 30). An acceleration voltage of 10 kV was chosen, yielding beam currents of about 18− 20 μA. Secondary electrons (SE) were detected in all cases, as they provide a better morphology contrast than the backscattered electrons (BSE).

3.8 Pressing techniques

For cold pressing of powder to form pellets or bars uniaxially or isostatic techniques have been used. Isostatically, the powder could be pressed to form bars of 6 – 10 mm diameter and up to about 15 mm in length. Uniaxially the powder was pressed to form pellets of 6 - 10mm diameter and 1 – 2 mm in thickness.

3.9 Polishing and Profilometer

Pellets were polished with a polishing machine (Rotopol-V, Struers, Copenhagen, Denmark) using polishing discs of different roughness down to 1 μm. This was used mostly to get a smooth and uniform surface on the electrolyte material before electrode deposition on it. The Dektak 8000 profilometer (Veeco) instrument was used to determine the electrode film thickness by depositing the film on a silicon wafer with the same conditions used for the deposition of the electrode material on the electrolyte surface for further measurements.

[1] J.L. Langford, *Appl Cryst* **4,** 164 (1971)

[2] http://www.ionic-systems.de/Instrumente/PG_02.html

[3] D. O. Raleigh, *J. Phys. Chem Solids.,* **26**, 320 (1965)

Chapter 4

4. Experimental part: Sample preparations and measurement methods used

This chapter describes the experimental details for the preparation of the electrode and solid electrolyte materials used for this work. The structural and electrical characterization techniques used are described with experimental parameters performed in this work.

The electrolyte materials described in this work were synthesized either by solid state reactions or sol-gel techniques.
In the case of solid state reactions, the starting materials are oxides, nitrates, carbonates of transition metals, lanthanum trioxide and titanium dioxides (dried in a furnace and kept in dry box before use). The sintering temperatures were from 700°C to 1100°C and the reaction processes took place in air with proper monitoring to avoid moisture presence with observable color changes and weight measuring after keeping in air for long time and drying in a furnace. Sol-gel technique was used only for the preparation of NASICON and is well explained under the preparation of NASICON.

4.1 Electrode materials and preparations

In this section, the preparation of electrodes for this work will be explained. The electrode materials used are Pt, Au and $Li_{1-x}CoO_2$. And also for the powder mixture samples, graphite was used, which is of course ready-made powder purchased from Aldrich. The Pt and Au electrodes were prepared by pasting on the electrolyte sides for some measurements and also using sputtering techniques to make a thin solid film of Au and Pt to be used as a current collector as well as an active electrode in some cases. Thin film $Li_{1-x}CoO_2$ was also used as an active electrode material. The $Li_{1-x}CoO_2$ was made in a sputtering thin film preparation method. The sputtering was carried out by RF magnetron (Alcatel 450, France). After each film deposition, all the film thickness was measured using a surface Profilometer (Dektak 8000).

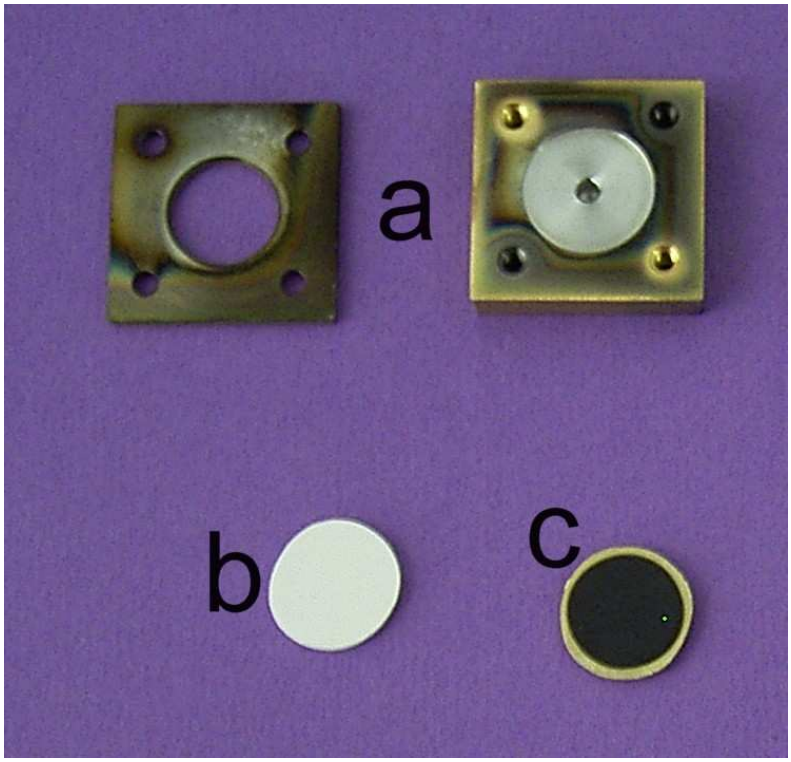

Fig. 4.1 Photographic representation of the electrode preparation by sputtering method. (a) the masks used for sputtering pellets, (b) polished garnet pellet before sputtering and (c) $LiCoO_2$ electrode sputtered on garnet electrolyte pellet.

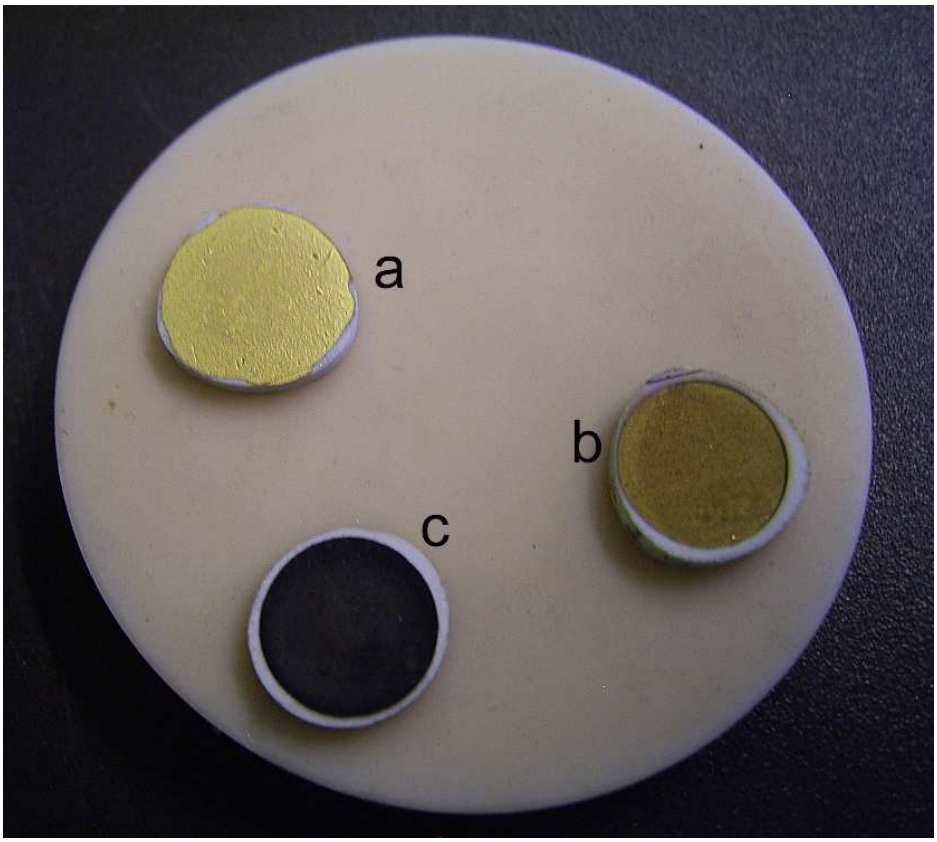

Fig. 4.2 Photographic representation of the electrodes made by sputtering and paste methods. (a) gold pasted on garnet pellet, (b) gold sputtered on garnet pellet and (c) $LiCoO_2$ electrode sputtered on garnet electrolyte pellet.

4.2 Electrolyte materials and their preparations

For this work only solid electrolytes are used. It is clear that the ionic conductivities of liquids are higher than solids, but there are many advantages of solid electrolytes over liquids. For example the stability in different environmental conditions, easy to handle with less danger in case of cell damage, with no leakage problem compared to the liquid system. There are many solid ionic conducting electrolytes, mostly are of lithium, sodium and potassium ion conducting electrolytes. The most commonly used solid electrolytes include, the Na^+ ion containing Nasicon, Nafion, β – alumina and the Li^+ ion containing – Lisipo, Lipon, $LiAlTi(PO)_4$ family, the Garnet-like family and the Ag^+ ion ionic conducting electrolyte families of AgBr, AgI, Ag_4RbI_5. For this work, the self synthesized Nasicon, Garnet, Nasicon-type LiAlTi(PO4) and the commercial available AgI were experimented.

4.2.1 Nasicon ($Na_{1+x}Zr_2Si_xP_{3-x}O_{12}$) solid electrolyte

The fast sodium ion conductor electrolyte, Nasicon was well explained [1] and it was prepared by sol gel method for this work with x = 2 [1, 2]. Nasicon was also prepared using the solid state reaction method but the product of sol-gel was found to be with very fine particle and less impurity when checked with XRD. So the sol-gel method was chosen over the solid state reaction method for the synthesis of Nasicon.

The required amount of each starting material was taken to get the proper composition based on the chemical formula of the product. First the required amounts of solid powders of NaOH (Merck, 99%) and $NH_4H_2PO_4$ (Aldrich, 99%) were dissolved with 250 ml of distilled water in a beaker separately with 20% excess NaOH to compensate for the loss of Na later in the heating processes. On a separate beaker, liquid $Zr(C_3H_7O)_4$ (Aldrich, 70%) and $Si(C_2H_5O)_4$ (Alfa, 99%) were dissolved with 250 ml of pure ethanol which was completely clean of possible H_2O with prior ethanol distillation. The liquid $Zr(C_3H_7O)_4$ and $Si(C_2H_5O)_4$ were kept in a glove box to avoid the possible formation of ZrO_2 and SiO_2 as these liquid materials are easily oxidizable in the presence of oxygen and water. Then the Na and P ion containing sample was then put in refluxing beaker as can be seen on Fig. 4.3 below. Then the Si and Zr containing sample was let into the refluxing beaker drop by drop while the refluxing was continuing with continuous stirring at an optimal reaction temperature controlled at 80°C. The reaction in the refluxing beaker at 80°C was run for 3 hours and then the gel formed was filtered using a filter paper and then dried in a drying oven at 120°C overnight. The dried

powder was then grained in a mortal to obtain fine particles size and calcined by keeping the powder to 400°C for 1 h and then to 900°C for 12 h with heating and cooling rates of 2°C/min. Then the powder was ball milled several times in zirconia cups with isopropanol and dried again at 120°C overnight. Finally, the powder was pressed isostaticaly (1 h at 130 KN) to form bars, which were then sintered inside alumina containers at 1100°C for 1 h, with heating and cooling rate of 2°C/min. The bars were afterwards cut into discs, which were polished and ready for the measurements to take place.

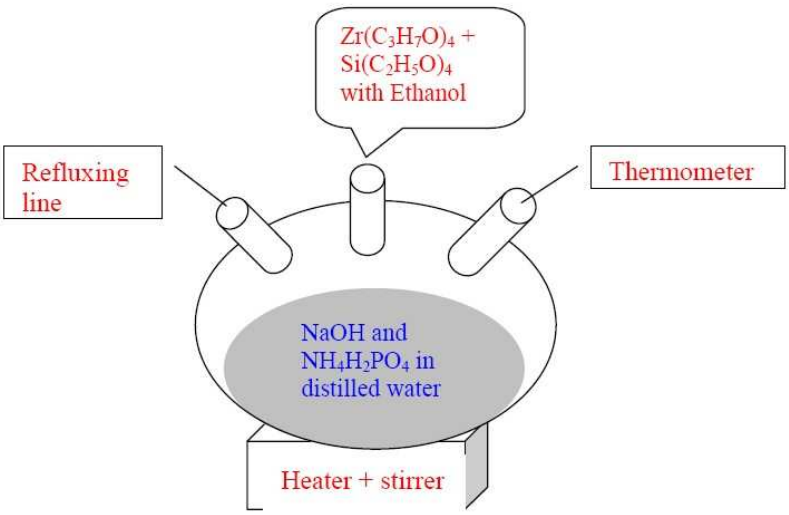

Fig. 4.3 Schematic show of the Nasicon preparation using a sol-gel technique. The reaction steps follow by dissolving NaOH and $NH_4H_2PO_4$ with distilled water (~ 250 ml) and putting inside the refluxing beaker which follows the slow addition of the $Zr(C_3H_7O)_4$ and $Si(C_2H_5O)_4$ solution dissolved in ethanol (~ 250 ml) with continuous stirring at a reaction temperature of 80°C for 2 to 3 hrs.

4.2.2 Nasicon type [$Li_{1+x}M_xTi_{2-x}(PO_4)_3$] solid electrolyte

Lithium ion conductors with high conductivity are especially attractive materials for the development of rechargeable batteries and CO_2 sensors [3, 4]. It has already been reported [5] that the conductivity of LiTi(PO4) increases noticeably if the Ti^{4+} cation is partially substituted by a cation such as M^{3+} = Sc^{3+}, Al^{3+}, Y^{3+}, Fe^{3+} or La^{3+}. In this work, only the one with Al^{3+} was prepared and measured. Synthesized compounds of the $Li_{1+x}M_xTi_{2-x}(PO_4)_3$ system are known as low temperature solid electrolytes with Li^+ ion transport [5]. The values of the ionic conductivity, their activation energy, and the lattice constants of the compounds of this system depend on the ionic radius of the substituting metal and on the x value.
At 298 K in a low frequency electric field (v = 10 kHz) the value of the total conductivity of the compound with M = Al was found to be $7x10^{-4}$ S/m [6, 7]. Its good chemical stability in air and high ionic conductivity at room temperature stimulate further investigation of this material.

Table 4.1 Total and bulk conductivities of the nasicon type electrolyte compound with different M values measured [8].

The values of σ_b, σ_{tot}, ΔE_b and ΔE_{tot} of the compounds of $Li_{1+x}M_xTi_{2-x}(PO_4)_3$				
Composition	σ_{tot} at 450 K (Scm^{-1})	ΔE_{tot} (eV)	σ_b at 300 K (Scm^{-1})	ΔE_b (eV)
$Li_{1.3}Sc_{0.3}Ti_{1.7}(PO_4)_3$	9.6×10^{-5}	0.42	2.1×10^{-4}	0.20
$Li_{1.3}Al_{0.3}Ti_{1.7}(PO_4)_3$	9.0×10^{-4}	0.33	3.5×10^{-3}	0.30
$Li_{1.3}Fe_{0.3}Ti_{1.7}(PO_4)_3$	1.2×10^{-3}	0.40	2.2×10^{-3}	0.31
$Li_{1.3}Y_{0.3}Ti_{1.7}(PO_4)_3$	8.0×10^{-4}	0.30	9.4×10^{-4}	0.19

Based on this exciting conductivity report of the literature, the Nasicon type solid electrolyte was prepared and analyzed in this work too. It has also showed a good ionic conductivity in this work too, which is comparable with the literature values mentioned above. Then it was used in some experiments with powder mixed (gold and carbon as electrode) technique for the supercapacitors preparation. The results obtained are discussed in the result and discussion part and here is only the general overview and preparation of the electrolyte using the solid state reaction synthesis method.

In this work the composition of $Li_{1.3}M_{0.3}Ti_{1.7}(PO_4)_3$ with x = 0.3 [13] of the general formula $Li_{1+x}M_xTi_{2-x}(PO_4)_3$ was prepared using the solid state reaction synthesis method. Using appropriate amounts of high purity (>99.9%) $LiNO_3$, TiO_2, Al_2O_3, and $NH_4H_2PO_4$ all obtained from Aldrich. To obtain the right stochiometry of the required electrolyte compound was then weighed. 10 wt% excess of $LiNO_3$ was added to compensate loss of Li due to volatilization of Li_2O during the preparation. The mixtures were then mixed in a ball-milling beaker of zirconia using isopropanol. Then it was ball milled for 6 and 12 hours (in two different beakers for comparisons and different analysis) using a gate mortal with a pestle, which followed by drying in open air inside a hood. Then it was followed by calcinations in air at 900°C for 2 hrs and then the powder was pressed isostatically into pellets, which was then annealed at 950°C and 1100°C for 24 hrs and 2 hrs respectively by covering the pellet with powder of the same material to reduce the loss of lithium because of volatilization. The heating and cooling rates were 2°C/minute for both calcining and sintering steps. After that the pellet was polished and ready for XRD and other electrical measurements.

The Process is summarized in the following flow-chart:

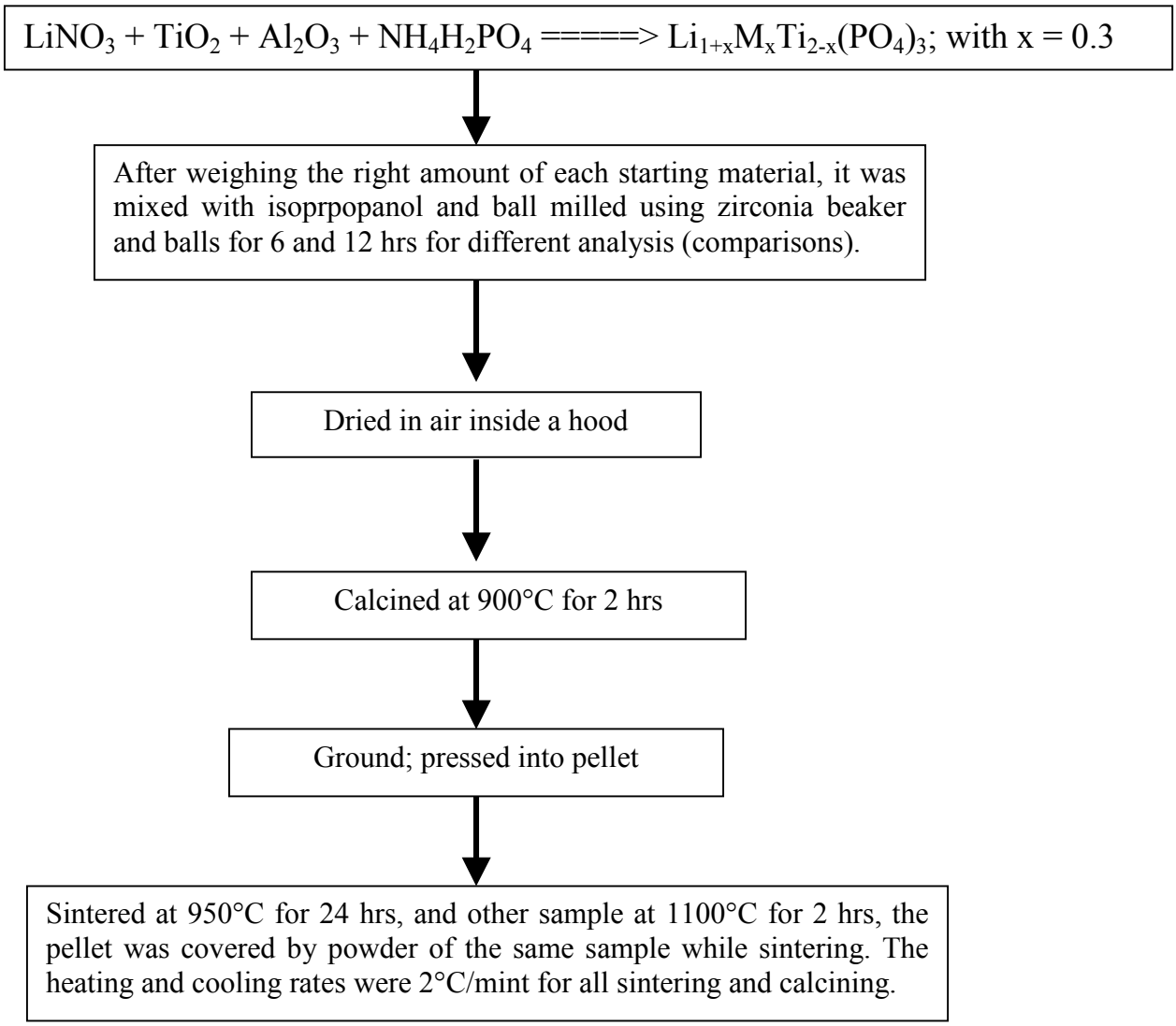

Fig. 4.4 Flow chart for the processes of Nasicon Type ($Li_{1+x}M_xTi_{2-x}(PO_4)_3$; with x = 0.3) *electrolyte preparation.*

4.2.3 Garnet ($Li_6BaLa_2Ta_2O_{12}$) solid electrolyte

Garnets are orthosilicates with the general structural formula, $A_3^{II} B_2^{III} (SiO_4)_3$, where A and B refer to eight-coordinated and six-coordinated cation sites [8, 9], respectively. SiO_4 tetrahedral are isolated and connected to each other through ionic bonds with the interstitial B-cations. A large variety of complex oxides have also been found to crystallize in garnet-like structures with other elements replacing silicon, for example, $A_3B_5O_{12}$ (A=Ca, Mg, Y, or Ln=La, or rare earth; B= Al, Fe, Ga, Ge, Mn, Ni, V). Compound with the chemical formula $Li_6ALa_2Ta_2O_{12}$ (A=Sr, Ba) were also found to have a garnet-like structure [10, 11, 12]. In this work the composition of $Li_6BaLa_2Ta_2O_{12}$ was prepared using the solid state reaction synthesis method.

Using appropriate amounts of high purity (>99.9%) La_2O_3 (pre-dried at 900°C for 24 h), $LiOH.H_2O$, $Ba(NO_3)_2$, and Ta_2O_5 obtained from Fluka or Aldrich, to obtain the right stochiometry of the required electrolyte compound, was then weighed. 10 wt% excess of $LiOH.H_2O$ was added to compensate loss due to volatilization of Li_2O during the preparation. The mixtures were then mixed in a ball-milling beaker of zirconia using isopropanol. Then it was ball milled for 12 hours using a gate mortal with a pestle, which followed by drying in open air inside a hood. Then it was followed by calcinations in air at 700°C for 24 hrs and then the powder was pressed isostatically into pellets, which was then annealed at 950°C for 24 h by covering the pellet with powder of the same material to reduce the loss of lithium because of volatilization.

The Process is shown in the following flow-chart:

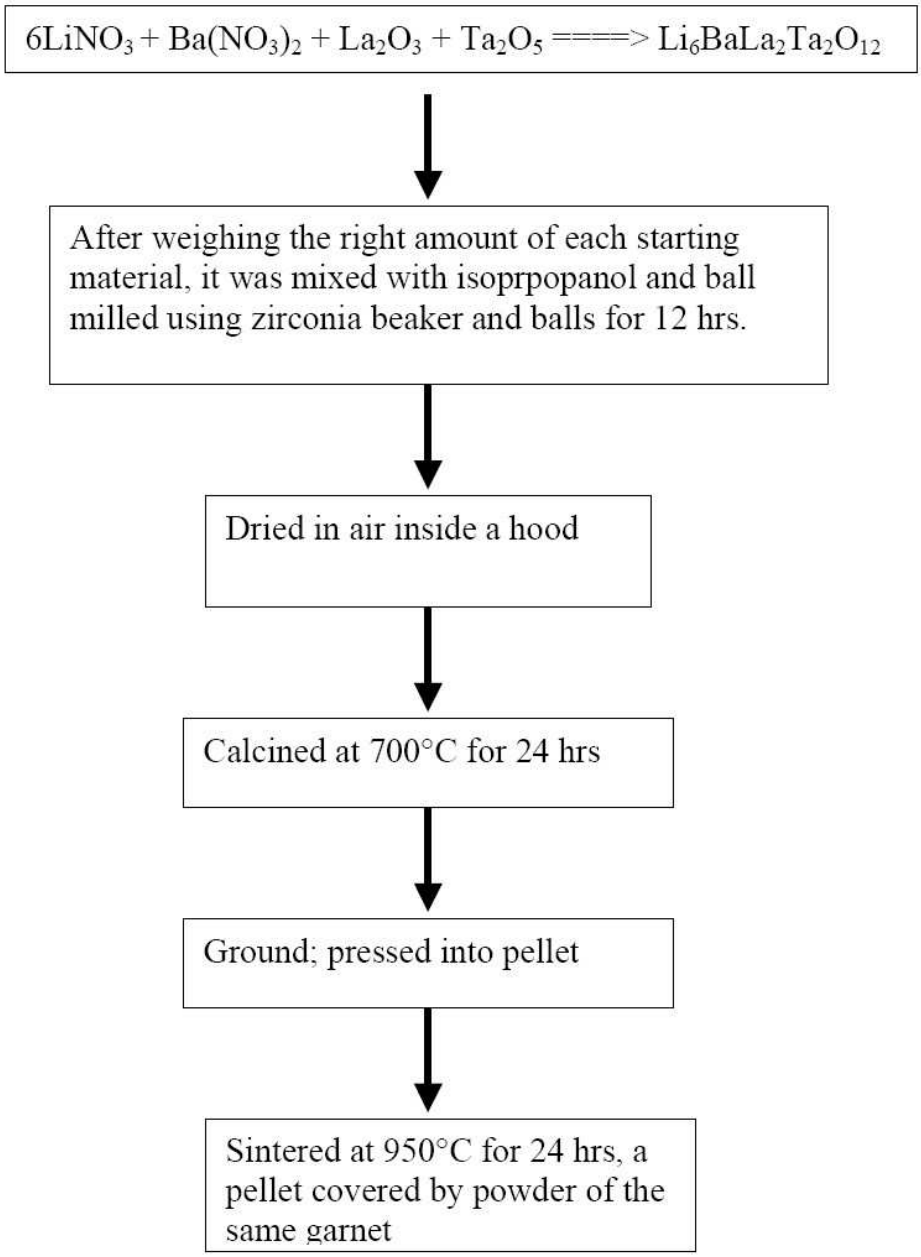

Fig. 4.5 Flow chart for the processes of garnet electrolyte preparation.

The final sintered pellet was then cut with appropriate size for the next characterization processes to follow. The pellet was very dense and smooth at the surfaces of the cut side, which creates good contact for electrode films made on it.

[1] V. Leonhard, H. Erdmann, M. Ilgenstein, K. Cammann, J. Krause, Sensors and Actuators B 18-19, 329-332 (1994)

[2] E. Steudel, Dr.-Ing. Thesis, University of Kiel (1998)

[3] Brousely M, Planchat JP, Rigobert G. Virey D, Sarre G., Journal of Power Sources **68**, 8 (1997)

[4] Subramanian MA, Subramanian R., Clearfield A., Solid State Ionics, 18-19, 562 (1986)

[5] V. Thangadurai, A. K. Shukla and J. Gopalakrishnan, J. Mater. Chem., **9**, 739–741 (1999)

[6] Aono H, Sugimoto E, Sadaoka Y, Imanaka N, Adachi G, J. Electrochm. Soc., **137**, 1023 (1990)

[7] Adachi G, Imanaka N, Aono H, Sugimoto E, Sadaoka Y, Yasuda N, Hara T, Nagata M, US patent 4,985,317, Jan 15 (1991)

[8] H. Y-P. Hong, Mat. Res. Bull.**10**, 635 (1975)

[9] A. F. Wells, Structural Inorganic Chemistry, 5th ed., Oxford Science Publications, Clarendon Press, Oxford, UK 1984.

[10] V. Thangadurai, W, Weppner, *Adv. Funct. Mater*. **15**, No. 1, January 2000

[11] S. Stramare, V. Thangadurai, and W. Weppner, *Chem. Mater.*, ***15,*** 3974-3990 (2003)

[12] V. Thangadurai, and W. Weppner, J. of Solid State Chemistry, **179**, 974–984 (2006)

[13] K. Arbi, S. Mandal, J. M. Rojo and J. Sanz, Chem. Mater., **14**, 1091-1097 (2002)

Chapter 5

5. Results and Discussion:

5.1 Electrode materials: preparations and some measured results.

In most of this work the electrode used was thin film $LiCoO_2$ prepared using the RF sputtering method. But for some part, $LiCoO_2$ with PVDF and carbon black was made using the tape casting method like the way used for battery systems. But as the contact between the casted film and the solid electrolyte in pellet form was very bad, the conductivity measured was so bad and the experiment was suspended. Other electrodes used were gold and platinum in both paste and sputtered-thin film forms. The pasted ones were used only for the electrolyte conductivity measurements. The sputtered ones were made on $LiCoO_2$ side when the full cell was made for further analysis.

$LiCoO_2$ was sputtered, as explained in the experimental part, on different electrolyte materials. The film thickness was measured using the profilometer after each deposition, where a film is made on a silicon wafer with the same sputtering conditions at the same time.

Most of the $LiCoO_2$ films were 650 – 800 nm when sputtered for 11 hours and 1400 –1500 nm when sputtered for 16 hours. But for most of this work, it was used those films sputtered for 11 hours, means with a thickness of ~ 700 nm range. On the other hand, the film thickness of gold and platinum was measured to be ~ 450 nm sputtered for 5 minutes and ~ 650 nm when sputtered for 10 minutes. In this case, the 5 minute sputtered film with a thickness of ~ 450 nm was used for most of this work. In all cases, the sputtering conditions were the same. The sputtering chamber pressure was ~ 10^{-5} mbar and with a substrate-target distance of ~ 7 cm. The maximum power was ~ 600 W while the gas flow into the sputtering chamber was ~ 100 sccm. For the $LiCoO_2$ film preparation, oxygen gas was also flown into the chamber used as a reaction gas while only argon gas was used when Au or Pt was sputtered.

The sputtering steps of the electrode films are shown in Fig. 5.1.

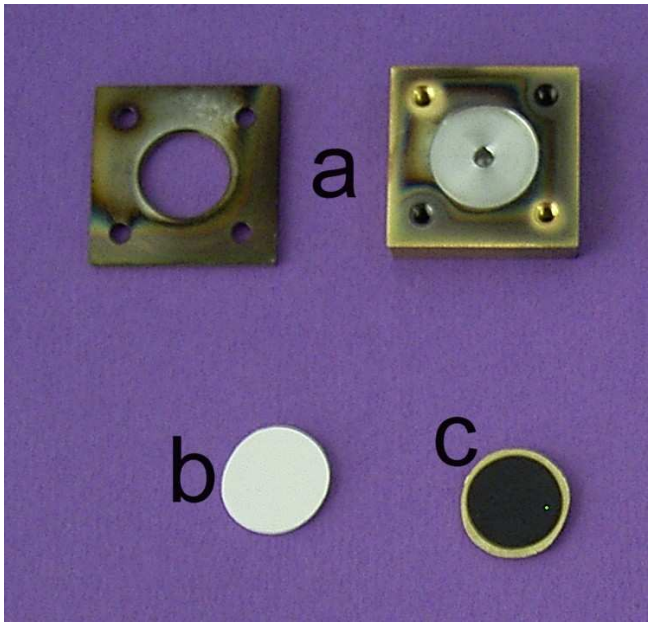

Fig. 5.1 Photographic representation of $LiCoO_2$ electrode made by sputtering method. (a) masks used for sputtering pellets, (b) polished garnet pellet before sputtering and (c) $LiCoO_2$ electrode sputtered on garnet electrolyte pellet.

The sputtering steps of gold and platinum electrodes were the same for $LiCoO_2$ demonstrated in the picture above. The only difference is that the $LiCoO_2$ has to be sintered after deposition to make it crystalline as the deposited film before heating is usually amorphous form [1]. Gracing incident XRD measurements were done before and after sintering of $LiCoO_2$ just to control the nature of the film whether it was amorphous or crystalline. The sintering duration was 2 hours at 700°C with heating and cooling rates of 1 °C/min.

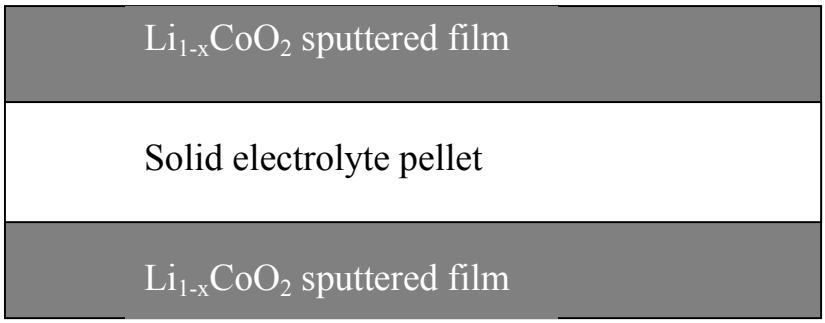

Fig. 5.2 Schematic representation of $LiCoO_2$ electrode made by sputtering method for the symmetric cell of supercapacitors.

When conductivity of the system shown in Fig. 5.2 was measured, it showed a poor contact between the $LiCoO_2$ and the platinum/gold sheet, used as current collector, attached to it by using the Kiel-cell where there was a continuous gas flow. To prevent that, Au or Pt was deposited on to the $LiCoO_2$ film to be used as a current collector where there is a sufficiently good contact area. Therefore, after each $LiCoO_2$ film deposition, it was sintered to 700°C and then Au/Pt was deposited on it. In some experiments it was tried to sputter Au immediately after $LiCoO_2$ deposition, before sintering, and then later sintered all the system together. In this case it was visible, even with eyes, that there was segregation of Au into $LiCoO_2$ which became brown and that experiment had to be stopped.

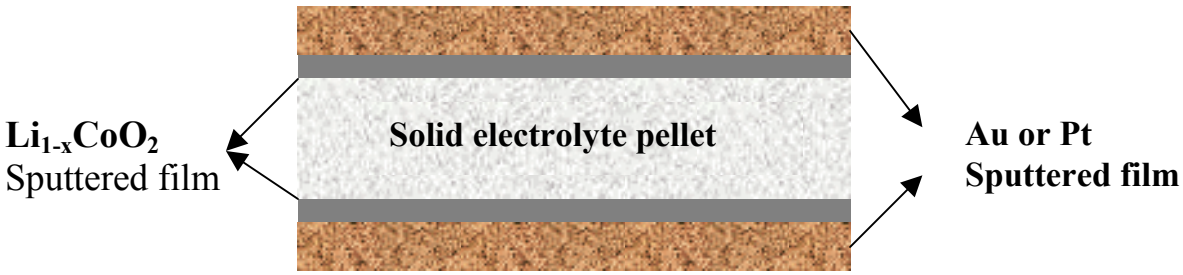

Fig. 5.3 Schematic representation of $LiCoO_2$ and Pt/Au electrode made by sputtering method on a solid electrolyte pellet for the symmetric cell of supercapacitors. Pt/Au were sputtered after the sputtered $LiCoO_2$ was sintered at 700°C.

Other electrodes used in this work were $LiCoO_2$, Au and carbon in different ways. That was used in a powder mixed form and will be explained in the electrolyte and whole cell evaluation later in this chapter.

5.2 Electrolytes used and their analysis results

5.2.1 XRD and Impedance analysis of Nasicon ($Na_{1+x}Zr_2Si_xP_{3-x}O_{12}$) solid electrolyte

As mentioned in the material preparation part, Nasicon ($Na_{1+x}Zr_2Si_xP_{3-x}O_{12}$) with x = 2 has shown better conductivity [2] and it was the same stochiometry prepared and analyzed in this work. The fast solid state ionic conducting electrolyte [3] was prepared using the sol-gel method where a very fine and homogenous powder was obtained. For the control of the purity

of the solid electrolyte prepared by all methods used in this experiment, there was always an XRD measurement taken after calcinations, sintering and even after long period of time to check the long-term stability of the material in the working environment. A SEIFERT XRD 3000TT and 3000PTS, with monochromized Cu K_α radiation, where Cu K_α radiation was used at room temperature with the operation conditions U = 40kV and I = 30mA was used for all measurements. Samples were analyzed in both powder and pellet forms. Most of the XRD graphs of Nasicon showed a very noisy background but when compared with literature scans, the most important lines were there and the lines of unreacted particles became smaller when the samples were sintered longer and higher temperatures.

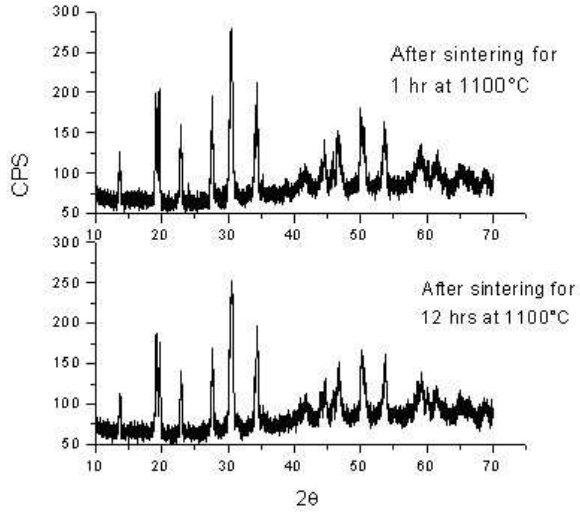

Fig. 5.4 XRD scans of Nasicon after sintering at 1100 °C with two different sintering times.

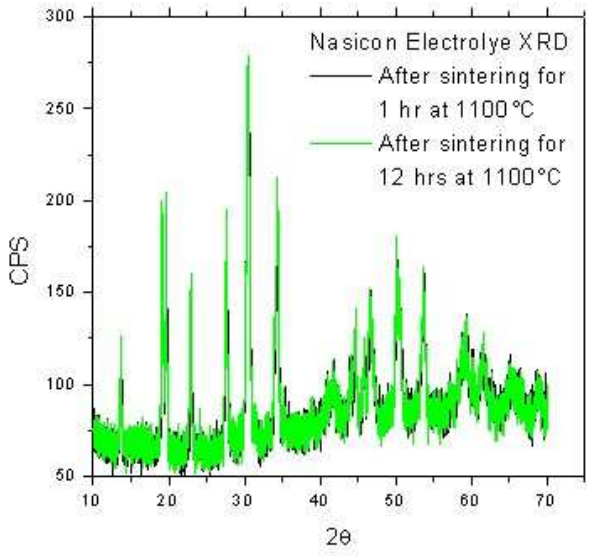

Fig. 5.5 XRD scans of Nasicon after sintering at 1100 °C with two different sintering times when they are put in one plot to show the temperature and time dependence of the sintering.

As can be seen from Figs. 5.4 and 5.5 the longer the sintering time, the less the additional phases. Other than that, there is no significant change observed between these two different durations of sintering. As can bee seen from the conductivity measurements as well, the difference is very small with respect to sintering time. But it has a big effect on the sintering temperatures.

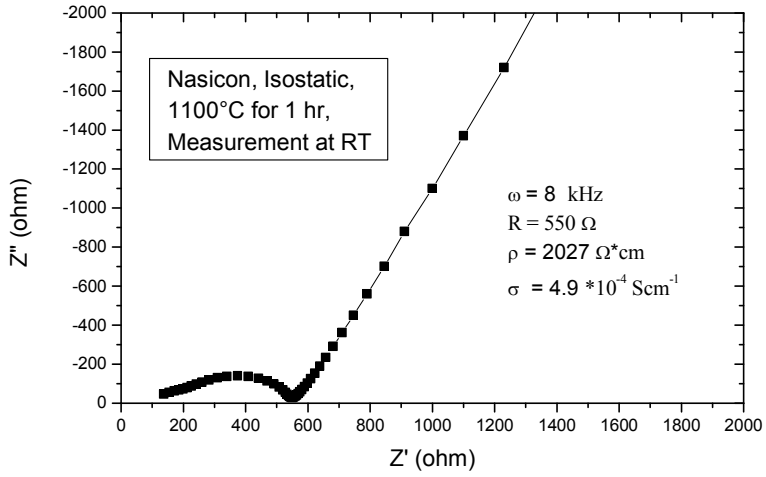

Fig. 5.6 Impedance (Nyquist) plot of Nasicon pellet with Au electrode after sintering at 1100 °C for 1 hr measured at room temperature.

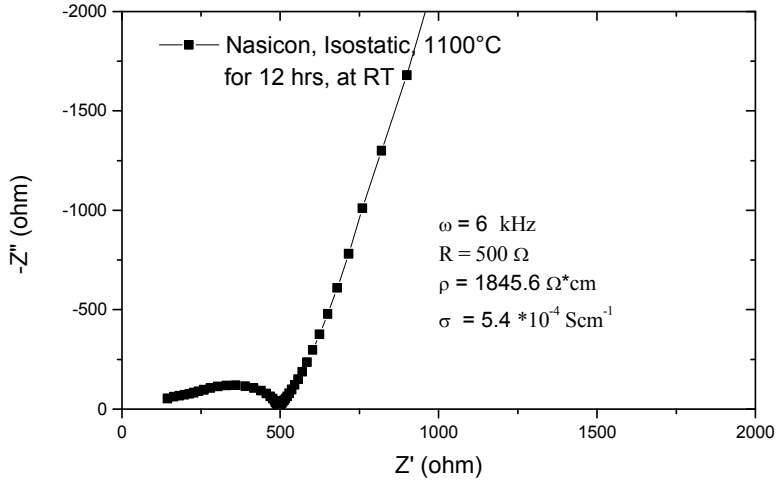

Fig. 5.7 Impedance (Nyquist) plot of Nasicon pellet with Au electrode on both sides, after sintering at 1100 °C for 12 hrs, measured at room temperature.

From Figs. 5.6 and 5.7 it is possible to see that the impedance plot shows only a very small difference in the conductivity because of the duration of sintering. The one sintered for only 1 hour at 1100°C showed a conductivity of 4.9 $*10^{-4}$ S/cm while the other one sintered for 12 hours at 1100°C showed a conductivity of 5.4 $*10^{-4}$ S/cm. Based on these results, most of the samples for the rest of experimental works were sintered for 12 hours, though the difference is not significant.

The impedances of these two samples were measured at some different temperatures to see the temperature dependence and plotted in Arrhenius plot. At all the temperatures measured, there was a small increase in conductivity of the sample sintered for longer time at a temperature of 1100°C as shown in Fig. 5.8. It shows that the conductivity result of this experiment is reasonably comparable with literature values and even at lower temperatures better than the literature values.

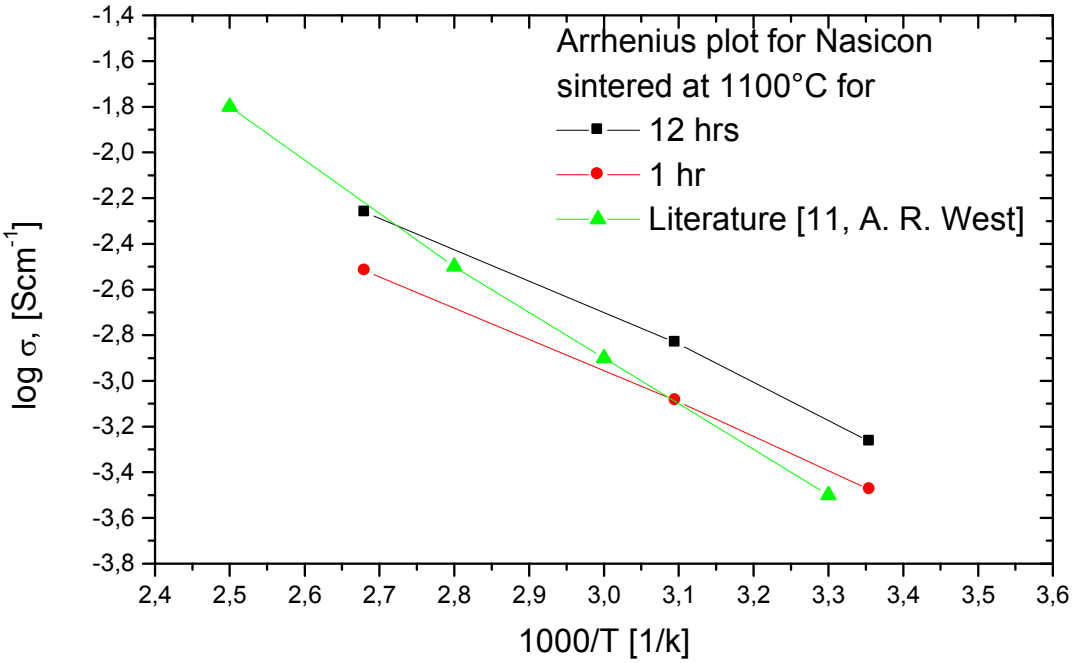

Fig. 5.8 Arrhenius plot of Nasicon pellet with Au electrode on both sides, after sintering at 1100 °C for 1 and 12 hrs, measured at RT, 50 and 100°C plotted together with literature values.

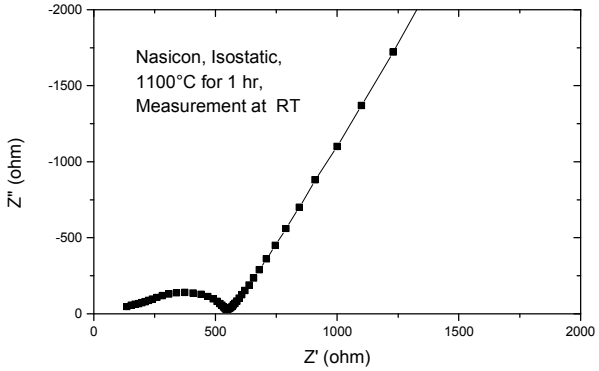

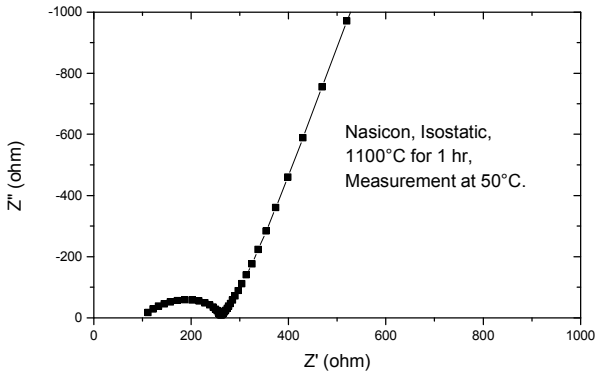

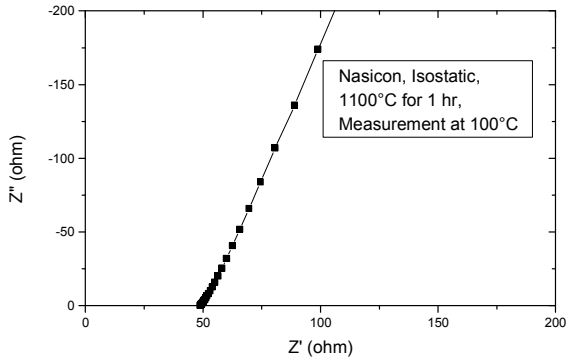

Fig. 5.9 Impedance (Nyquist) plot of Nasicon pellet with Au electrode on both sides, after sintering at 1100 °C for 1 hr, measured at RT, 50 and 100°C.

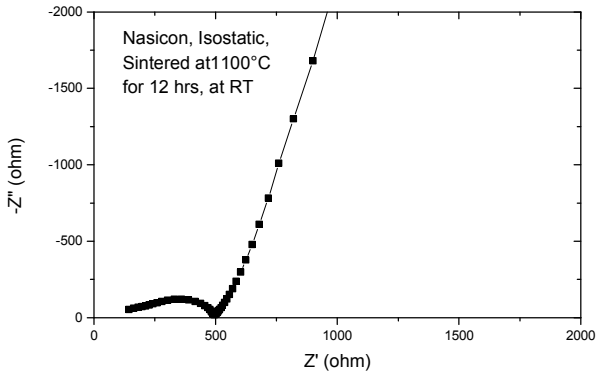

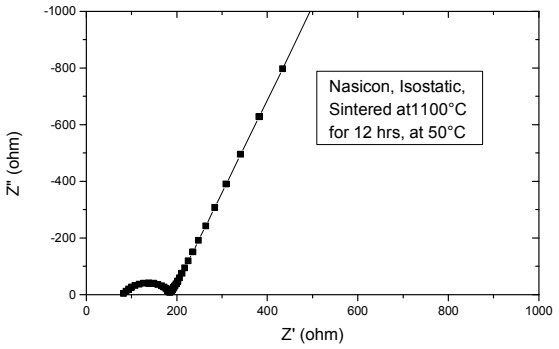

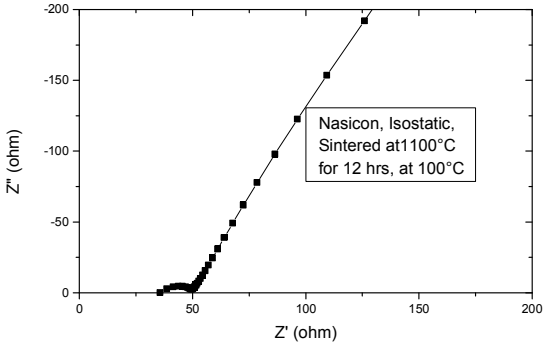

Fig. 5.10 Impedance (Nyquist) plot of Nasicon pellet with Au electrode on both sides, after sintering at 1100 °C for 12 hrs, measured at RT, 50 and 100°C.

Figures 5.9 and 5.10 show the comparison of the Nyquist plots of the two different nasicon electrolyte samples as a function of temperature. The linear increase in conductivity as the increase of temperature is observed in both samples, which are sintered at the same temperature for different sintering times. These impedance analyses showed a good ionic conductivity of the nasicon solid electrolyte and then these samples were used for the supercapacitors cell preparation.

Then, after a good ionic conductor nasicon was obtained, different forms of a capacitor were assembled. First a symmetrical cell of Nasicon as electrolyte and graphite as electrode on both sides was assembled. But the contact between graphite powder electrodes pressed on both sides of the nasicon pellet was very poor and the impedance showed an over flow. Then another way was designed to have powder mixtures of graphite and Nasicon with different weight percentages. In parallel, there was a sample prepared with a mixture of nasicon powder with Au to get a high surface area, which is the most advantage to get a higher capacitance at the electrode and electrolyte interfaces.

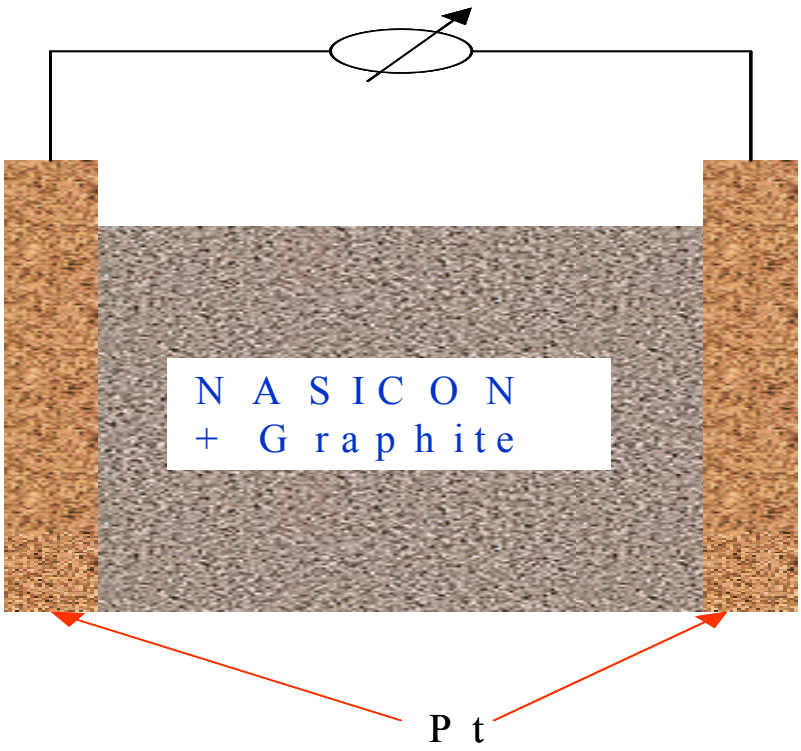

Fig. 5.11 Graphical illustration of the assembled cell with Nasicon and Graphite powders pressed into a pellet at different weight percentages supported by Au or Pt as current collectors. The same arrangement was also used with Au mixed with Nasicon instead of graphite.

The Nasicon-graphite powder mixtures with different volume percentages of 2, 5, 10 and 20 % graphite were prepared. The right volume percentage of these powders was mixed using isopropanol to have a uniform mixture. Then it was dried at 120 °C and then pressed into pellet, but the pellets were not dense enough and were sintered at higher temperatures to get them dens. The 10 and 20 volume percent of graphite showed high electronic conductivity, short circuited, and only the 2 and 5 % were tried to be measured for the ionic conductivity measurements. Here the problem was that without sintering, the resistance was too high and when sintered the pellet was always cracked and unable to be used for further measurements.

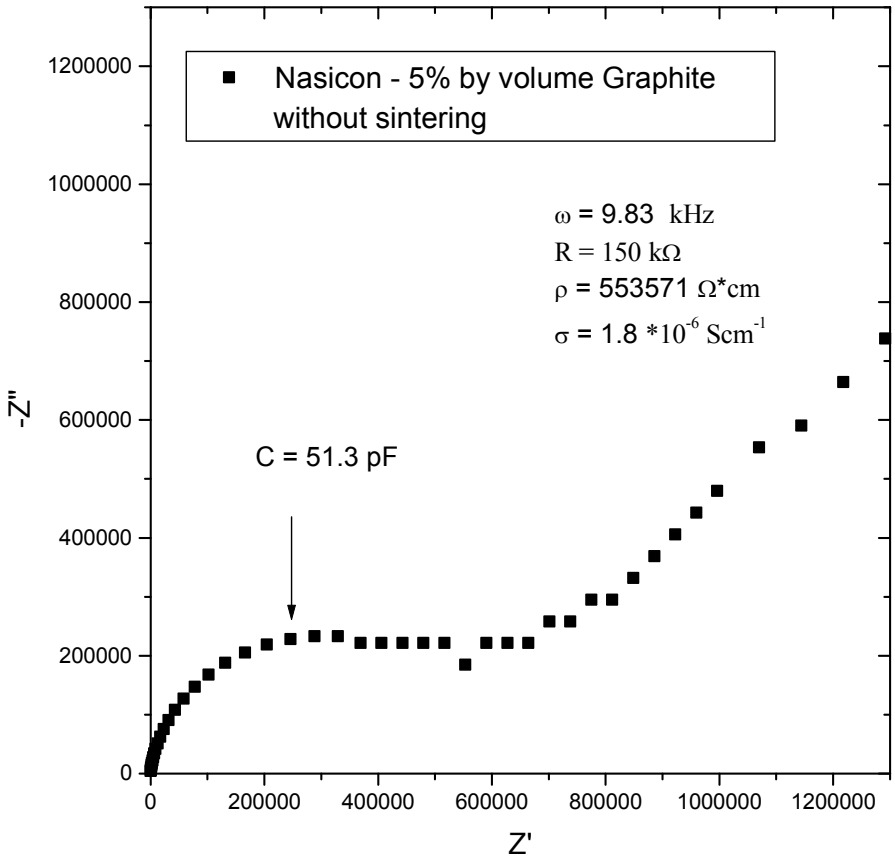

Fig 5.12 Impedance (Nyquist) plot of Nasicon-graphite powder mixed pellet measured after uniaxial pressing without any further sintering. The units of the plot are in Ω.cm.

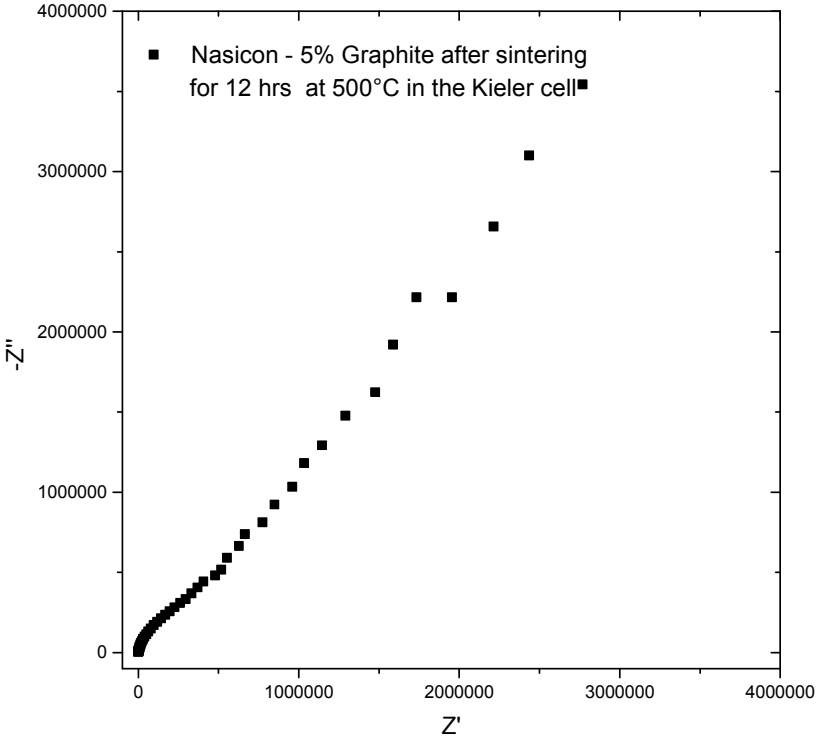

Fig 5.13 Impedance (Nyquist) plot of Nasicon-graphite powder mixed pellet measured after uniaxial pressing and sintering in a kiel-cell. The units of the plot are in Ω.cm.

In the same way the Nasicon-graphite mixture made, a nasicon-gold mixture was prepared so that to have an easy dense sintered pellet. Gold paste was used as a source of Au for the preparation. The amount of gold present in a given weight of the Au-paste was determined by weighing before and after burning the paste at 500 °C and then the right amount of Au-paste was mixed with a nasicon powder to achieve the right weight percentage of nasicon-gold mixture. The unwanted part present in the gold paste was removed when later the mixed material was sintered at 500 °C. For first trials 2 and 10 weight percentage of Au with Nasicon were prepared and further analyzed using the impedance measuring technique for the conductivity and capacitance determinations.

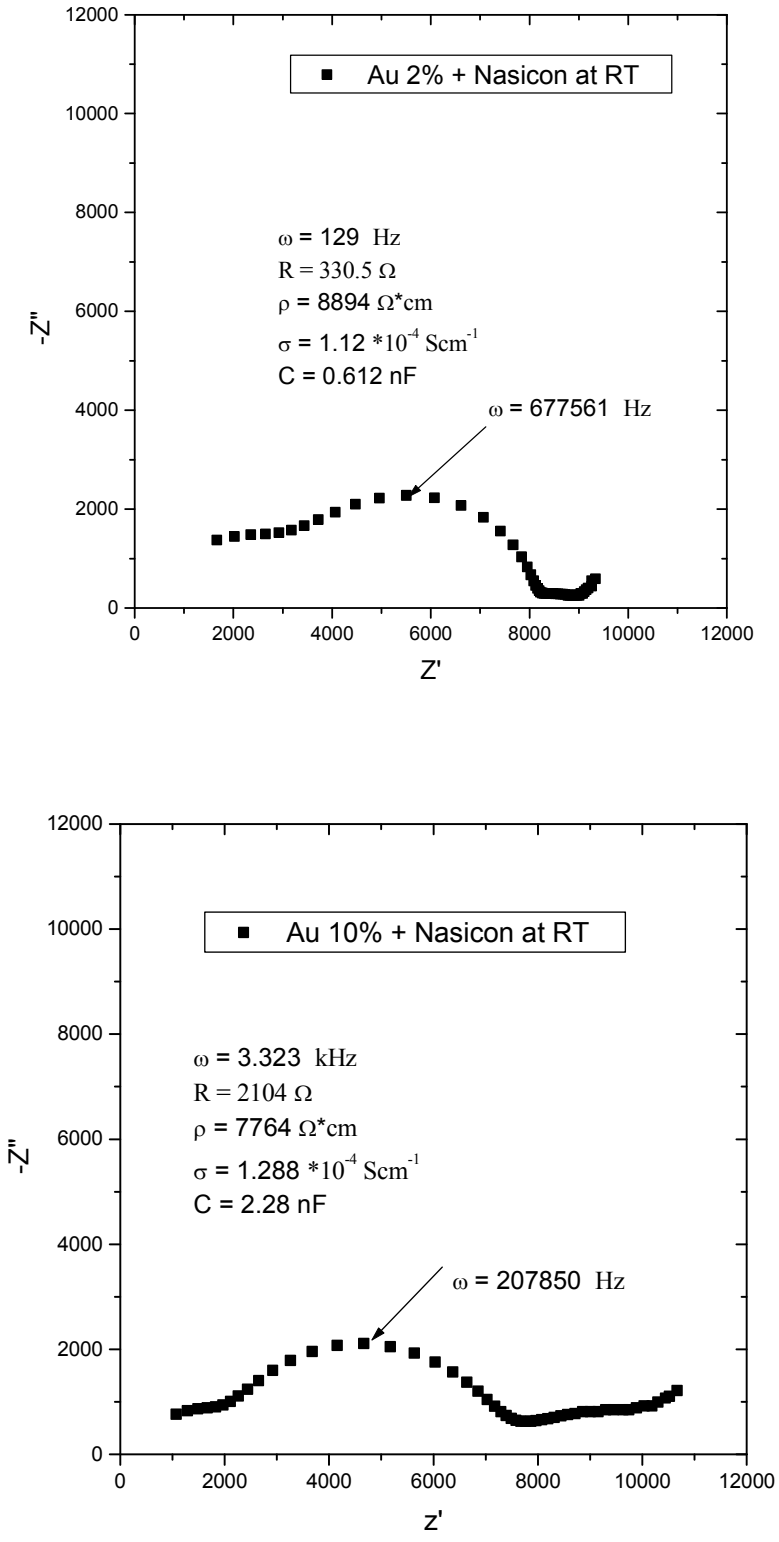

Fig 5.14 Impedance (Nyquist) plots of Nasicon-Gold mixed pellet at room temperature after uniaxial pressing. The units of the plots are in Ω.cm.

The impedance measurements of the Nasicon-Gold cell with 2 and 10 weight percentage didn't show significant difference at room temperature and then became heated using the Kiel-cell.

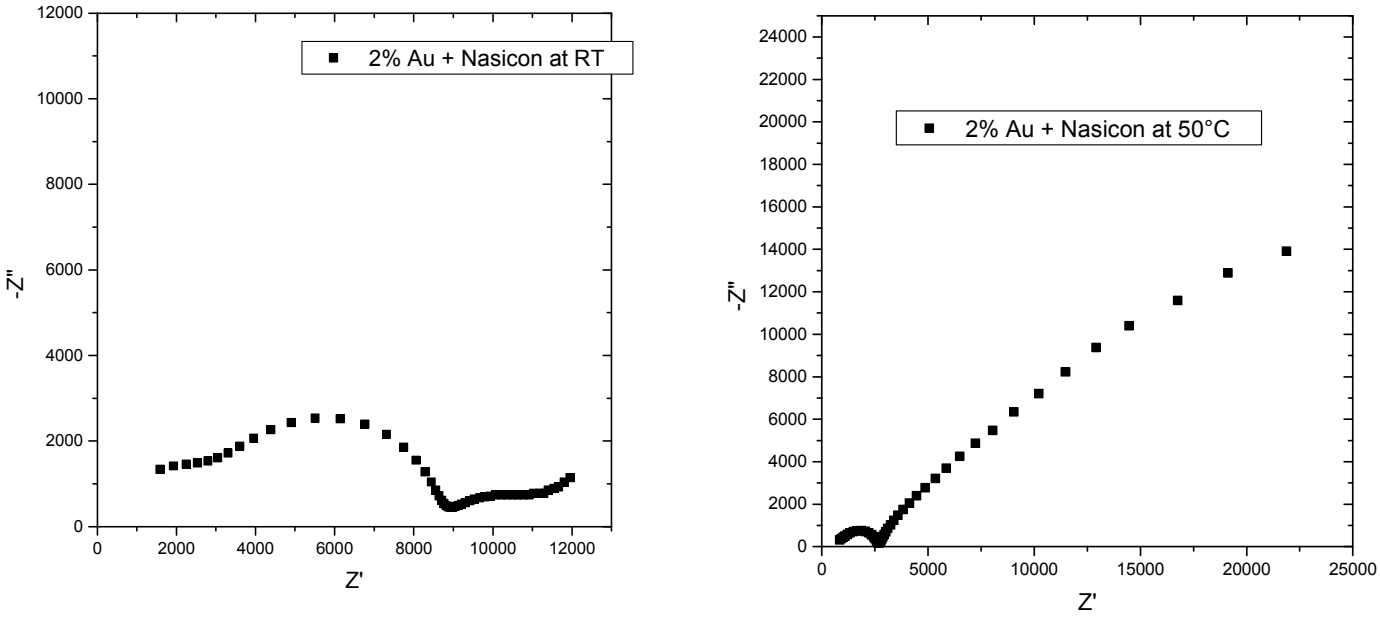

Fig 5.15 Impedance (Nyquist) plots of Nasicon-Gold mixed pellet at room temperature after uniaxial pressing. The units of the plot are in Ω.cm.

When impedance was measured while heating up, there was a large decrease of the resistance as can be seen from the plots above but when it was measured back after sintering at 500°C, there was an overflow of the impedance and there was no reproducibility, specially at lower frequency. Then the sample was taken out and checked if there was a side product formed. A DTA of both 2 and 10 % sample was measured and there was no any redox processes at 500°C as there was no any color change of the sample after the DTA measurement in addition to the none existence of peaks from the DTA measurements at this temperature other than the endothermic peak at 1060^{o}C, the melting point of gold. That indicates that the sample can be analyzed in air and even can be heated above 500^{o}C. Even the distribution of gold particles in the nasicon electrolyte was uniform both before and after sintering when checked using a simple microscope unless there was segregation of gold particles beyond the reading scale of the microscope. XRD plots of the mixture pellet was taken before and after sintering where there was no any difference except the sizes of the scanned lines. Because of that failure, again another electrolyte with different electrodes were tried.

5.2.2 Nasicon Type [$Li_{1+x}M_xTi_{2-x}(PO_4)_3$] solid electrolyte

The good Nasicon type solid ionic conducting electrolyte was prepared using a solid state reaction method as explained in the experimental part. Then the dense, sintered, polished solid electrolyte with a required dimension with the chemical formula $Li_{1.3}Al_{0.3}Ti_{1.7}(PO_4)_3$ was ready for further investigations.

5.2.2.1 Thermal analysis (DTA)

There were not too many thermal analysis experiments carried for this work. But there was one additional experiment for the Nasiscon-gold system performed for the determination of the stability of the Nasicon type $Li_{1+x}Al_xTi_{2-x}(PO_4)_3$ solid electrolyte in contact with $LiCoO_2$, which was used as an electrode where there were visible color changes at temperatures above 500°C. This happens when the whole cell was heated in the Kiel-cell for electrochemical analysis. Therefore, there was doubt that these two materials, the electrolyte and electrode, form another product, side product, which could affect the measurement to be done. But there was no clear information from the thermal analysis as the pure parts, electrode and electrolyte separately, and the cell after electrode/electrolyte contact showed the same scans on the thermal analysis experiment.

5.2.2.2 XRD

Before the assembling of the whole supercap cell, the impurity presence in the material prepared, was checked by XRD analysis using the literature data for comparison. It was in a good agreement with literatures [4, 5]. The XRD of the material was taken after calcination and sintering in both powder and pellet forms to have a comparison where there was the same lines except the height differences and background noise effects in the powder form.

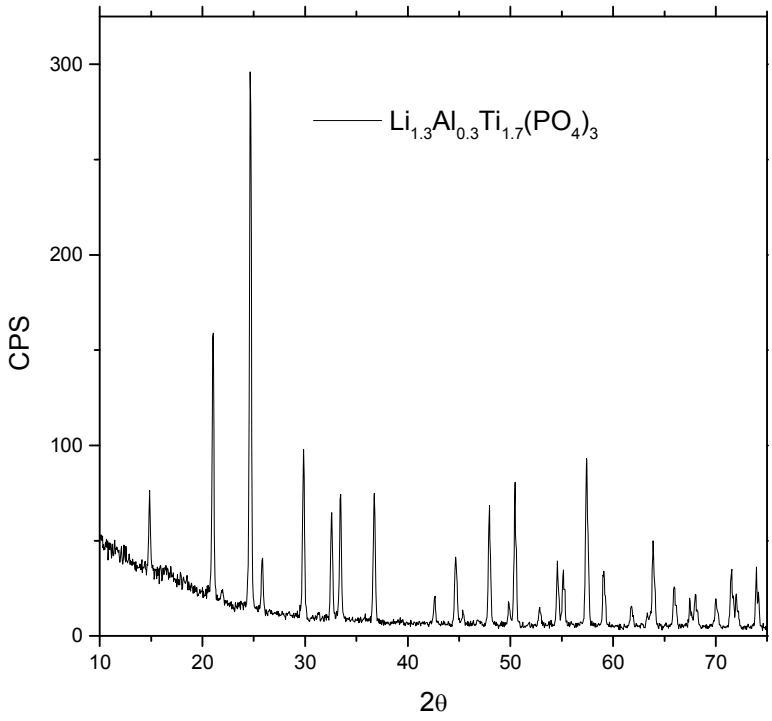

Fig. 5.16 XRD scans of Nasicon type solid electrolyte after sintering at 1100 °C for 2 hours with a cooling/heating rate of 2°C/min.

5.2.2.3 Impedance analysis of the solid electrolyte with the Kiel-cell for the conductivity

After the solid electrolyte with a good purity was prepared, then the cell was assembled for the conductivity measurements of the electrolyte with Pt/Au as current collectors on both sides of the electrolyte pellet either in paste form or sputtered thin films. The impedance measurements took place at different temperatures starting from room temperature.

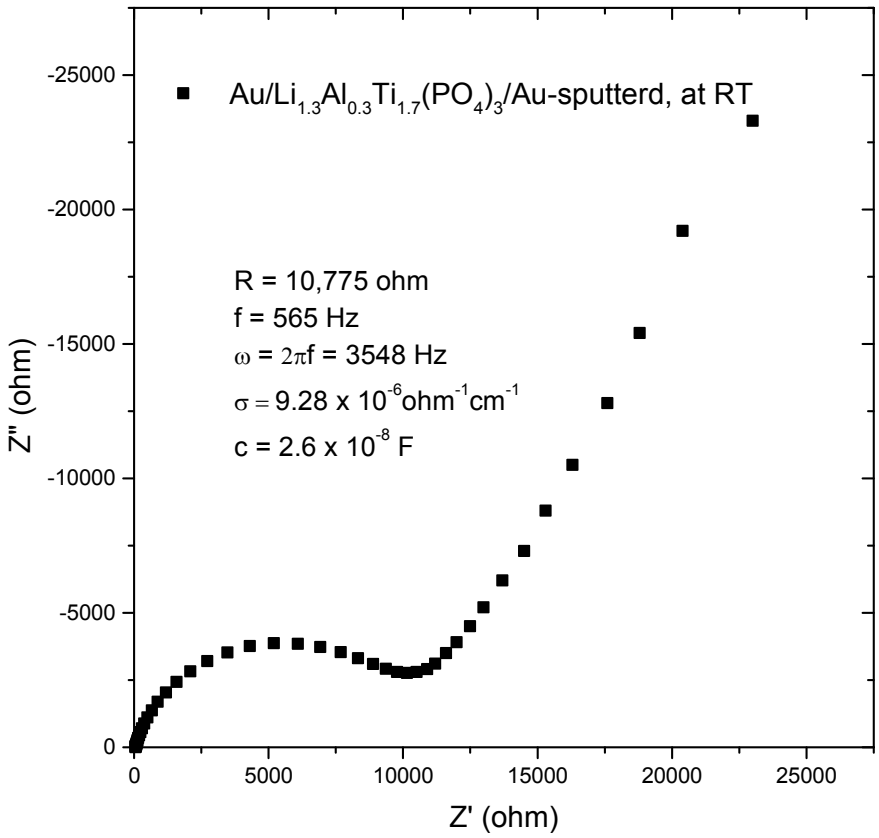

Fig. 5.17 Impedance plot of a nasicon type solid electrolyte at room temperature.

As can be seen from the impedance plot above, the conductivity of the electrolyte at room temperature was not good compared to nasicon and was needed to be heated up for better conductivity at least above 50°C. But at the same time it was not very bad and further experiments were performed with the material synthesized with the same procedures.

The next step was to assemble supercaps, which can store more charges at the interface. For that reason, LiCoO2 electrode was chosen as it is being used in the lithium ion battery system which is related to the supercaps studied in this work.

Two different ways of assembling the whole cell were performed here. First the commercially available LiCoO2 powder was pressed separately into pellet and placed on both sides of the solid electrolyte and the impedance was tried to be measured for the system Pt or Au (current collector)/$LiCoO_2$/ $Li_{1.3}Al_{0.3}Ti_{1.7}(PO_4)_3$/$LiCoO_2$/Pt or Au full cell. But in this case, the contact between the electrode and electrolyte pellets was very

poor and there was an overflow when the impedance was tried to be measured. Then the next step was to look for a better interfacial contact of $LiCoO_2$ electrode and the electrolyte pellet by putting a paste of $LiCoO_2$ on to the electrolyte pellet. Again this has failed as it was pealed off when heated above 100°C for the impedance measurements. After that, it was tried to make a sputtered film of $LiCoO_2$ on both faces of the electrolyte pellet. That was ok when measured at lower temperatures but when heated to ~ 500 °C, the impedance measurement showed a very poor conductivity when cooled down and of course there was a physical observation, color change, at the interface of the electrolyte and electrode. That gave some hint that might have happened with some side product, phase formation or too high diffusion processes between the electrode and electrolyte materials.

To check that, DTA and XRD analysis were done where it was nearly impossible to see any possible phase formation. The following XRD plot for example shows that there was no significant difference between the scans of the electrolyte pellet before and after sintering with $LiCoO_2$ electrode.

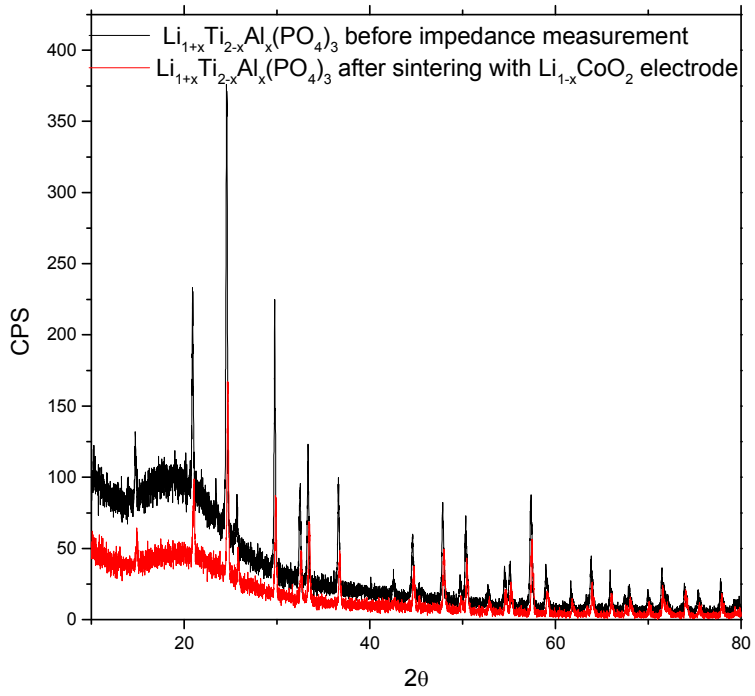

Fig. 18 XRD scans of Nasicon type solid electrolyte before and after sintering with $LiCoO_2$ electrode plotted together.

The XRD of the sample before the impedance measurement and after the sintering with the $LiCoO_2$ didn't show any difference except the intensity of the lines and background change. The DTA measurement also didn't show any possible phase formation when powders of the electrolyte and electrode were analyzed at the temperature of sintering, 500°C. Another sample was analyzed and the XRD of that was nearly with no much difference too.

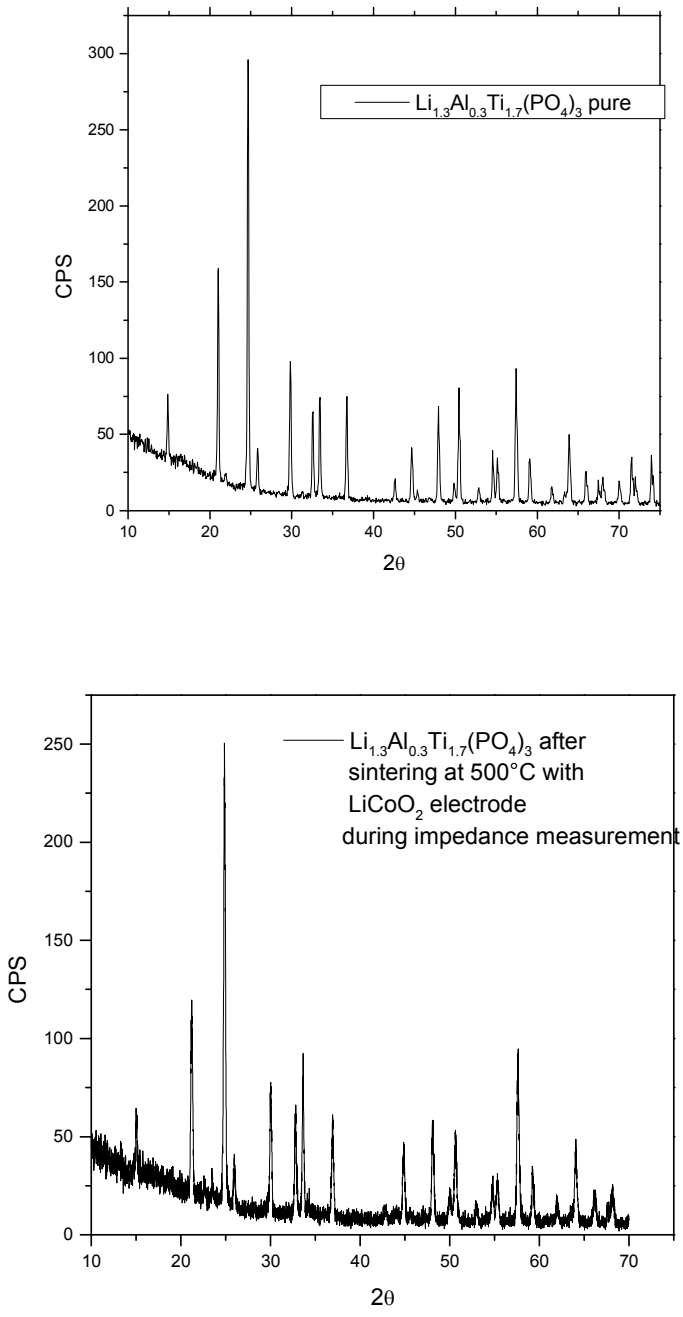

Fig. 5.19 A different XRD scans of Nasicon type solid electrolyte before and after in contact with $LiCoO_2$ measured after heated in the Kiel-cell of the impedance measurement.

5.2.3 Garnet ($Li_6BaLa_2Ta_2O_{12}$) solid electrolyte

The garnet solid electrolyte was mostly used one in this work and most experiment were done using garnet electrolyte than the others two. First of all, it was easy to prepare with the right stochiometry using the solid state reaction method than the others mentioned earlier. The conductivity was also good and it was easy to handle it as it was done intensively at the Chair of Solid State Ionics and Sensors [6]. The material was very dense when pressed and easy to polish and get smooth surface to have good contact with the electrode materials.

5.2.3.1 XRD of Garnet ($Li_6BaLa_2Ta_2O_{12}$) solid electrolyte

Like in the case of other electrolytes, after every garnet material synthesis, XRD measurements were taken to control the purity of the material both after calcination and sintering in both powder and pellet forms. It was almost always the same and showed that the synthesis was reproducible.

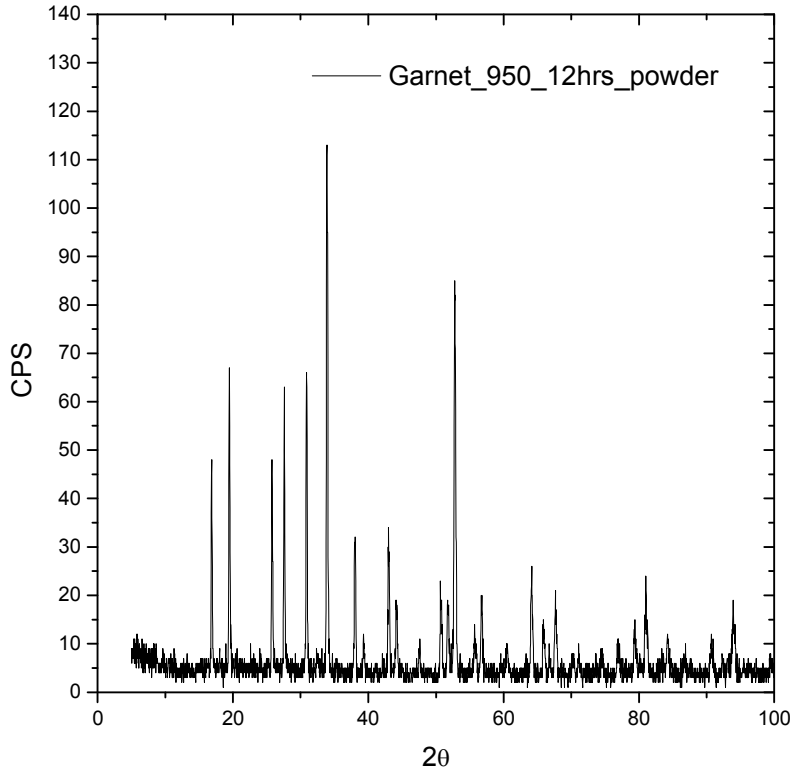

Fig. 5.20 XRD scan of garnet solid electrolyte powder after sintering at 950°C for 12 hours.

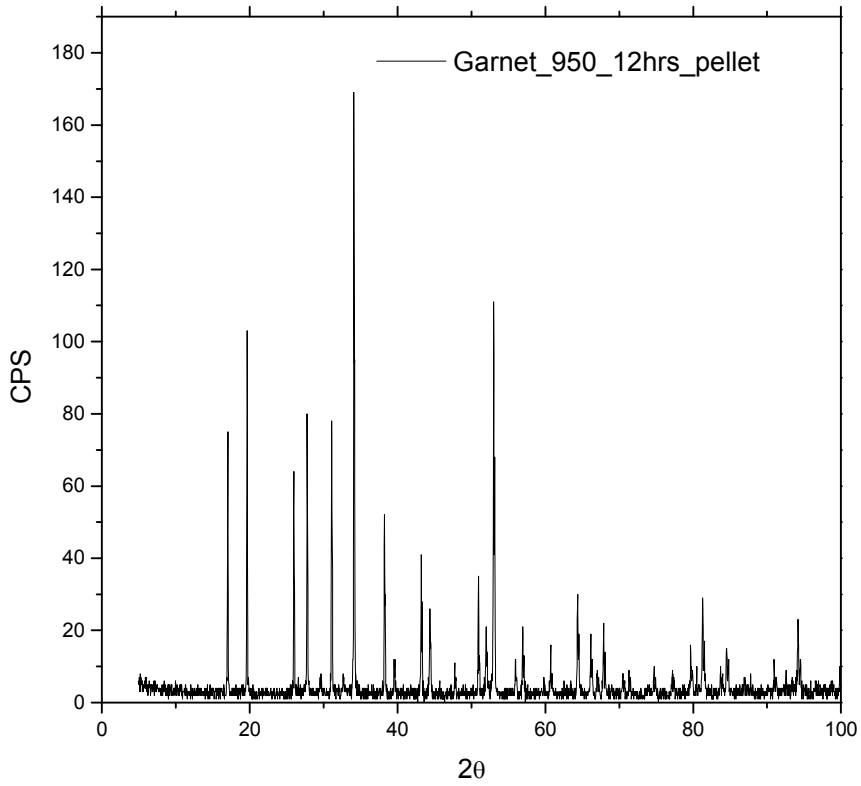

Fig. 5.21 XRD scan of garnet solid electrolyte pellet after sintering at 950°C for 12 hours.

Many samples were checked by XRD after preparations and almost all showed the same scan results showing that there was no significant impurity while preparation. The only difference can be seen from the powder and pellet sample scans is the reduction of background in the case of the pellet scan. But all the important lines are seen in both forms of scans.

5.2.3.2 Impedance analysis with the Kiel-cell for the conductivity and diffusion constant determination of garnet and complete supercap cell

After the XRD was taken and checked with JCPDS and all the lines fit with no impurity, then further experiments were made. First the conductivity of the garnet solid electrolyte was measured using gold paste and gold sputtered films as electrode.

First the garnet pellet was cut with the dimensions required and polished so that there will be good contact with the electrode. For example, a thickness/diameter of 0.85 mm/ 9.85 mm, 1.25 mm/ 10.10 mm, 0.8 mm/ 10 mm and 1.35 mm/ 10.05 mm dimensions were taken. Of course for every experiments, there were different dimensions, though there was no big difference in pellet size. Then the gold pasted electrolyte pellet was sintered at 800 °C for 2 hours. Then the conductivity was measured at different temperatures.

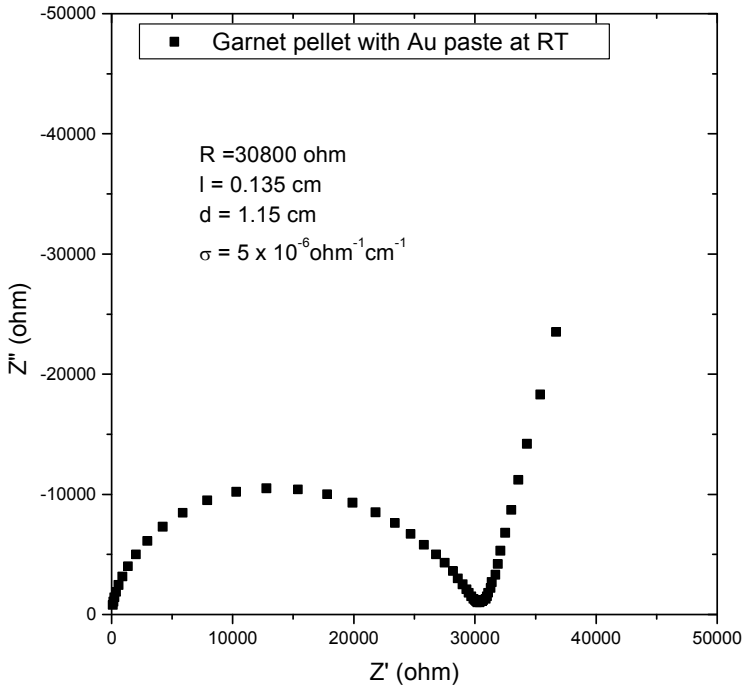

Fig. 5.22 Impedance plot of a garnet solid electrolyte at room temperature with gold paste on both sides of the electrolyte pellet as electrode.

The impedance of the garnet solid electrolyte with gold paste showed a higher resistance but when the measurements were done higher than 50^{o}C, there was improvement of conductivity and the system looked a reasonable good solid electrolyte.

The same garnet electrolyte material was also checked with a gold sputtered electrode and the conductivity showed some improvement as there was good contact of the electrolyte-electrode interface compared to the pasted one, which helps to have high surface area for the storage of charges at the interface.

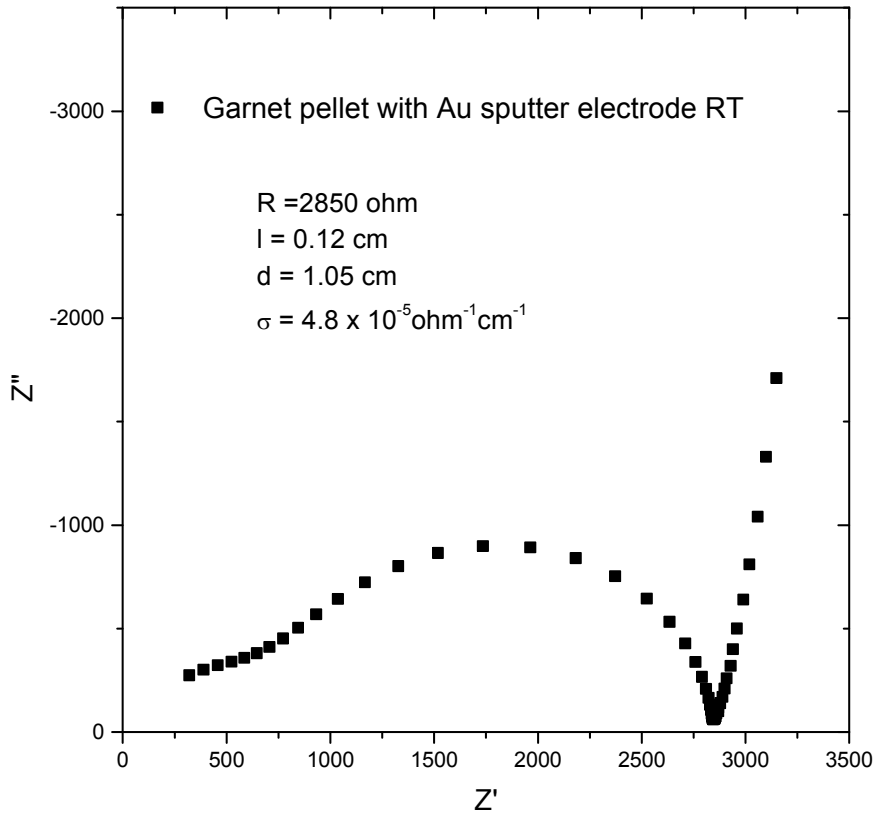

Fig. 5.23 Impedance plot of a garnet solid electrolyte at room temperature with gold sputtered on both sides of the electrolyte pellet as electrode. The units of the plot are in Ω.

From Figs. 5.22 and 5.23, there is a big difference in the conductivity, which might be from the contact improvement for the sputtered case, even though there is also a dimension difference of the electrolyte pellets, that wouldn't make such an order of magnitude change at

the conductivity. Based on these two results, most of the electrodes for this work were by sputtering than the pasted ones.

After the good ionically conducting solid electrolyte was prepared, then the whole supercap cell was made in different ways. First like other electrolytes, the powder mixtures of garnet with graphite and $LiCoO_2$ powders at different weight percentages were prepared. The percentages tried were 5, 10, 30 and 50 % of graphite and $LiCoO_2$ with garnet powder. First the powders were mixed simply by stirring with the proper weights and then pressed into pellets. Then ready for the impedance measurements using the kiel cell.

The other way was to put the electrode and electrolyte unmixed. In this case, the well polished garnet pellet was taken and a $LiCoO_2$ electrode was sputtered on both sides of the electrolyte pellet. The $LiCoO_2$ film thickness was of course dependent on the time of sputtering and in most of the experiments 11, 16 and 20 hours were chosen which yields a film thickness of 650-800 nm, 1400-1500 nm and 2000 nm respectively. Then gold electrode was sputtered on both sides with different thickness (sputtering time). For most of the experiments the gold electrode was sputtered for 5 and 10 minutes yielding a thickness of 450 and 650 nm respectively. Then the cell was sintered in two different ways. First immediately after $LiCoO_2$ was sputtered on the garnet pellet, which was sintered at 700^{o}C for 2 hours with a heating and cooling rates of 2^{o}C/min. In the other case, both $LiCoO_2$ and gold were sputtered on both sides of the electrolyte pellet one after the other, where $LiCoO_2$ was sputtered first and then gold, and then the whole cell was sintered at 700^{o}C for 2 hours.

Of course the aim of sintering here is just to get the crystallized form of the sputtered $LiCoO_2$ [7] and also it creates a good contact with the solid electrolyte pellet interface. In some experiments gold paste was also used instead of sputtered gold. But the gold-pasted film didn't have a good contact with the $LiCoO_2$ film on garnet pallet and pilled off later when it was heated in the Kiel-cell for the impedance measurements. The impedance measurements at low frequencies showed also an overflow. For that reason, most of the results presented here are from the gold sputtered film experiments.

The system arrangement looks like:

$Au/LiCoO_2/ Li_6BaLa_2Ta_2O_{12})/LiCoO_2/Au$

Fig. 5.24 Schematic representation of the supercapacitor assembled from Garnet pellet as electrolyte, Sputtered $LiCoO_2$ as electrode on both sides, and Au paste Or Au sputtered film as a current collector.

The above assembled cell was then kept in the Kiel-cell for the impedance measurements and the following results were obtained at different temperatures.

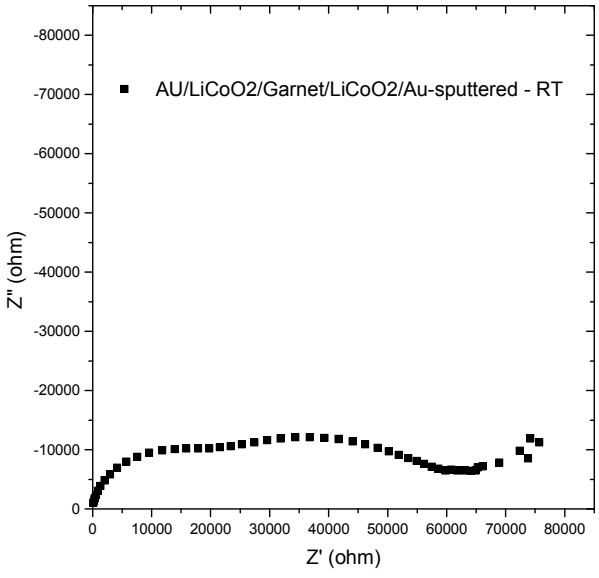

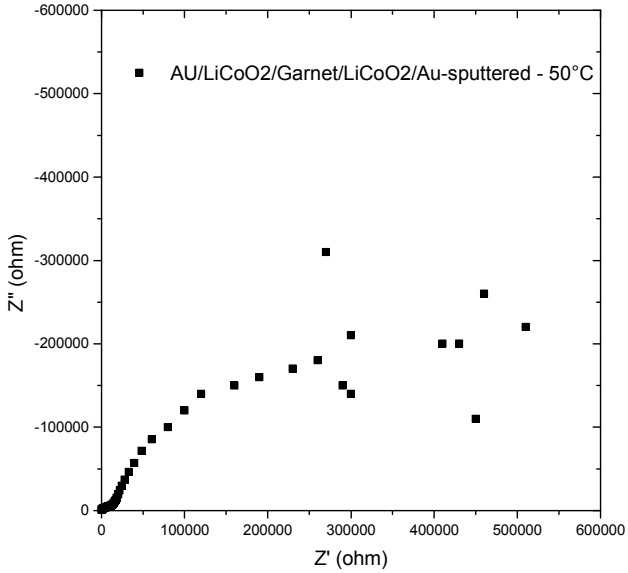

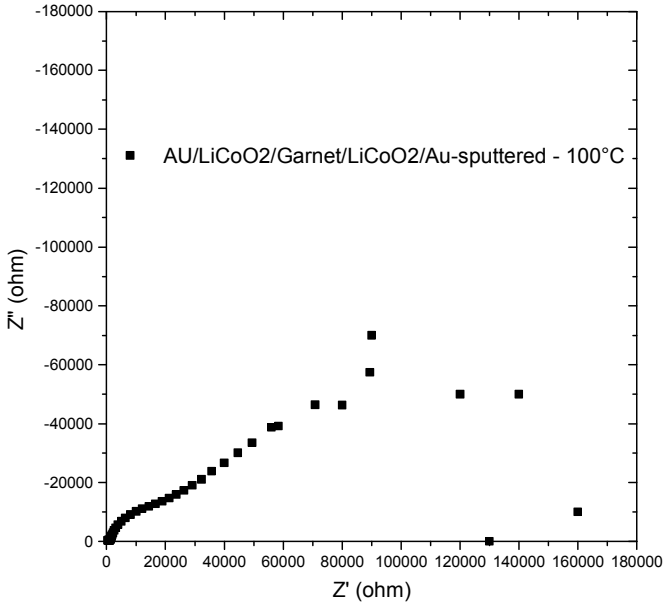
AU/LiCoO2/Garnet/LiCoO2/Au-sputtered - 100°C
Z'' (ohm)
Z' (ohm)
-180000
-160000
-140000
-120000
-100000
-80000
-60000
-40000
-20000
0
0
20000
40000
60000
80000
100000
120000
140000
160000
180000

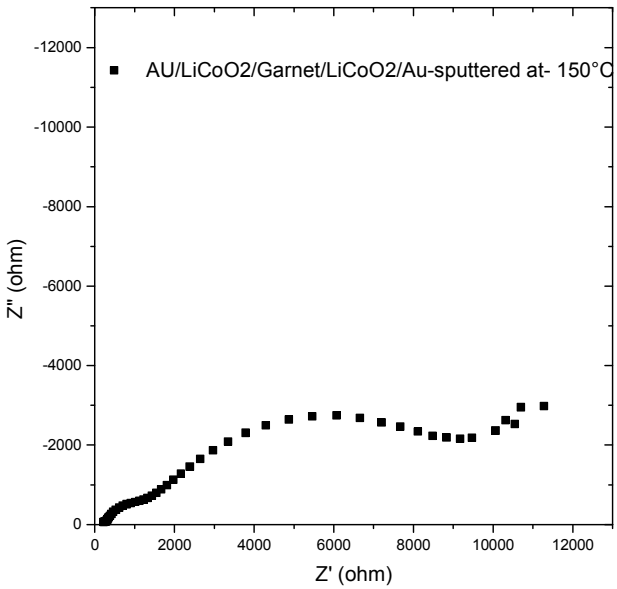
AU/LiCoO2/Garnet/LiCoO2/Au-sputtered at- 150°C
Z'' (ohm)
Z' (ohm)
-12000
-10000
-8000
-6000
-4000
-2000
0
0
2000
4000
6000
8000
10000
12000

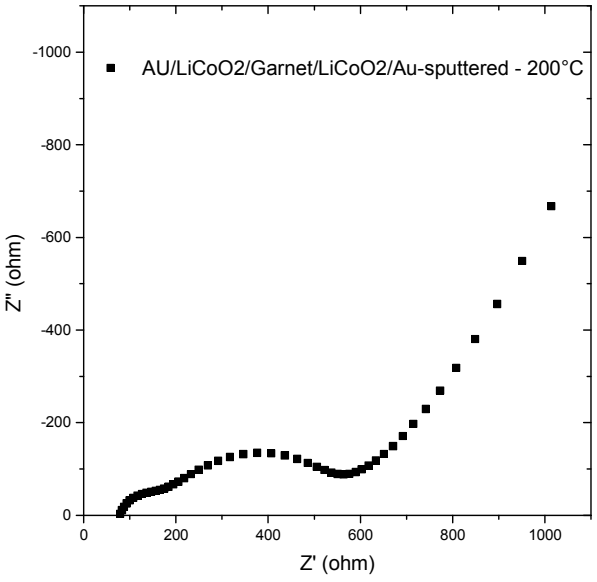
AU/LiCoO2/Garnet/LiCoO2/Au-sputtered - 200°C
Z'' (ohm)
Z' (ohm)
-1000
-800
-600
-400
-200
0
0
200
400
600
800
1000

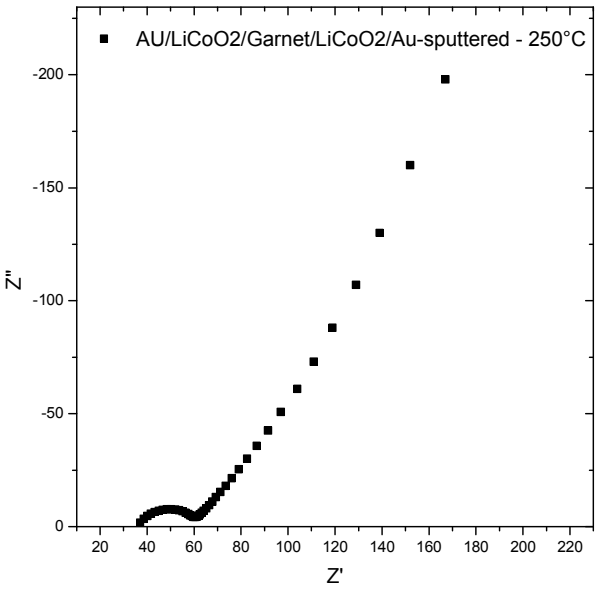
AU/LiCoO2/Garnet/LiCoO2/Au-sputtered - 250°C
Z''
Z'
-200
-150
-100
-50
0
20
40
60
80
100
120
140
160
180
200
220

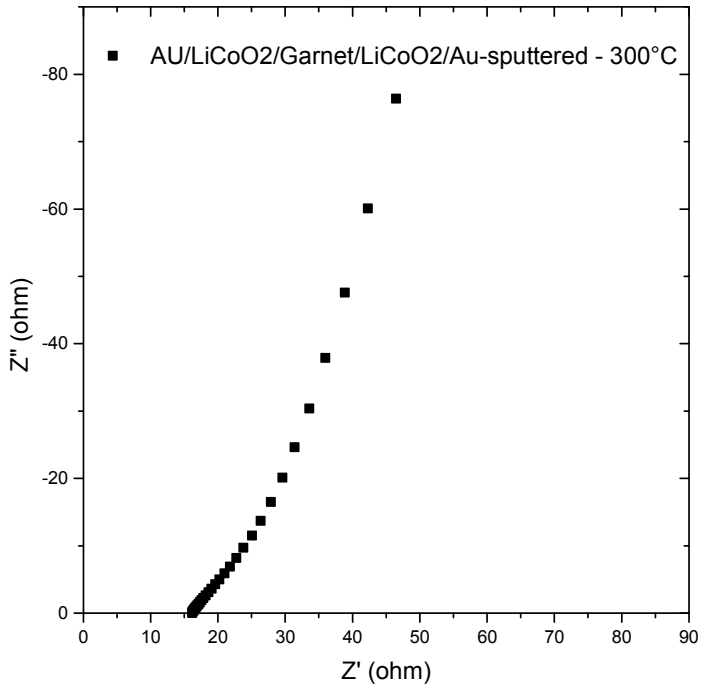

Fig. 5.25 Nyquist plots of the whole cell (all the above 7 figures) at different temperatures to show the nature of the semi-circles with respect to the temperature change.

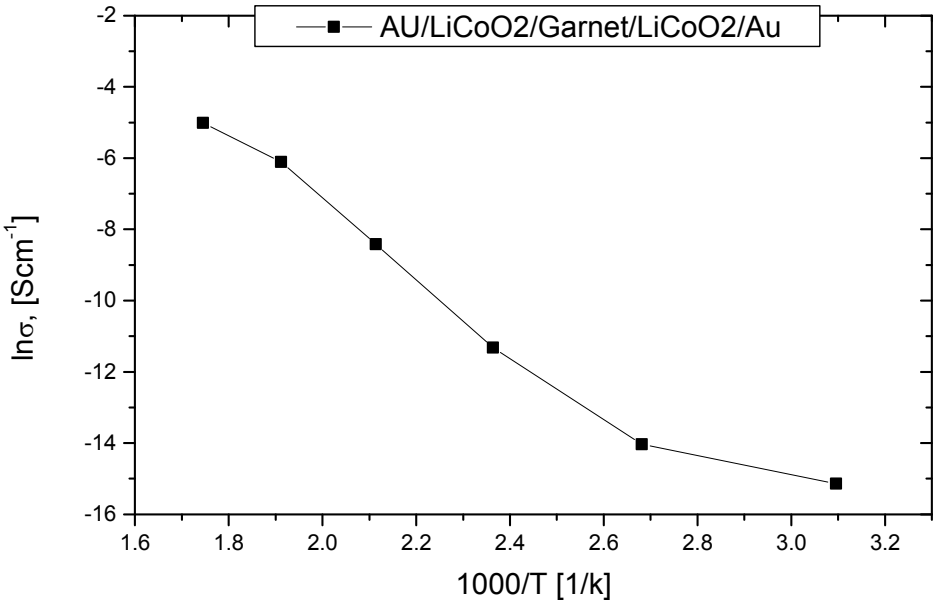

Fig. 5.26 Arrhenius plot of the whole cell of the Garnet electrolyte with $LiCoO_2$ electrode.

The Nyquist plots of the complete cell above in Fig. 5.25 show how unclear the semicircles are at lower temperatures. It was possible to see the clear semicircles only above 150 °C of the temperatures of the cell. Even when further heated, the second big semicircle becomes a line showing the presence of diffusion at those temperatures. For that matter the chemical diffusion coefficients at some temperatures were calculated using the equation below (eq. 5.1) and the values showed good agreements with lithium ion diffusion in $LiCoO_2$ as presented in other works [1]. As can be seen from the above Nyquist plots, at higher temperatures with low frequencies there is Warburg-like line, which definitely shows the presence of diffusion [7-9]. The chemical diffusion cal be calculated using the formula of equation 5.1.

$$|Z| = \left| \frac{V_M (dE/dx)}{zFa\sqrt{\tilde{D}}} \cdot \frac{1}{\sqrt{\omega}} \cdot \right| \tag{5.1}$$

where $|Z|$-impedance of the cell, V_M-molar volume, z-elemental charge, F-Faraday constant, a-area of the electrode-electrolyte interface, $\omega = 2\pi f$ –angular frequency, dE/dx-slope of coulometric titration of LiCoO2 and $\tilde{D}$-chemical diffusion constant.

Therefore from the plot of the impedance - $|Z|$ versus $1/\sqrt{\omega}$, it is possible to get the chemical diffusion coefficient from the slope, as all the other parameters in the equation are available.

Based on these calculations, the chemical diffusion coefficients were 3.1 x 10^{-13}, 1.2 x 10^{-12}, and 2.4 x 10^{-12} Scm^{-1} at temperatures 200, 250 and 300 °C respectively.

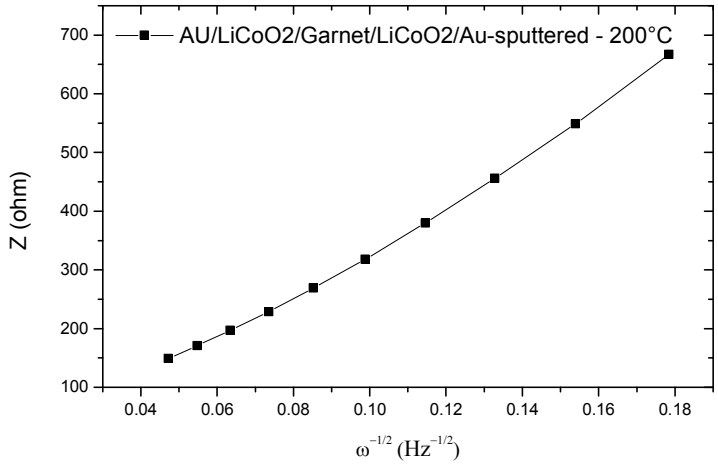

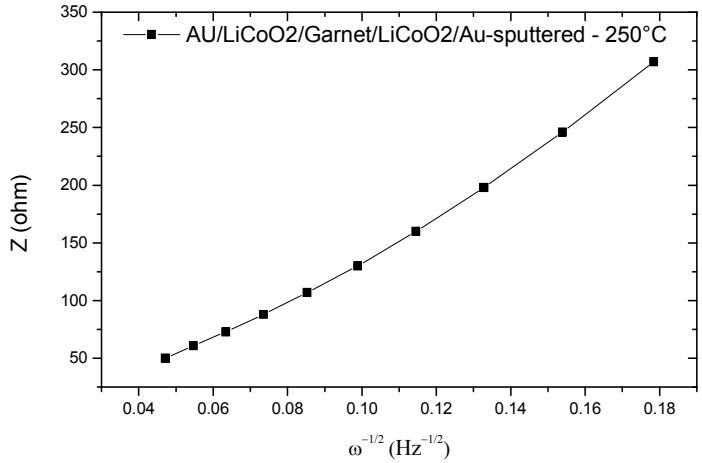

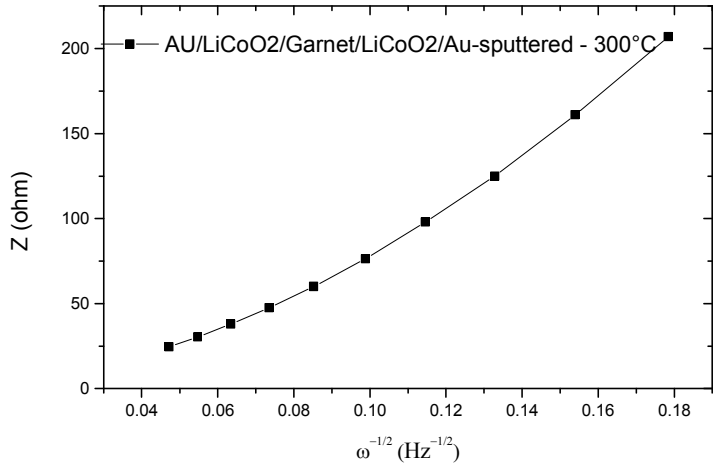

Fig. 5.27 Plots of the impedance of the Au/$LiCoO_2$/Garnet/$LiCoO_2$/Au cell as a function of the frequency at lower frequency values where Warbung is shown in plots of Fig. 5.25 due to the diffusion of lithium.

The natural logarithm of the chemical diffusion was plotted against temperature to calculate the activation energy. For this measurement, the activation energy was found to be ~ 0.45 eV.

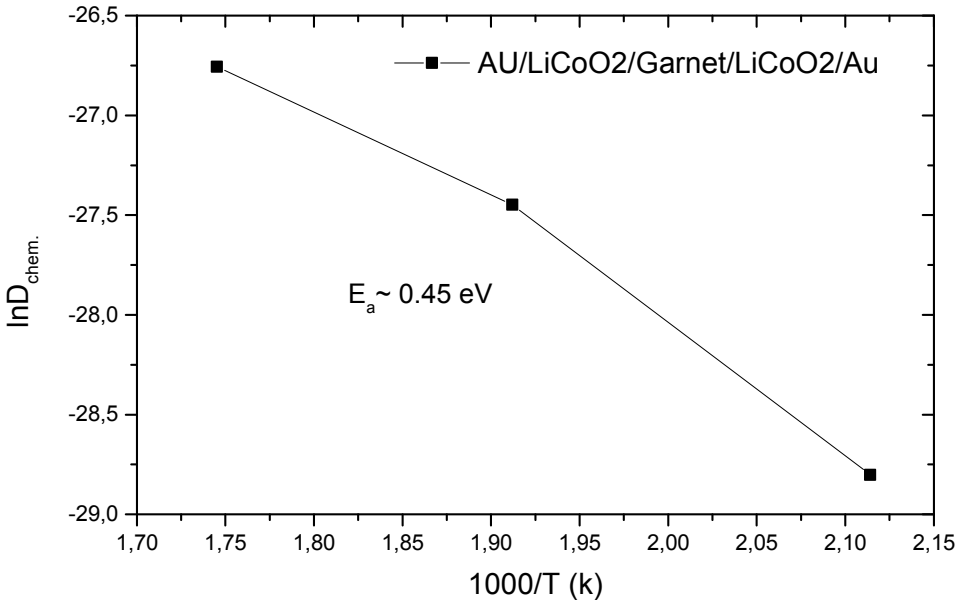

Fig. 5.28 Plot of the natural logarithm of the chemical diffusion coefficient ($\ln \tilde{D}$*) versus temperature for the determination of the activation energy.*

It was also possible to calculate the capacitance of the cell from the impedance measurements but only for those at higher temperatures where there is a clear vertical like line where one can use the formula $C = 1/\omega R$ with a known frequency and the corresponding resistance. For the temperatures 200 and 250 it was in the range of 2 –5 μF which of course varies a bit as the line is not clear vertical where the resistance is not the same for the different frequency values.

The stability of $LiCoO_2$ against garnet at the interface was checked by DTA and XRD [10] and didn't show any phase formation at the interface other than the diffusion of Li-ion into the $LiCoO_2$, which is of course very slow diffusion even at those high temperatures. That indicates that there is a good chance of charge storage at the interfaces which may yield good capacitance at the interface.

5.2.3.3 Electrochemical analysis (charging and discharging) with constant current

In this electrochemical analysis the complete symmetrical *Au/LiCoO$_2$/Garnet/LiCoO$_2$/Au* cell was analyzed by applying a constant current. Also a comparison with some literature analysis is made, though there are differences in the ways the capacitances are calculated.

Two different constant currents were applied for comparison matter in this system, 5 and 10 μA. First the sample was charged and discharged to see the nature of its cyclability and latter a current on and off measurements were taken to see the nature of the curves. The charging/discharging curves at these selected currents show a good cyclability except the presence of the expected high IR drops, which is because of the contact problems at the solid-solid interfaces.

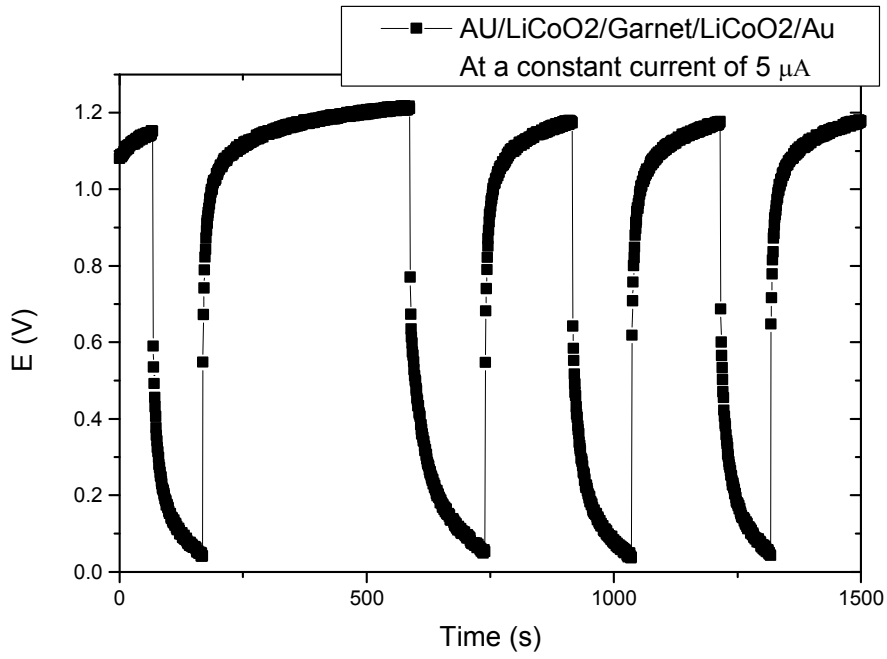

Fig. 5.29 Plot of electrochemical charging/discharging process of the Au/LiCoO2/Garnet/LiCoO2/Au cell at a constant current of 5 μA.

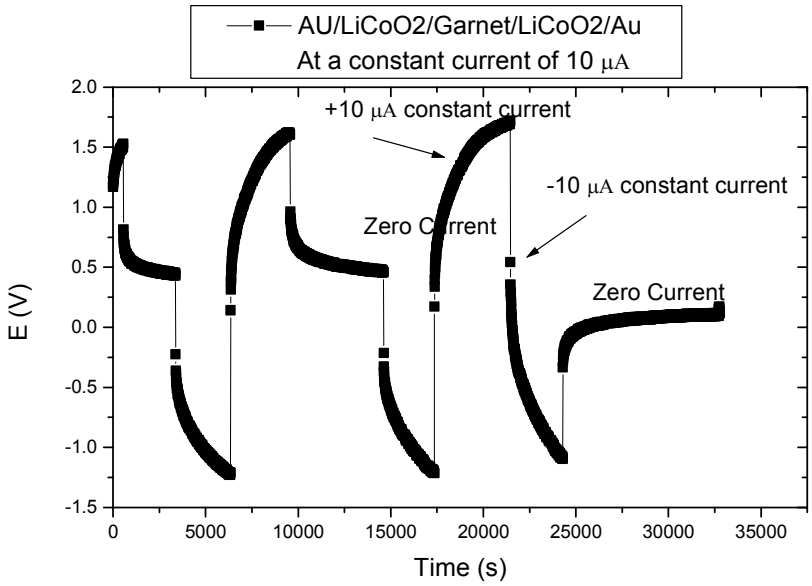

Fig. 5.30 Plot of electrochemical charging/discharging process of the Au/LiCoO2/Garnet/LiCoO2/Au cell at a constant current of 10 μA with the current switched on and off in-between.

Just to see the IR drop nature of the cell an experiment was done at the same applied current but at two different temperatures, room temperature and 200 °C. And the result clearly shows the improvement of the high IR drop with temperature changes and that tells when a measurement is made a bit higher than RT, it is possible to minimize the IR drop observed in the plots above.

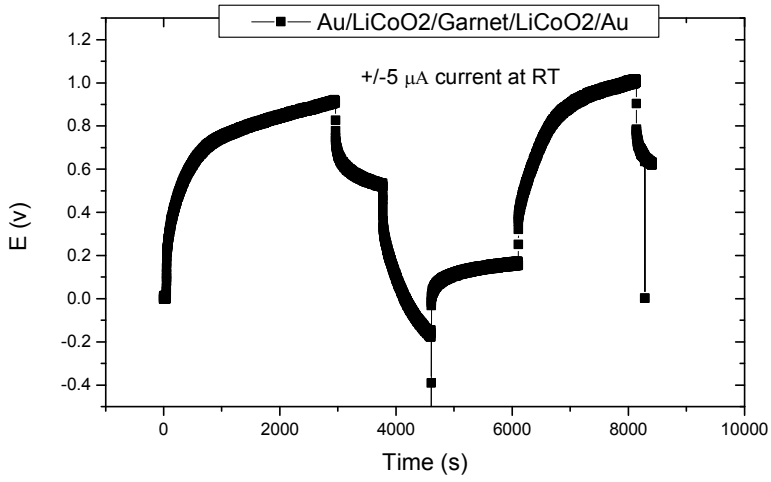

Fig. 5.31 Plot of electrochemical charging/discharging process of the Au/LiCoO2/Garnet/LiCoO2/Au cell at a constant current of 5 μA at RT.

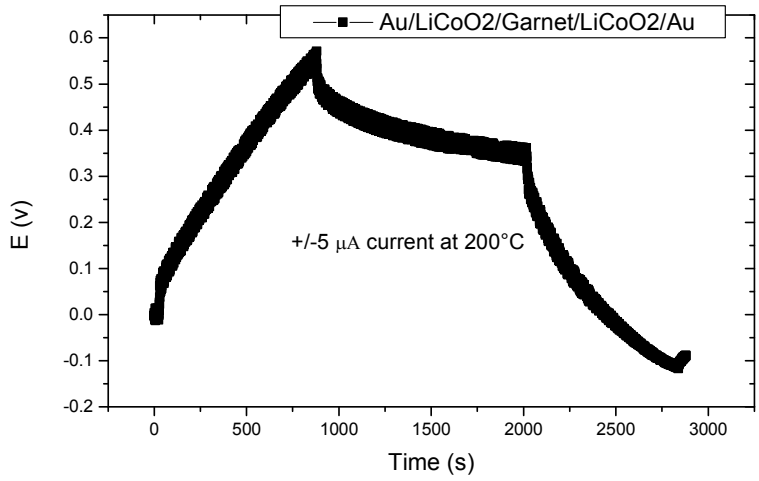

Fig. 5.32 Plot of electrochemical charging/discharging process of the Au/LiCoO2/Garnet/LiCoO2/Au cell at a constant current of 5 μA at 200 °C.

In all the above galvanostatic charging-discharging graphs, there is an initial sharp change in potential with time during both charging and discharging processes which is due to an ohmic-loss which arises from the internal resistance of the cells. This is also observed when there was a sharp decrease of capacitance when the applied current increases [12].

A constant current of 1 and 2 μA were also tried but it was too small and the signal was very weak which also take longer time for charging and discharging fully. But for the 5 and 10 μA measurements, it was clear to have a better voltage against time values where one can calculate the charge stored at the interface using the equation:

$$Q = I.t \tag{5.2}$$

and that also leads for the determination of the capacitance using the equation:

$$C = Q / V = I\Delta t / \Delta V \tag{5.3}$$

and the specific capacitance, C_m, of the cell can be calculated from:

$$C_m = C / m = I\Delta t / \Delta V.m \tag{5.4}$$

where I is the current of the charge-discharge, Δt the time of charge/discharge, ΔV the change in voltage, m-mass load of active materials (both positive and negative electrodes).

The values, Δt and ΔV can be taken from charging/discharging plots and the load of active material is also known for this system and then the capacitances can be calculated for each of the charging and discharging processes at the applied constant current. For example, for the first two charging and discharging processes for Fig. 5.29, the values are given in the table 5.1 below.

Table 5.1 Capacitance calculated from charging-discharging data of the garnet/LiCoO2 system at constant current of 5 μA.

Charging/discharging steps	Capacitance (μF)	Specific capacitance (mF/g)
Second charging	541	7
Third charging	583	7.7
First discharging	1224	16
Second discharging	1105	15

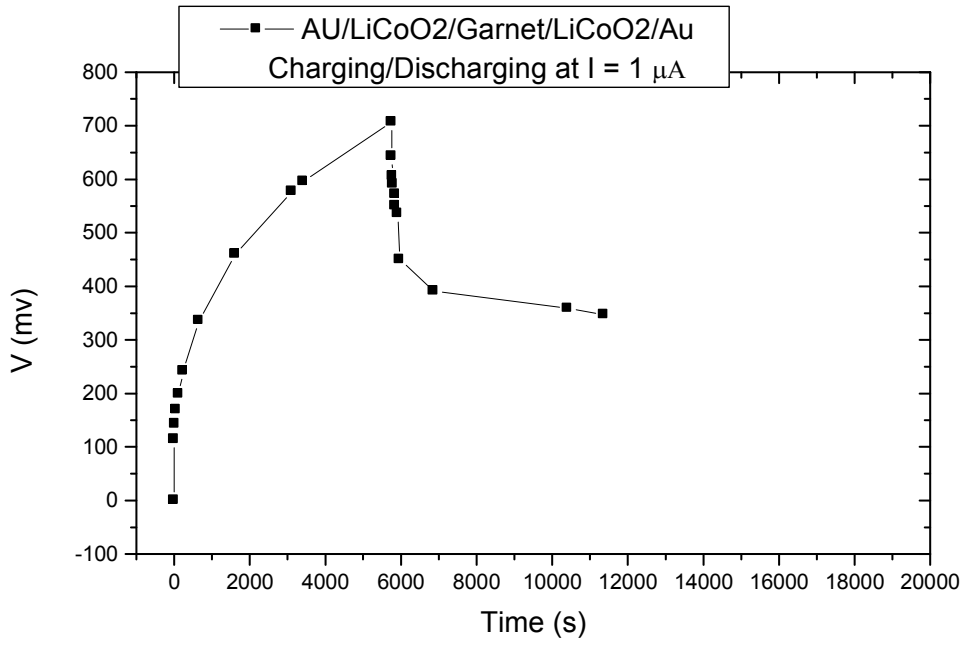

Fig 5.33 Plot of electrochemical charging/discharging process of the Au/$LiCoO_2$/Garnet/$LiCoO_2$/Au cell at a constant current of 1 μA

Fig. 5.33 shows that the lower the applied current is the lower the out put voltage and it takes too long for charging to the highest voltage value. At the same time it shows that the lower the current is the lower is the IR drop.

For the calculation of the capacitance and charge stored at the interface of the cell, Fig. 5.29 was taken as it has undergone smooth charging-discharging steps without current interruption. The calculations were done only for the first two charging/discharging steps at the beginning of the processes too.

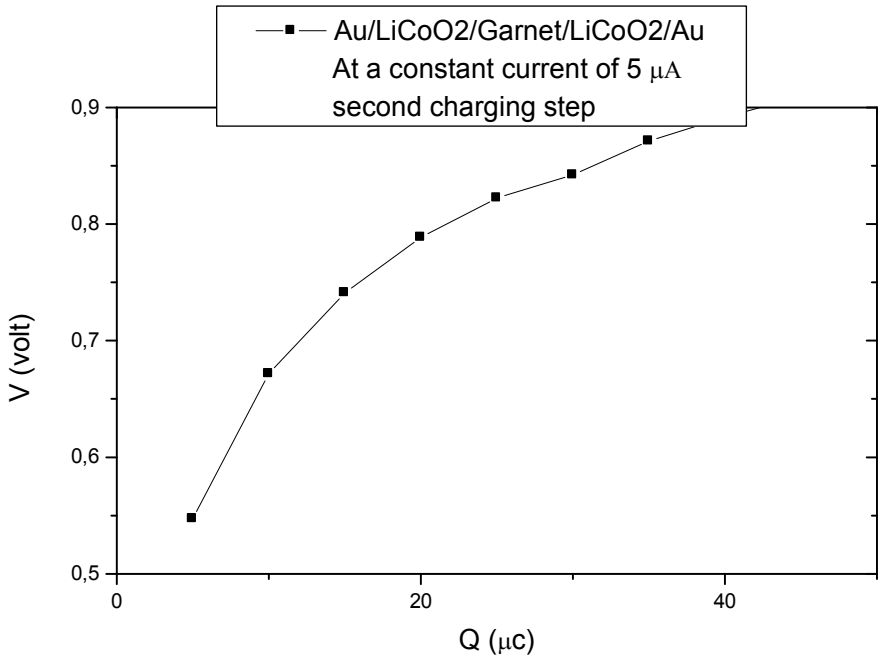

Fig. 5.34 Plot of voltage versus charge for the charging process of the Au/LiCoO$_2$/Garnet/LiCoO$_2$/Au cell at a constant current of 5 μA for the second charging step (Fig. 5.29).

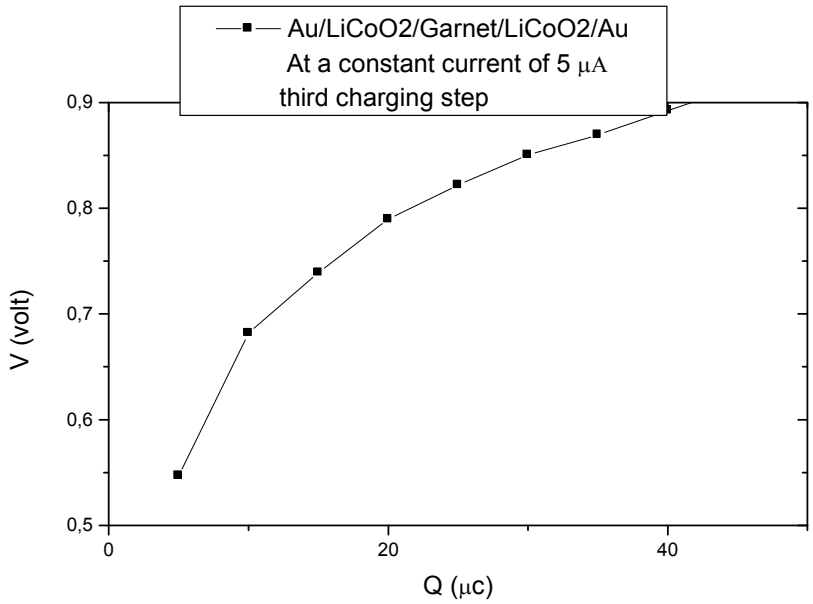

Fig. 5.35 Plot of voltage versus charge for the charging process of the Au/LiCoO$_2$/Garnet/LiCoO$_2$/Au cell at a constant current of 5 μA for the third charging step (Fig. 5.29).

The calculation for the first charging step was escaped because of the less data recorded at the beginning. As can be seen from Fig. 5.29, the first charging step jumps very fast to the highest voltage when the current was applied and that might be because of presence of some potential difference across, though it should have been zero for the symmetric cell in principle.

Figures 5.34 and 5.35 show the nature of the charge stored when the cell is charged at the beginning. With the time goes, the increase in charge is low and only the first data were taken where there is sharp increase. As can be seen from Fig. 5.29, the nature of the charging and discharging cycles are the same and that is also proved from Figs. 5.34 and 5.35 where they show nearly the same plots.

The same was done for the discharging processes of the first and second steps and presented in Figs. 5.36 and 5.37 below.

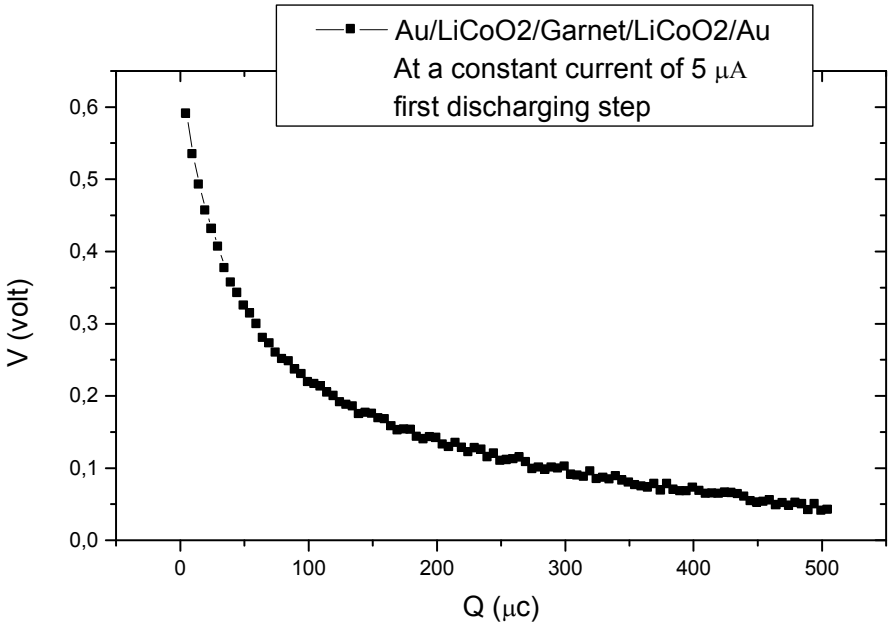

Fig. 5.36 Plot of voltage versus charge for the discharging process of the Au/LiCoO₂/Garnet/LiCoO₂/Au cell at a constant current of 5 μA for the first discharging of (Fig. 5.29).

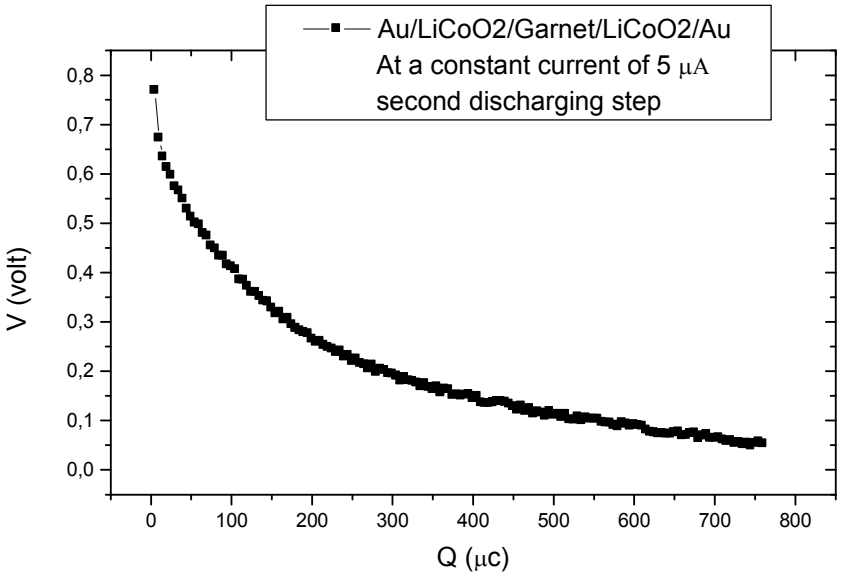

Fig. 5.37 Plot of voltage versus charge for the discharging process of the Au/LiCoO₂/Garnet/LiCoO₂/Au cell at a constant current of 5 μA for the first discharging of (Fig. 5.29).

It is also possible to determine the chemical diffusion coefficient from the galvanostatic measurements [13]. Using equations 5.5 and 5.6 it is possible to calculate the chemical diffusion coefficient of this cell mentioned above from the slope of plots $dE/dt^{1/2}$.

$$\frac{dE}{dt^{1/2}} = \left(\frac{2V_M}{ZFA} . I_o . \frac{dE/dy}{\left(\tilde{D}\pi\right)^{1/2}} \right) \tag{5.5}$$

$$\tilde{D} = \left(\frac{2V_M}{ZFA} . I_o . \frac{dE/dy}{\Delta E/\Delta t^{1/2}} \right)^2 . \frac{1}{\pi} \tag{5.6}$$

where V_M-molar volume of the electrode, I_o-applied constant current, dE/dy-slope of a coulometric titration, Z-elementary charge number, F-Faraday constant, A-area of the electrode interface with the electrolyte, and $\tilde{D}$-the chemical diffusion constant.

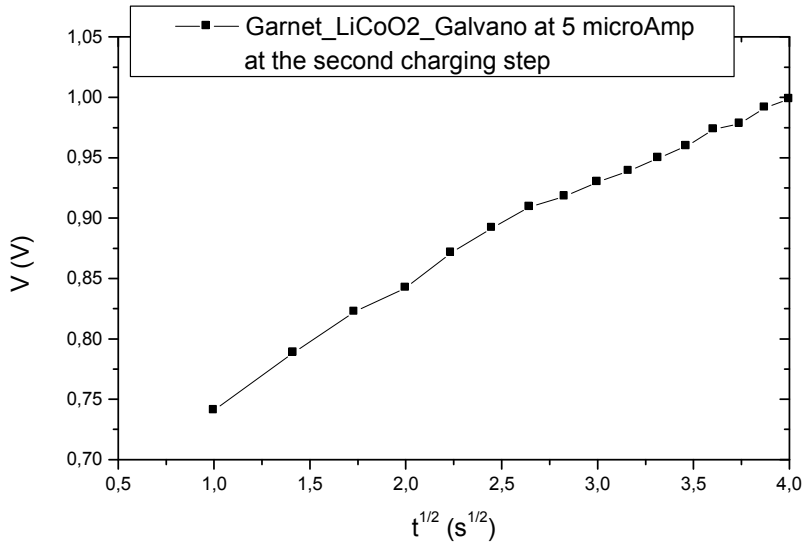

Fig. 5.38 Plot of voltage versus square root of time in order to calculate the chemical diffusion coefficient from the slope.

Based on equations 5.5and 5.6 with all the parameters available and the slope obtained from Fig. 5.38 the chemical diffusion coefficient for this cell was found to be ~ 7 x 10^{-13} cm^2/s which is also close to the value determined from the impedance analysis.

5.2.3.4 Oscilloscope method with constant voltage applied

The electrochemical double-layer capacitance of solid AgBr has been determined against Pt and Au electrodes, using the cell $C,Br_2(g)|AgBr(s)|(Pt\ or\ Au)$ [16]. In a similar way using the cell arrangement $Ag|Ag_4RbI_5|carbon$ [17] was used for the determination of the electrochemical double layer capacitance. The measurement method for the Ag_4RbI_5 system was by applying a constant current and measuring the voltage versus time steps where as in the AgBr case a constant voltage was applied and the current response with time was recorded where the capacitance is calculated from the integral of the current versus time plots.

With the same arrangement but *AgI* as solid electrolyte and *Pt* and *Ag* as electrodes was analysed in this work using the oscilloscope method by applying a constant voltage where current response of the cell versus time was recorded at different temperatures. The *AgBr* system in the literature was tried at temperatures 246 and 293^{o}C which are below the decomposition temperature of *AgBr* but with a good increasing of the ionic conductivity of the electrolyte. In this work different temperatures in these range were tried and the results will be presented below.

The AgI used for this work was a commercial available powder, which was pressed uniaxially into a pellet with a diameter of 10 mm and different thicknesses close to 1 mm. As electrode, Ag mesh and Pt sheet were used which were pressed together with the electrolyte pellet. Then the whole cell was put in the kiel-cell where it was possible to heat the cell at different temperatures. The kiel-cell was directly connected to the potentiostat machine with which a controlled voltage was applied to the cell. Again the cell was connected to the oscilloscope machine where the current response with time was displayed and later converted to a computer editable digital data. The whole experimental setup is shown with Fig. 5.39 below.

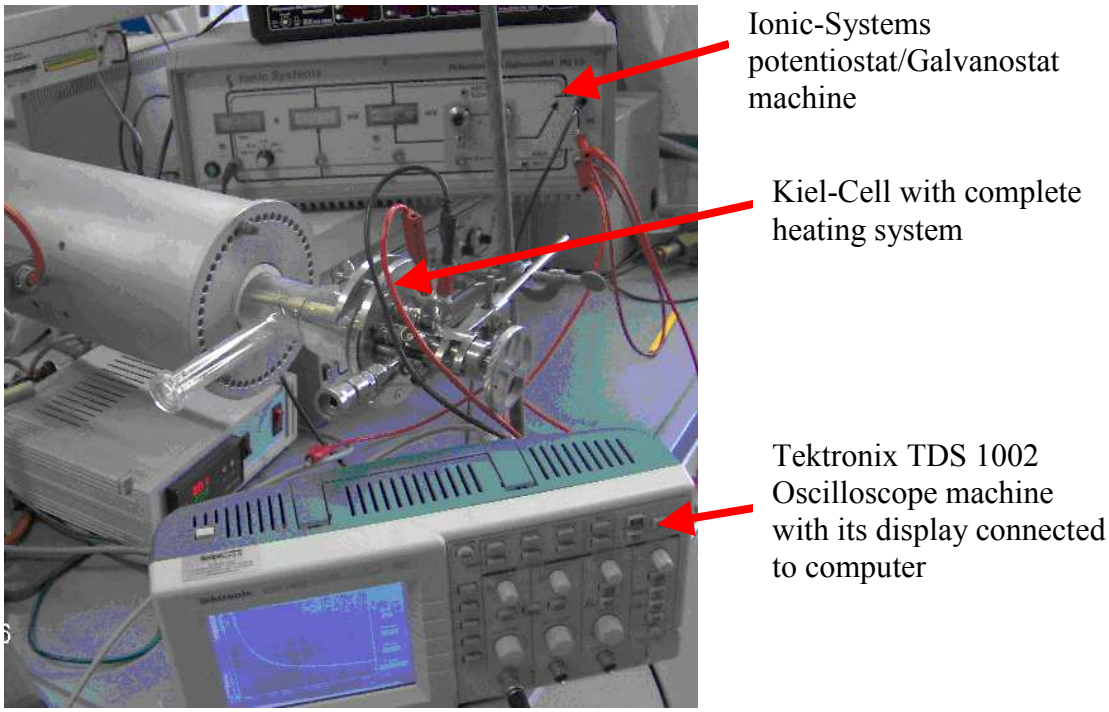

Fig. 5.39 Photographic representation of the electrochemical oscilloscopic measurement used for this work.

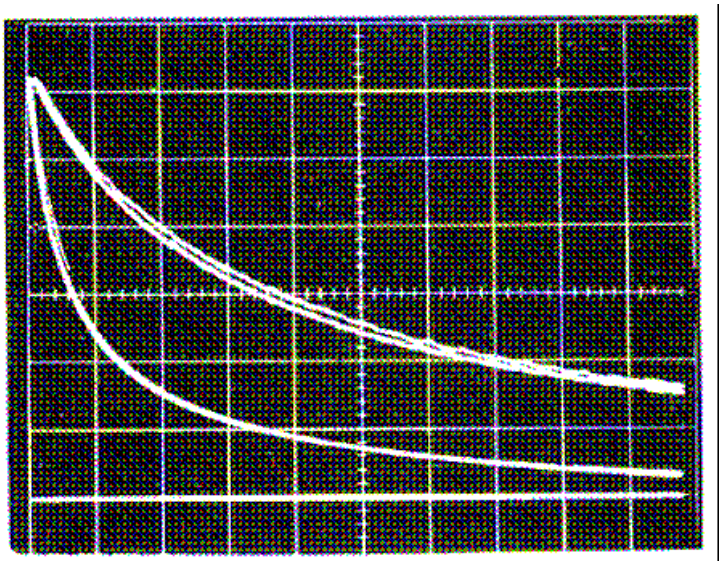

Fig. 5.40 Cell currents in response to 0.1-V step for forward and reverse (0.5 to 0.6 V) at temperature of 293^{o}C with a complete cell of C,Br_2(g)|AgBr(s)|Pt [16].

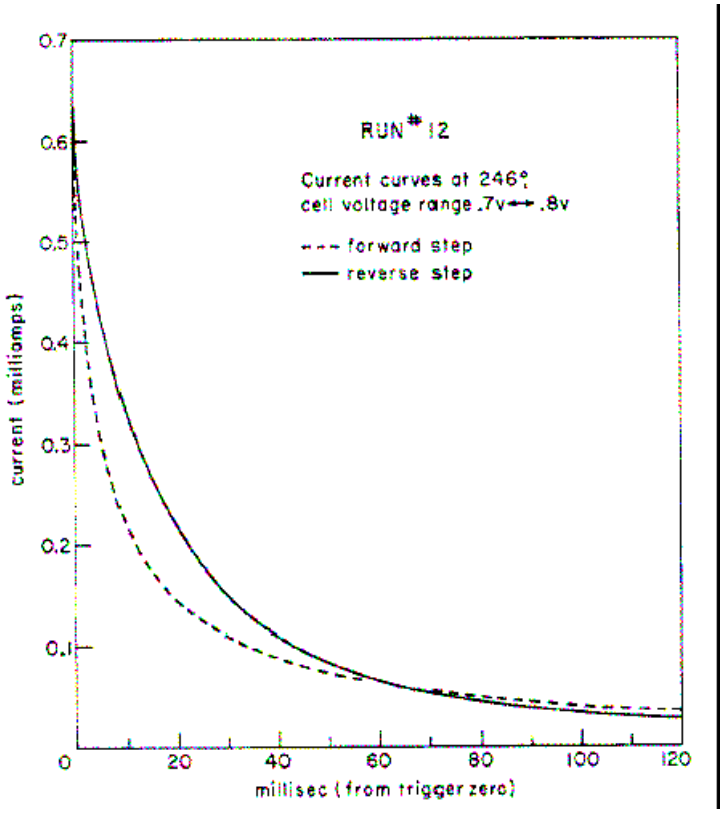

Fig. 5.41 Cell currents in response to a 0.1-V step for forward and reverse (0.7 to 0.8 V) at temperature of 246°C with a complete cell of C,Br_2(g)|AgBr(s)|Pt [16].

Figures 5.40 and 5.41 above show the photographic image from the oscilloscope and the data plotted respectively of the AgBr electrolyte system [16]. From these data, the capacitance was calculated from the integral of the current versus time plots and found to be in the range of 200 and 300 μf/cm^2 for Pt and Au electrodes respectively [16, 17].

The voltage range chosen was 0.4 to 0.7 V, where the silver at the blocking electrode is low, using voltage steps in the range 50-200 mV and cell temperatures 246 and 293°C. The temperatures chosen correspond to an approximate fivefold change in the ionic conductivity of AgBr.

At higher silver activities, there is an abrupt increase in the apparent capacitance which is attributed to the build-up of a monolayer of plated Ag on the metallic electrode as the decomposition potential of AgBr is approached. A theory due to Grimley and Mott accounts

for a portion of the large double-layer capacitance as resulting from a high cation defect concentration in lattice layers of the electrolyte near the electrode interface. To explain the major portion, however, it is necessary to consider additional sources of capacitance, which are believed to involve the layer of electrolyte ions in contact with the electrode and the precise surface condition of the electrode. The time dependence of the charging current indicates that more than one relaxation process is involved in the double-layer charging.

Fig. 5.42 shows the nature of the original plots and the tails subtracted and plotted with time to see the presence of more relaxation processes which involve in the double-layer charging of the capacitors.

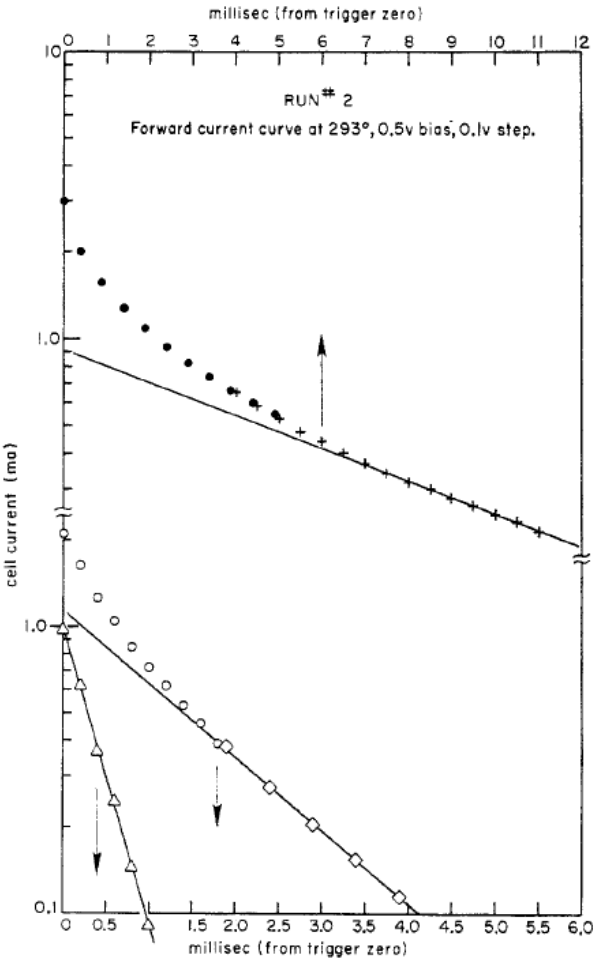

Fig. 5.42 Three-component graphical resolution of a typical current-time curve from an early run. Dots and crosses are original current-time data; circles and diamonds are the results of the first tail subtraction; triangles are the results of the second tail subtraction. Point designations indicate data extracted from curves at various sweep rates and time delays. The lower two curves are displaced one decade downward for illustration [16].

The findings in this system concern both the shape of the current-time curves and the total integrated current. Comparative photographs under various conditions with the cell $C,Br_2/AgBr/Pt$ showed that in the cell voltage range 0.4 to 0.7 V, both the shape and the total amount of repolarization current varied but little with initial cell voltage, direction of voltage step, and temperature. The first two dependences are shown for the cell at 293 ^oC in Figs. 5.40 and 5.41, using photographs from different runs.

At higher cell voltages, approaching the decomposition potential (0.853 V at 246 ^oC and 0.824 V at 293 ^oC) there was an abrupt increase in the characteristic repolarization time, indicating a considerable increase in the total integrated current. The effect was larger at the higher temperature and was accompanied by the onset of a considerable asymmetry in the current curves in response to forward and reverse voltage steps.

In this work the complete cell with garnet electrolyte, *Au/LiCoO$_2$/Garnet/LiCoO$_2$/Au,* and *AgI* solid electrolyte were treated at different temperatures and applied voltages the same way the *AgBr* and *Ag$_4$RbI$_5$* system were done in the literatures mentioned above. Some of the oscilloscope measurements at different temperatures and applied voltages are presented in the following results.

5.2.3.4.1 The silver iodide solid electrolyte system

The complete cell with *AgI* electrolyte, *Ag/AgI/Pt*, was pressed together and placed in the Kiel-cell. Then the whole cell was heated to different temperatures and those measured at 200, 250 and 250 ^oC are presented below. Keeping the sample at these different temperatures, different values of constant voltages, from 400 to 700 mV, were applied and the current responses with time were recorded for all these steps. For curiosity, measurements at room temperatures were tried where there was no any signal on the oscilloscope display as expected.

Also measurements at voltages lower than 400 mV were tried which showed a very small signal which was difficult to have the integral area for the calculation of the charge stored in the cell from which the capacitance was to be calculated.

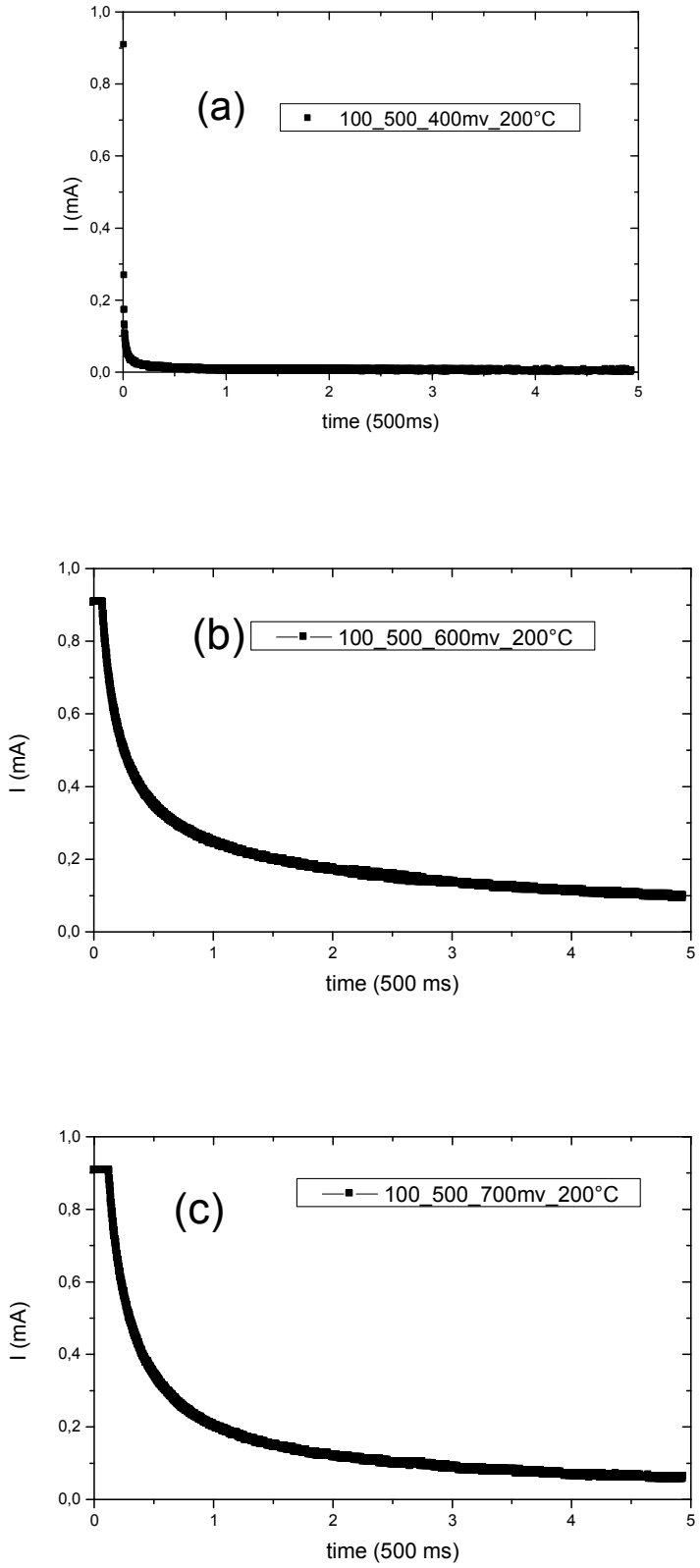

Fig. 5.43 Current versus time plots of the Ag/AgI/Pt system at 200 ^{o}C and (a) 400 mV, (b) 600 mV and (c) 700 mV applied voltages.

In Fig. 5.43 one can see the effect of the magnitude of the applied voltage which contributes for the increasing integrated area that is the source of high charge storage. There is a big jump at the start when 700 mV was applied and because of that the plots look to have a small area compared to the 600 mV. It is also possible to see that the current signal at lower voltage, for example 400 mV, is very low but decreases very slowly where as at higher voltages the initial current signal was higher and decreases faster with time. That can also be seen from plots at the 600 and 700 mV where the decrease at 700 mV is faster than the one at 600 mV as the time goes.

It was also of interest to develop a graphical method to characterize the current-time behavior and measure the total charge passed in the repolarization. Plots of natural log (current) vs. time were of interest since the cell at least formally resembles an *RC* series, *R* being the resistance of the electrolyte and *C* the capacitance of the blocking interface. Unlike an *RC* series, however, plots of log *i* versus *t* in this case were found to be linear only in the limit of long time, indicating that the current decay could not be represented by a single time constant.

To see if the current decay could be represented by a mixture of time constants, the linear tail portion was back-extrapolated to $t = 0$, subtracted from the total current curve, and the process was iterated if necessary. In this way, it was found that current-time traces from several early runs could invariably be resolved into a mixture of more time constants. Figure 5.44 shows a typical graphical resolution of this type where one can easily calculate the integral area for the determination of the charge (capacitance) of the cell.

Figure 5.44 shows that there appear to be two components to the decay. It is likely, in consequence, that other factors such as the existence of more than one relaxation mechanism for the repolarization process may be involved. In fact, the achievement of resolution into straight exponential decay components may have been fortuitous but provides a convenient method of calculating the total integrated current.

In consequence, we do not have a true *RC* series since one end of our resistor is one face of the capacitor, and, with a non-unidimensional current flow geometry, partial currents flowing to various portions of the blocking interface will encounter different resistances.

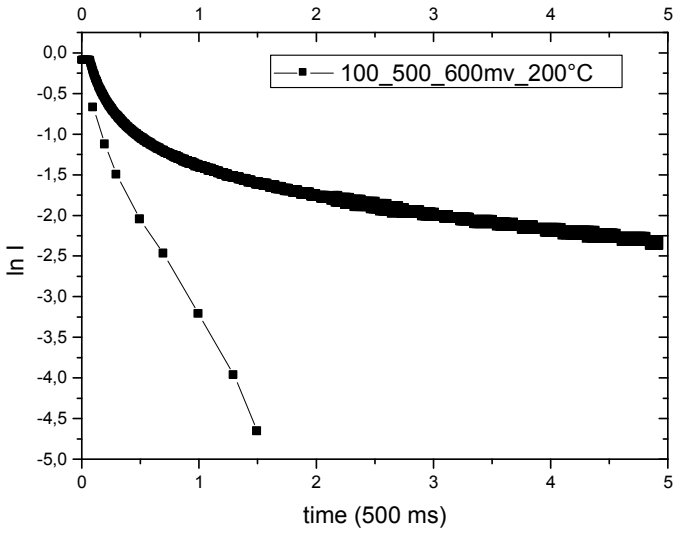

Fig. 5.44 Current versus time and natural logarithm versus time plots of the Ag/AgI/Pt system at 200 ^{o}C and 600 mV applied voltage.

In general, the exact contributions of the various components of the current decay, considered as shape parameters, were somewhat sensitive to the exact manner in which the graphical analysis was performed and showed nothing definite by way of consistent trends as a function of initial cell voltage or from one run to another. **A** clear-cut result, however, was obtained in the temperature dependence of the current decay shape in the cell voltage range 400 to 700 mV.

Plots of the current response with times of the system at different temperatures are show in Fig. 5.45. It is possible to see from these figures the effect of the temperature on the nature of the current response which is directly related to the charge stored that can be calculated from the integral of the plots. That is magnified specially at the start when the voltage is applied and fast decrease in the current with time as the temperature and voltages increase.

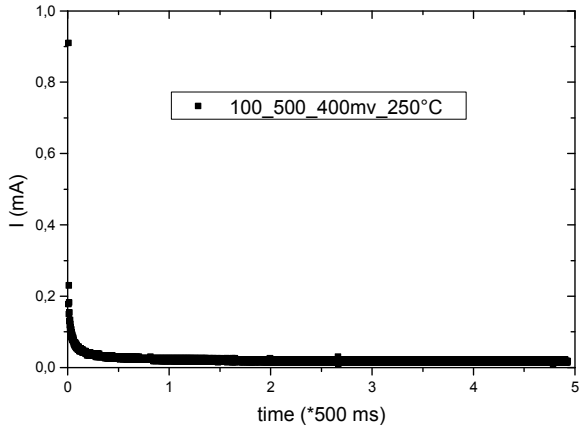

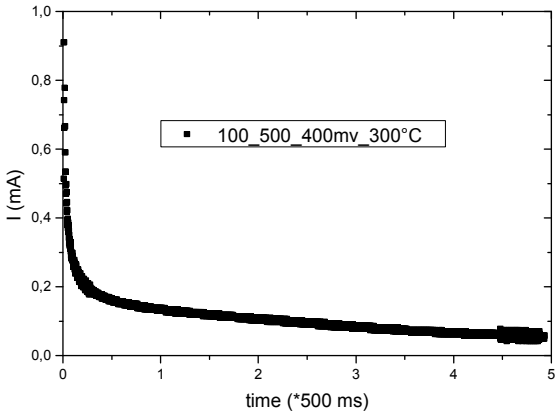

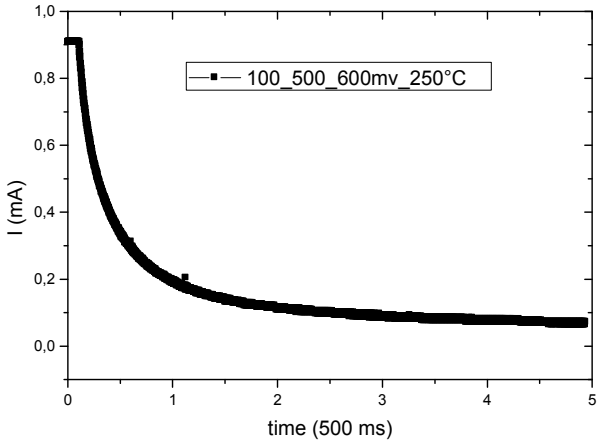

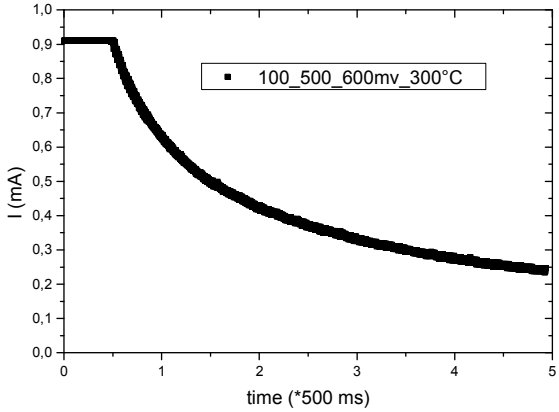

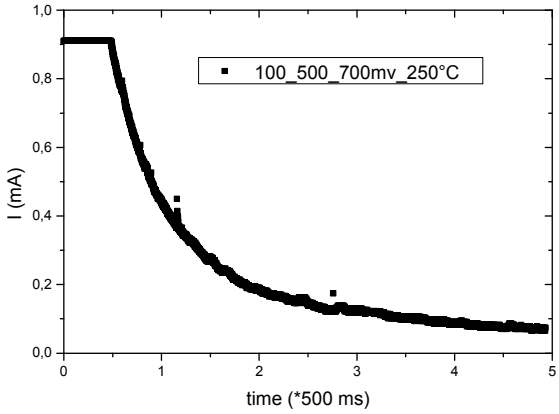

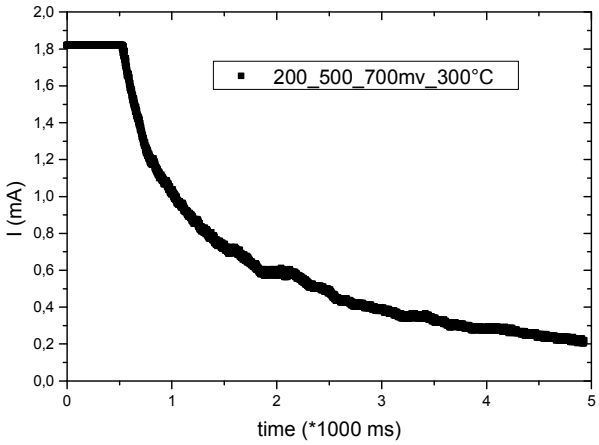

Fig. 5.45 Current versus time plots of the Ag/AgI/Pt system at temperatures 250 and 300 ^{o}C which were exposed to the same applied voltages of 400, 600 and 700 mV.

The total integrated current in response to a voltage step is readily calculated from the graphical analysis procedure of Fig. 5.44 since, for an exponentially ignores any possible long-time, low-level contributions to the integrated current but measures directly the charge transfer accompanying repolarization of the blocking electrode, the rest being extrapolated on this basis. One feels that any low-level contributions not significant on the observed time scale would belong to an independent electrode process.

5.2.3.4.2 The garnet solid electrolyte system

The same way the AgI solid electrolyte cell treated, but with different values, the *Au/$LiCoO_2$/Garnet/$LiCoO_2$/Au* complete cell was treated at different temperatures and applied voltages where the current response at these conditions with time was recorded. In the garnet electrolyte system, signals of the current response were very poor for voltages below 500 mV and the measurements were performed in the voltage ranges of 0.5 to 1.0 Volt. For example, at 200 mV it was possible to see a small signal at higher temperature, 350 ^{o}C where as there was nearly no signal at the lower temperature, 265 ^{o}C, in this case.

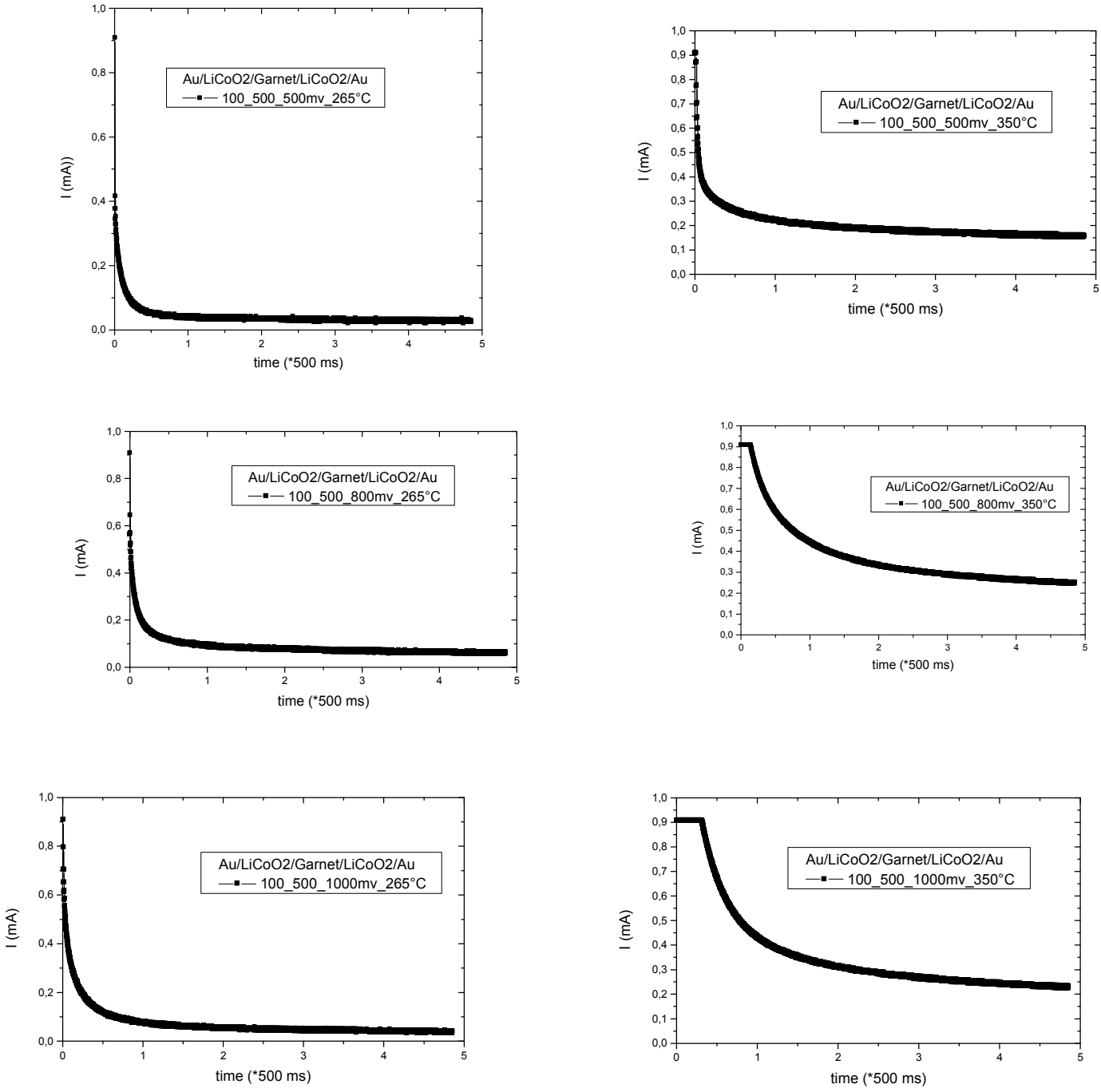

Fig. 5.46 Current versus time plots of the Au/$LiCoO_2$/Garnet/$LiCoO_2$/Au system at temperatures 265 and 350 ^oC which were exposed to the same applied voltages of 500, 800 and 1000 mV.

The charges stored under these current-time plots were calculated manually, which was of course difficult to get the precise values as the measurement was done only for short time. For the starting part, some extrapolation was done while for the data after the 5*500 ms were ignored for all the evaluations, which is of course not the right way. What wanted here was not to put the precise values but to show the trends of the charge storage with temperature and applied voltages which is clear to see the effects.

Table 5.2 Some rough calculated values of charge stored under the current-time plots of the garnet/$LiCoO_2$ systems at two different temperatures and different applied potentials.

	265 °C		350 °C	
Voltage (V)	Charge ($\mu C/cm^2$)	Capacitance ($\mu F/cm^2$)	Charge ($\mu C/cm^2$)	Capacitance ($\mu F/cm^2$)
0.5	94	188	505	3010
0.8	141	176	950	1187
1	179	179	970	970

It is also possible to determine the chemical diffusion coefficient from the galvanostatic measurements which are similar to the potentiostatic ones where a constant potential is applied and the output current is recorded with time [14, 15]. Using equations 5.7 and 5.8 it is possible to calculate the chemical diffusion coefficient of this garnet solid electrolyte cell with $LiCoO_2$ electrode.

$$\frac{\Delta I}{\Delta t^{-1/2}} = \left(\frac{ZFA}{V_M \sqrt{\pi}} \cdot \frac{\Delta E}{dE/dy} \right) . \sqrt{\widetilde{D}} \tag{5.7}$$

$$\widetilde{D} = \left(\frac{V_M}{ZFA} \cdot \frac{dE/dy}{\Delta E} \cdot \frac{\Delta I}{\Delta t^{-1/2}} \right)^2 . \pi \tag{5.8}$$

where $\Delta I/\Delta t^{-1/2}$ is slope of the plot measured current with inverse square root of time, V_M-molar volume of the electrode, ΔE-applied voltage, dE/dy-slope of a coulometric titration, Z-elementary charge number, F-Faraday constant, A-area of the electrode interface with the electrolyte, and $\widetilde{D}$-the chemical diffusion constant.

The slope is obtained from the linear fit of the plot of output current with inverse of the square root of time through which the current is recorded at the applied constant potential. All the parameters to be used in this equation are available and when all inserted a chemical diffusion coefficient of 1 x 10^{-12} cm^2/s can be obtained, which is also close to the values determined using the impedance analysis and galvanostatic methods.

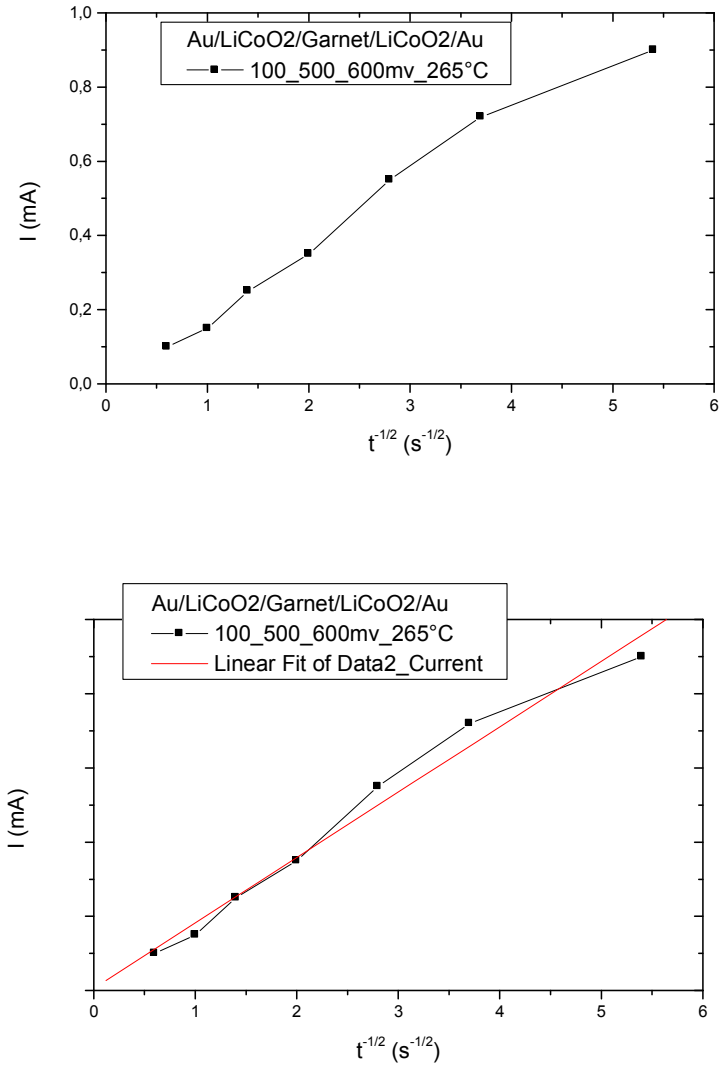

Fig. 5.46 Current versus inverse square root of time and the linear fit of the $Au/LiCoO_2/Garnet/LiCoO_2/Au$ system at temperature of 265 ^oC and at voltages of 600 mV from which the chemical diffusion coefficient can be calculated.

[1] Julian Schvenzel Ph.D thesis, CAU Kiel, 2003.

[2] J. B. Goodenough, H. Y-P. Hong, and J. A. Kafalas, Companion paper.

[3] H. Y-P. Hong, J. A. Kafalas, and J. B. Goodenough, J. Sol. State Chem., **9**, 345 (1974)

[4] Brousely M, Planchat JP, Rigobert G. Virey D, Sarre G., Journal of Power Sources **68**, 8 (1997)

[5] Subramanian MA, Subramanian R., Clearfield A., Solid State Ionics, 18-19, 562 (1986)

[6] V. Thangadurai, W, Weppner, *Adv. Funct. Mater*. **15**, No. 1, January 2005

[7] C. Ho, I.D. Raistrick, R. A. Huggins *J. Electrochem. Soc.,* **127**, 343 (1980)

[8] W. Weppner. R. A. Huggins, *J. Electrochem. Soc.*, **124**, 1569 (1977)

[9] W. Weppner. R. A. Huggins, *J. Electrochem. Soc.*, **125**, 7 (1978)

[10] Hao Ding, Master thesis, CAU Kiel, Chair For Sensors and Solid state Ionics, 2006

[11] A.R. West, Solid State Chemistry and it's Applications, Chapter 13, Wiley (1984)

[12] S. Mitra, A. K. Shukla and S. Sampath, J. of Power Sources, 101, 213-218 (2001)

[13] I.D. Raistrick, C. Ho, R.A. Huggins, *J. Electrochem. Soc.* **123**, (1976), 1469.

[14] W. Weppner, *J. Solid State Chem.* **20**:305-14 (1977)

[15] H. Rickert, W. Weppner, Z. *Naturforsch.* **29a** : 1849-59 (1974)

[16] D. O. Raleigh, *J. Phys. Chem.,* **70**, 689 (1966)

Chapter 6:

Conclusion and Summary

Supercapacitors for reversible electrical energy-storage are presently being developed for a number of applications. Electrochemical capacitors are complementary to secondary batteries and offer applications primarily in hybrid-power systems for electric vehicles, utility load-maintenance, cold-start assist, and memory back-up systems. The energy-storage mechanism in electrochemical capacitors is based on the separation of charges at the interface between a solid electrode and an electrolyte, and/or fast reactions at the interface that are pseudo-faradiac in nature.

An effective method of fabricating electrochemical double-layer capacitors with high power-density is to use a thin-layer solid electrolyte. Parameters, such as low conductivity, poor contact, presence of crystalline domains, high internal-resistance and low mechanical-strength limit, however, the use of solid electrolytes as well as solid polymer electrolytes in electrochemical capacitors.

Organic solvent-based polymer electrolytes with high stability have been reported to be favorable materials for supercaps. In addition, gel electrolytes based on a combination of polyethylene oxide (PEO), polymethylmethacrylate (PMMA) and propylene carbonate (PC) with lithium perchlorate salt have been reported by Ishikawa et al. It is claimed that these gels are superior to solid polymer-electrolytes based on PEO which contains lithium salts in terms of their conductivity and they also posses adequate mechanical strength. Nevertheless, PEO-lithium perchlorate solid-polymer electrolytes have high internal-resistance at ambient temperatures, which makes them unattractive for several applications.

Lithium-ion batteries have been applied in a wide range of uses including portable computers and mobile telephones just to name a few. Phone batteries must be able to supply repetitive high-current pulses, perhaps up to a 10 C discharge rate, i.e., full discharge in $1/10^{th}$ of an hour. This can severely stress many of the battery systems, particularly during operation at low temperatures. While batteries store a large amount of energy and release the stored charge stably, supercapacitors deliver a high current, but only for a very short period of time. That is, although supercapacitors release their peak current when the devices begin operation, batteries give off a stable current while in use. The performance of portable electronic

equipment can often be improved by including a supercapacitor alongside the battery. The capacitor extends a battery's life by reducing its peak output power in many cases. A supercapacitor can provide high power density as well as sufficient energy density. As shown in the Ragone plot in chapter one, clearly, the supercapacitor offers the best combination of power and energy density. Furthermore, by combining the best features of the battery and the supercapacitor, a superior system will result.

At a high discharge rate, such as the pulse current, the heat generated inside a battery is significant. This not only reduces the efficiency of the electrical energy generation, but also causes deleterious effects (i.e. shortened cycle life and increased internal resistance). With an electrochemical capacitor, it is expected that only a minimum amount of heat is generated (I^2R). Clearly, electrochemical capacitors should possess a high efficiency even at a rapid rate of discharge. Therefore, for pulse power applications, the electrochemical capacitor should help the battery to deliver higher power in a more efficient manner.

So, in general the electrochemical characteristics of the supercapacitor can provide a much higher pulse current capability than a battery system. The better pulse performance of nanocrystalline powder is due to the smaller particle size. Shorter diffusion distances promote faster and uniform Li intercalation into $LiCoO_2$ crystallites during the discharge process compared to that of coarse-grained powder, thus improving pulse performance. Although sufficient time is needed, high-pulse performance is improved due to combination with an electrochemical capacitor.

Though the use of the supercapacitors together with batteries is the best to get out of the two, supercapacitors have their own advantages over batteries. Supercapacitors are well suited to replace batteries in many applications. This is because at the moment their scale is comparable to that of batteries, from small ones used in cellular phones to large ones that can be found in cars. Even though supercapacitors have a lower energy density compared to batteries, they avoid many of the battery's disadvantages.

Batteries have a limited number of charge/discharge cycles and take time to charge and discharge because the process involves chemical reactions with non-instantaneous rates. These chemical reactions have parasitic thermal release that causes the battery to heat up.

Batteries have a limited life cycle with a degrading performance and acidic batteries are hazardous to the environment.

Supercapacitors can be charged and discharged almost an unlimited number of times. They can discharge in matters of milliseconds and are capable of producing enormous currents. Hence they are very useful in load levelling applications and fields where a sudden boost of power is needed in a fraction of a second. They do not release any thermal heat during discharge.

Supercapacitors have a very long lifetime, which reduces maintenance cost. They do not release any hazardous substances that can damage the environment. Their performance does not degrade with time. Supercapacitors are extremely safe for storage as they are easily discharged. They have low internal resistances, even if many of them are coupled together.
Even though they have a lower energy density, are bulkier and heavier than an equivalent battery, they have already replaced batteries in many applications due to their readiness in releasing power.

Different solid electrolytes with different electrodes were tested in this work to make a supercapacitor, including powder mixtures of electrolytes and electrodes to get a high surface area where many charges could be stored to provide high capacitance in response. But due to mechanical failures during the pellet pressing, it was not possible to get the supercapacitor as needed. Other than that, the supercapacitor assembled from garnet pellet electrolyte and $LiCoO_2$ thin film electrode showed reasonable results and appears to be a good supercapacitor, though it needs more intensive work and modifications.

The capacitances obtained from the cell assembled in this way were far too low when compared to the others with polymer and liquid electrolytes which is of course due to the bad contact at the electrode-electrolyte interfaces. That was also shown from the impedance analysis.

From all these results, we can see that supercapacitors made in this way have more of a bad-battery nature than a common supercapacitor. That is mainly due to the electrode material used which has less surface areas to store large amount of charges compared to the carbon-

electrode material based supercapacitors. But if further improvements on the materials preparation and assembling is made, a much better supercapacitor can be prepared.

From the electrochemical analysis, we observed that the nature of the cyclability is a good indication that the material can store the same amount of charges when recycled for longer times at the charging/discharging processes.

Most of the electrochemical capacitors are based on high surface area carbon, conducting polymer or some oxide electrodes. The common electrode materials for supercapacitors are carbon (most advanced and is already on the market as high-performance devices), metal oxides like RuO_2, MnO_2, $NaNO_3$, $Li_4Ti_5O_{12}$ (very fast and reversible Faradaic – where a transfer process takes place at the electrode like batteries and are therefore named Pseudocapacitances) and electrical conducting polymers (ECP) like Polypyrrole (Ppy), Poly(methyl)thiophene (PMeT), pseudocapacitances arise from fast and reversible redox reactions: oxidation – p-doping process (positiveve electrode) and reduction – n-doping process (negative electrode). But most of these electrodes are used either with aqueous or organic electrolytes both in symmetric and asymmetric combinations. For example when carbon is used as electrode in aqueous and organic electrolyte, a capacitance of 75 – 175 and 40 – 100 F/gm, respectively, was obtained.

In this work, a different combinations of electrodes and solid electrolytes were assembled for which the capacitance was very low. In spite of the low capacitance obtained, if further modification is done a better product can be made with the big benefits of using solid electrolytes compared to the liquid ones.

7. List of symbols, Abbreviations and Physical Constants

LIST OF SYMBOLS

The following principal symbols have been used throughout in this work.

a_i	Activity of species i
A	Electrode area
c_e	Concentration of electrons
c_i	Concentration of species i
C	Capacitance
C_{dl}	Overall double layer capacitance
C_D	Diffuse layer capacitance
C_g	Geometric capacitance
C_H	Helmholtz layer capacitance
d	Determinant of stoichiometric numbers, thickness
D_i	Diffusion coefficient of species i
$\tilde{D}_i$	Chemical diffusion coefficient of species i
D_{Ti}	Tracer diffusion coefficient of species i
E	Electromotive force (emf)
F	Faraday`s constant, degrees of freedom
G	Gibbs energy
ΔG_{fo}	Standard Gibbs energy of formation
ΔH	Change in enthalpy
I	Electrical current
J	Electrical current density
J_0	Exchange current density
J_i	Flux density of particle i
k	Boltzmann`s constant
L	Diffusion length, inductance
L_{Deb}	Debye length
m_i	Mass of species i
M_i	Molecular weight of species i
n_i	Number of species i
P_i	Partial gas pressure of the component i
q	Electron charge

R	Gas constant, electrical resistance
S	Entropy
t	Time
T	Absolute temperature, period
t_i	Transference number of species i
u_i	Electrical mobility of species i
U	Applied voltage
U_0	Amplitude of applied voltage
V	Volume
W	Enhancement factor (Wagner Factor)
x	Distance coordinate
z	Charge number of species i
$\bar{Z}$	Complex impedance
Z′	Real part of complex impedance
Z″	Imaginary part of complex impedance
$\bar{Z}_W$	Complex Warburg impedance
ε	Dielectric constant
ε_0	Permitivity of vacuum
η_i	Electrochemical potential of species i
$\mu_{e-,\ h+}$	Chemical potential of electrons and holes, respectively
μ_i	Chemical potential of species i
μ_{io}	Chemical potential of species i in the standard state
ρ	Charge density
σ	electrical conductivity
σ_i	Partial electrical conductivity of species i
τ	Relaxation time
φ	Phase shift between input voltage and output current
ϕ	Electrostatic potential
ω	Angular frequency

ABBREVIATIONS USED IN THIS WORK:

AC	Alternate Current
ALD	Atomic Layer Deposition
CPS	Counts Per Second
CVD	Chemical Vapour Deposition
CV	Cyclic Voltammetry
DC	Direct Current
DLC	Double Layer Capacitance
DTA	Differential thermal analysis
EC	Electrochemical Capacitors
ECP	Electrical Conducting Polymers
GITT	Galvanostatic Intermittent Titration Technique
JCPDS	Joint Committee on Powder Diffraction Standards
PITT	Potentiostatic Intermittent Titration Technique
RF	Radio Frequency
SEM	Scanning electron microscope
TGA	Thermogravimetric analysis
WE	Working Electrode
XRD	X-ray diffraction

Physical constants

$F = 96485.3415$	C mol $^{-1}$	Faraday's constant
$K = 1.38066\times10^{-23}$	J K^{-1}	Boltzmann's constant
$q = 1.60218\times10^{-19}$	C	Electron charge
$R = 8.314472$	J K^{-1} mol^{-1}	Gas constant
$\varepsilon_0 = 8.85418\times10^{-12}$	F m^{-1}	Permittivity of vacuum

8. Acknowledgement

The author of this thesis would like to express his sincere appreciation to the following peoples for their contribution to this thesis.

I would foremost like to thank my thesis advisor Prof. Dr. W. Weppner for his constant guidance, support and readiness for stimulating scientific discussions during the whole accomplishment of this work. His analytical approach to scientific problems has been essential to make this thesis possible. In addition to the scientific advises, I was grateful to get his support in my personal life during my stay in Kiel.

I express special thanks to Dr W.F. Chu for his assistance in most of my experimental startings with ordering and obtaining the right starting materials, useful discussions, and sharing his valuable experience on most experimental aspects including in laboratory works.

I would also like to thank T. Metzing for providing technical assistance in the laboratory and computer related supports in office.

I would like to acknowledge Dr. J. Schwenzel for his help on the thin film preparation methods using the evaporation and sputtering machines in our laboratory.

I would also like to thank all the members of the Sensors and Solid State Ionics group for an excellent atmosphere, and the library team for being always helpful.

Thanks to my fellow Ethiopians, Mr. Beyene Aleme and Mr. Tsega Fiseha who were the causes for my coming and persuade my study here in Kiel together with the help of Prof. Dr. F. Fauple. I also would like to thank Prof. Dr. Fauple for the opportunity he gave me to do my master thesis under his group.

I thank my parents and friends for their continuous moral support and encouragement throughout my studies.